The Dissertation Committee for Guangliang Wu Certifies that this is the approved version of the following dissertation:

Continental extension in orogenic belts: Modes of extension, origin of core complexes, and two-phase postorogenic extension

Committee:

Luc L. Lavier, Supervisor

Ronald J. Steel

Nicholas W. Hayman

Whitney M. Behr

Daniel F. Stockli

W. Roger Buck

Continental extension in orogenic belts: Modes of extension, origin of core complexes, and two-phase postorogenic extension

by

Guangliang Wu, B.E.

Dissertation

Presented to the Faculty of the Graduate School of

The University of Texas at Austin

in Partial Fulfillment

of the Requirements

for the Degree of

Doctor of Philosophy

The University of Texas at Austin

May 2016

Dedication

For my wife and my family.

Acknowledgements

It was a great privilege to study at Jackson School of Geosciences. First and foremost, I must thank my supervisor, Luc Lavier, for his immense patience, insightful guidance, and unreserved support through my PhD study, and for keeping me as sane as he possibly can. The dissertation would not have been possible if not for his trust, encouragement, and financial support. Many thanks to Paul Mann for the opportunity to study at UT.

Special thanks to my committee members: Ron Steel for his support all along, especially during the difficult years in 2010-2011; Nick Hayman for support and the wonderful memory during the field trip to Death Valley; Whitney Behr for the fun class and field trip to California; Danny Stockli and Roger Buck for their encouragements. Thanks to all committee members for discussions and their comments on the dissertation. Special thanks also to Eunseo Choi, Eh Tan, Nansheng Qiu, Kirk McIntosh, Ian Norton, John Goff, and Adam Papendieck.

I thank Philip, Mark, Judy, Nancy, and Lisa for their support. Thank Anna, Baiyuan, Becky, Bobby, Dan, Dennis, Greg, Maria, Ryan, Trasha, Yang, Yawen…, friends at ACCCF, HPBC and TCACF, and roommates through these years for the friendship, companionship and interesting conversations. I also thank my fellow students in Jackson School for having classes and/or field trips, or being TAs together. They all make my life at UT more enjoyable.

I would like to thank my parents for their unconditional love and support, and above all my beautiful wife Tiffany for the best memories of my life and incredible life forward.

天 下 同归 而殊途 ，一致而百虑 。

By diverse means we arrive at the same end.

Continental extension in orogenic belts: Modes of extension, origin of core complexes, and two-phase postorogenic extension

Guangliang Wu, Ph.D.

The University of Texas at Austin, 2016

Supervisor: Luc L. Lavier

Continental extension principally occurs in orogenic belts, however, most of numerical simulations use uniform crust that cannot represent an orogenic belt. We simulate lithospheric extension in an orogenic hinterland approximated by a crustal wedge. We first show that the presence of a preexisting weak mid-crustal shear zone dipping at low angle exerts a critical control on whether crustal and mantle deformation are decoupled or coupled. When the lower crust and the mid-crustal shear zone are weak, decoupling occurs and crustal deformation is compensated by lower crustal flow. When the lower crust is strong or a weak shear zone is absent, coupling occurs and crustal deformation is compensated by flow in the mantle. By varying the strength of the lower crust and the weak shear zone in numerical lithospheric extension experiments, we examine structures developed and compare them with structures observed in extended and collapsed orogenic belts. In models with a weak mid-crustal shear zone, we find that decoupling is particularly effective. In these models, we distinguish three modes of extension: 1) localized, asymmetric crustal exhumation in a single metamorphic massif with a weak lower crust, 2) the formation of rolling-hinge normal faults and the exhumation of lower crust in multiple metamorphic core complexes with an intermediate strength lower crust, and 3) distributed domino faulting over the weak mid-crustal shear

zone with a strong lower crust. In models without a mid-crustal shear zone, extension is coupled and structures similar to those observed in continental margins form.

We further analyze my model to better explain and understand the core complexes and low-angle normal faults which develop when a preexisting weak mid-crustal shear zone is present. We define three types of detachment systems and present four models which produce core complexes that bear striking resemblance to natural examples: 1) bivergent core complexes, 2) metamorphic core complexes, 3) boudinage structures, and 4) flexural core complexes. We also discuss intracrustal isostasy and the thermal history of material particles sampled in modeled detachment. Finally, based on a geological and geophysical synthesis and using numerical simulations, we propose a two-phase postorogenic extensional scenario that approximates the evolution and the structures observed in the South China Sea margins.

Table of Contents

List of Tables

List of Figures

List of Illustrations

Chapter 1: Introduction

Continental extension generates some of the most impressive topographic features on Earth in both continental rifts and mid-ocean ridges. Through the past several decades since the era of plate tectonics, researcher have recognized that the thermal structure and crustal thickness of the lithosphere at the time of rifting can result in continental rifts with a variety of geometries, faulting patterns, and subsidence histories (e.g., Sonder et al., 1987; Braun and Beaumont, 1989; Dunbar and Sawyer, 1989; Buck, 1991; Bassi, 1991; Buck, 2007). Rifting has also been found to be influenced by magmatic activity (e.g., White and McKenzie, 1989) and large-offset faulting (e.g., Lavier and Manatschal, 2006). With the advent of more advanced numerical methods, some subtle effects previously not easily studied have been extensively analyzed, for instance, the effects of extensional rate (e.g., Rey et al., 2009) and depth-dependent extension (e.g., Huismans and Beaumont, 2011).

Continental extension often evolves over 10s Myr and few examples of active rifting are available for study, resulting in lacking in evidences and our understanding of the physics behind the rifting processes. Many variables can be studied numerically, especially when dynamic effects are considered. During the past several decades, researchers have developed thermo-mechanical codes to simulate a variety of rheologies suited for long-term tectonic processes, such as the Fast Lagrangian Analysis of Continua (FLAC, e.g., Poliakov et al., 1993; Tan et al., 2012). The rheology of the lithosphere is often prescribed with a yield strength envelope (YSE, e.g., Burov and Diament, 1995). The upper crust is usually modeled as an elastic-plastic medium using Mohr-Coulomb failure criterion (e.g., Lavier et al., 2000), while the lower crust is modeled as a viscoelastic medium using nonlinear creep laws to calculate the viscosity (e.g., Ranalli,

1995). Commonly used creep laws for the viscous part of the crust as well as mantle are extrapolated from lab experiments on rock samples performed at a relatively fast rate compared with those of naturally deformed rocks (e.g., Hirth et al., 2001; Hirth and Kohlstedt, 2003). Together with the variation in petrology of the lower crust and mantle, significant uncertainties in the long-term rheology of lithosphere are common.

Most studies of continental extension use a lithosphere with initially uniform crust. For instance, using an initially uniform lithosphere Buck (1991) showed that a lithosphere generates core complex mode, wide rift mode and narrow rift mode depending on crustal thickness, initial heat flow, and strain rate. Continental extension, however, often occurs in orogenic belts where there are thicker and hotter continental crust, structural heterogeneities, and forces generated by extensional collapse (Dewey, 1988; Platt and Vissers, 1989; Wu et al., 2015). These unique characteristics likely have an important impact on the mechanics and style of rifting that initiates in orogenic belts. Firstly, variation in crustal thickness with topography and Moho relief generates a lateral material flow in orogenic belts (e.g., Bird, 1991). Secondly, heterogeneities including mid-crustal shear zone, décollement, and structures such as thrust faults in the foreland of the belt create multiple weak zones that may be reactivated during extension. Thirdly, during the orogenic collapse the inferred delamination of the mountain root might affect postorogenic extension (e.g., Platt and Vissers, 1989).

To address some of the issues mentioned above, in Chapter 2 we investigate the effects of lower crustal flow and a preexisting weak mid-crustal shear zone in an orogenic belt and in a continental margin approximated by a wedge-shape crust overlying the lithospheric mantle. We first analyze 1) how regional topographic loading and mantle buoyancy generates a pressure gradient that drives lower crustal flow from the highland towards the lowland in the crustal wedge, 2) the factors that contribute to the velocity of

lower crustal flow, and 3) the importance of lower crustal flow velocity compared to the tectonic velocity. We use PARAVOZ (Poliakov et al., 1993; Tan et al., 2012), an academic version of FLAC, to run the numerical experiments. We vary the strength of lower crust to mitigate the uncertainty in our knowledge of the rheology of the lower crust. We also include a mid-crustal shear zone in our models, an addition which is supported by geological and geophysical evidence (e.g., Jolivet et al., 1998; Lister and Davis, 1989) and numerical models (e.g., Lavier and Manatschal, 2006, Regnenauer-Lieb et al., 2006). We vary the shear zone's frictional strength when it is brittle and use a low cut-off viscosity (10^{19} Pa s) when it is viscous. In order to accommodate evidences of a gabbroic lower crust inferred in the US Cordillera and some parts of the Variscan orogeny in Europe (McGuire, 1994; Müntener et al., 2000), we also include a strong lower crust described as mafic lower crust throughout the models. We present two sets of models using 2-layer and 3-layer crusts with the lower crust ranging from very weak to very strong. We also explore these models both with and without a mid-crustal shear zone to provide a detailed description of the effects of lower crustal strength and mid-crustal shear zone on the modes of extension in the crustal wedge, and we discuss in detail the effects of the lower crust and mid-crustal shear zones in the formation of continental core complexes and continental margins.

The clustered distribution and striking similarities of continental core complexes in orogenic belts (e.g., Whitney et al., 2013), such as the US Cordillera and the Aegean, motivate us to investigate their origin in the context of postorogenic extension. They typically have 3 key elements: 1) a metamorphic core that exposes middle to lower crust up to 15-20 km (e.g., Lister and Davis, 1989), 2) a detachment fault (a décollement zone) as a resistant layer that contains mylonite, blastomylonite, and microbreccia shattered by closely spaced fractures (Davis and Coney, 1979), and 3) mid-to-high-angle hanging wall

normal faults lying above the detachment faults (Davis and Coney, 1979). Subhorizontal Moho is typically observed beneath the regions where core complexes are found (Klemperer et al., 1986; McCarthy et al., 1991; Sodoudi et al., 2006). Various models of core complexes have been proposed, such as stress rotation (e.g., Yin, 1989; Spencer, 1989; Melosh, 1990; Wills and Buck, 1997; Collettini et al., 2011), initial weak zone (e.g., Faulkner et al., 2006; Collettini et al., 2009), crustal flow (Block and Royden, 1990; McKenzie et al., 2000) and magmatic activity (Gans and Bohrson, 1998).

Each of these proposed models contributes only a partial explanation of the three key elements and subhorizontal Moho. For instance, the current most widely accepted rolling-hinge model (Wernicke, 1985; Buck, 1988; Lavier et al., 1999; Choi et al., 2013) successfully predicts the geometry of core complex, however, it gives little information on the nature of the detachment, the presence of hanging wall normal faults, the flow of deep crust, and the evolution to flat Moho. In addition, it predicts that the detachment fault is of high-angle origin, contradicting the view that some detachment faults are primary (e.g., Colletini et al., 2011). The flexural model (Spencer, 1984) is still largely a schematic model based on geological reconstructions and assumes an initial low-angle detachment with correlated domino normal faults as a prerequisite. Again, it gives little information on the nature of the deep crust and the flat Moho.

In Chapter 3, we summarize the geological and geophysical observations of continental core complexes and detachment faults in the US Cordillera and the Aegean Sea, and use numerical methods to investigate their origin in orogenic belts. We use identical methods as those doscribed in Chapter 2, but this time we mainly focus on the geological features predicted by the model. Based on numerical models, we define three types of detachment faults and describe their associated upper-crustal normal faults. We present the origin of primary low-angle normal faults in the context of a non-Andersonian

state of stress. We propose four models that we believe provide a consistent view of the origin of continental core complexes and detachment faults: 1) bivergent core complexes (or metamorphic massifs), 2) classic Cordilleran metamorphic core complexes, 3) boudinage structures (or multiple consecutive core complexes), and 4) flexural core complexes. We also investigate the lower crustal flow, its effects in intracrustal isostasy, and the thermal history of the modeled shear zone.

Continental rifts may develop even further and eventually lead to seafloor spreading. The Basin and Range extended shortly after Laramide orogeny (Christiansen et al., 1992). Though varying in time regionally, it generally underwent 2 phases of extension: phase 1 was dominated by directional lower crustal flow and by formation of core complexes where exhumed lower crusts juxtapose upper-crustal rocks along detachment faults (e.g., Wernicke, 1992); phase 2 was dominated by upper-crustal high-angle normal faults in the characteristic Basin and Range style. The South China Sea (SCS) region, an Andean-type orogenic belt before extension (e.g., Taylor and Hayes, 1983), seems to undergo similar phases of extension that develop much further and eventually lead to seafloor spreading.

In Chapter 4, we investigate a two-phase postorogenic extension scenario for the formation of the South China Sea (SCS) margins using recent seismic data and numerical simulations. In the same manner as in Chapter 2, we carry out numerical simulations of the extension of a single wedge with a mid-crustal shear zone to investigate the first phase, a phase characterized by grabens, half grabens, and migration of extension from North to South (Sun et al., 2009). We propose that as phase 1 evolves it leads to severe attenuation of the crust as well as a reduction of topography and Moho relief, and it may ultimately reach isostatic equilibrium. Phase 2 subsequently began in the highland in the SE SCS where the last known rift is active, but before which a period of tectonic

quiescence might have facilitated the transition between the two phases through thermal cooling and subsidence. We model phase 2 using identical methods but exclude the mid-crustal shear zone. Both seismic profiles (e.g., Hu et al., 2009, Sun et al., 2009; Franke et al., 2014; Lester et al., 2014) and our numerical models show that phase 2 is symmetric, coupled, and generates conjugate margins characterized by domino style normal faults dipping seawards. The model presented here is probably a highly simplified version of the rather complicated evolution of the SCS margins, however it illustrates what we believe are the key geological processes.

The main purpose of this dissertation is to (1) investigate the extension of orogenic belts approximated by extending a crustal wedge overlying the mantle and (2) apply the resulting models to explain the origin of core complexes and tectonic evolution of the SCS margins. In chapter 2, we study lower crustal flow, weak preexisting mid-crustal shear zones, and their potential effects on the modes of extension in a crustal wedge mainly through a physical perspective. We apply our results to explain the origin of continental core complexes and detachment faults mainly from a geological perspective in chapter 3. Finally, in chapter 4, we further develop our models and propose a two-phase scenario of postorogenic extension for the SCS margins based on a geological and geophysical synthesis and numerical simulations. Through these tasks, we also investigate issues such as the effects of decoupling between upper crust and mantle, and the isostatic equilibrium during the extension of a crustal wedge. Our models reproduce some key structures, such as core complexes and detachment faults, with striking resemblance. We suggest that our models could be widely applied in cases of continental extension of orogenic belts, and probably island arcs as well.

Chapter 2: Modes of continental extension in a crustal wedge

Note: Chapter 2 has been published in *Earth Planet. Sci. Lett.* 421, 89-97. doi:10.1016/j.epsl.2015.04.005. [1] Supplementary Fig. A1-A8 and Mov. A1-A3 are included in Appendix A.

ABSTRACT

We ran numerical experiments of the extension of a crustal wedge as an approximation to extension in an orogenic belt or a continental margin. We study the effects of the strength of the lower crust and of a weak mid-crustal shear zone on the resulting extension styles. A weak mid-crustal shear zone effectively decouples upper crustal extension from lower crustal flow. Without the mid-crustal shear zone, the degree of coupling between the upper and the lower crust increases and extension of the whole crust tends to focus on the thickest part of the wedge. We identify three distinct modes of extension determined by the strength of the lower crust, which are characterized by 1) localized, asymmetric crustal exhumation in a single massif when the lower crust is weak, 2) the formation of rolling-hinge normal faults and the exhumation of lower crust in multiple core complexes with an intermediate strength lower crust, and 3) distributed domino faulting over the weak mid-crustal shear zone when the lower crust is strong. A frictionally stronger mid-crustal shear zone does not change the overall model behaviors but extension occurred over multiple rolling-hinges. The 3 modes of extension share characteristics similar to geological models proposed to explain the formation of

[1] AUTHORS: Guangliang Wu[a,b,*], Luc L. Lavier[a,b], Eunseo Choi[c]
[a] Institute for Geophysics, University of Texas at Austin, 10100 Burnet Rd., Austin, TX 78758, United States
[b] Department of Geological Sciences, University of Texas at Austin, 2225 Speedway, Stop C1160, Austin, TX 78712, United States
[c] Center for Earthquake Research and Information, University of Memphis, 3890 Central Ave., Memphis, TN 38152, United States
[*] Corresponding author: glwu@utexas.edu (G. Wu)

metamorphic core complexes: 1) the crustal flow model for the weak lower crust, 2) the rolling-hinge and crustal flow models when the lower crust is intermediate and 3) the flexural uplift model when the lower crust is strong. Finally we show that the intensity of decoupling between the far field extension and lower crustal flow driven by the regional pressure gradient in the wedge control the overall style of extension in the models.

2.1 INTRODUCTION

The yield strength of the continental lithosphere is primarily constrained by the thermal structure and rheological composition of the lithosphere and is often represented as a yield stress envelope (YSE) (e.g., Burov and Diament, 1995). In extension, its yield strength is such that only when weakened by heating or magmatic processes, a continental lithosphere can breakup (e.g., Buck, 1991; Buck et al., 2005, 2009). For example, Buck (1991) showed that a hot, and therefore weak, orogenic lithosphere with a thick crust is weak enough to stretch in the "wide rift" or "core complex" mode. Some of the best examples of such extensional environments are the Basin and Range province in the western US, Papua New Guinea, and the Aegean.

Several intriguing observations have further driven the search for a more detailed mechanical model for the formation of a rift basin in similarly hot lithosphere including: 1) the lack of variations in crustal thickness over large wavelength, 2) the exhumation of lower crust in metamorphic core complexes (MCCs) and 3) the formation of large-offset low-angle normal fault. The first observation is a key characteristic of the extension of hot lithosphere. Hot ductile lower crust flows to smooth out variations in crustal thickness caused by differential extension (Block and Royden, 1990; McKenzie et al., 2000). Likewise, the topographic gradient in a differentially thickened crust can also drive the flow of ductile lower crust (Braun and Beaumont, 1989; Kruse et al., 1991; Bird, 1991).

Several mechanisms were proposed to explain the remaining characteristic observations, i.e., the exhumation of middle crust along shallow-dipping mylonitic shear zone and brittle normal faults (e.g., Gans, 1987; Wernicke, 1981; Buck, 1988; Block and Royden, 1990; Melosh, 1990; McKenzie et al., 2000). The rolling-hinge model proposed that the middle crust is exhumed from large depths by an offset greater than 15 km along a high- or low-angle normal fault rooted in the middle crust (Axen, 1988; Buck, 1988). Other models (Gans, 1987; Block and Royden, 1990; McKenzie et al., 2000) proposed that lower crustal flow caused by local or regional pressure gradients drives exhumation and causes the rotation of an initially high-angle normal fault to a low angle. Explaining the formation of large-offset normal faults in the rolling-hinge model remains the main issue. Hypotheses include fault strength decreasing with fault offset in a thin brittle upper crust (Buck, 1988; Axen, 1988; Lavier et al., 2000) and stress rotation caused by basal shear or along a weak frictional fault interface (e.g., Yin, 1989; Melosh, 1990). Accordingly, the low dip of a large-offset normal fault can be achieved either through the rotation of a high-angle normal fault (e.g., Buck, 1988) or as a primary fault (e.g., Yin, 1989; Melosh, 1990).

However, in spite of a few exceptions (e.g., Rey et al., 2010), most numerical and theoretical studies of lithospheric extension assumed an initially uniform crustal thickness and ignore regional pressure gradients that would be caused by preexisting variations in crustal thickness. For instance, Buck (1991) showed that a localized mode of crustal extension similar to core complex extension would occur in a uniformly thick lithosphere with weak lower crust. The rolling-hinge model (Buck, 1988; Lavier et al., 1999; Choi et al., 2013) also assumed a lithosphere that initially has a uniform thickness. Following the same mechanical principles with those of the rolling-hinge model proposed by Buck (1988) (i.e., that an active high-angle normal fault is rotated into a low-angle normal fault

when exhumed at the surface), sometimes with the addition of melt, numerical models of core complexes forming in a hot and uniformly thick lithosphere with a thick crust have shown that the high-angle rolling-hinge is successful at explaining some of the observations at core-complexes (e.g., Lavier and Buck, 2002; Tirel et al., 2008; Rey et al., 2009; Huet et al., 2011; Gessner et al., 2007). Although successful in explaining the low dip and geometry of normal faults observed at many MCCs, rolling-hinge models failed to explore the combined effects of regional flow due to gradients in crustal thickness (Bird, 1991) and differential stretching (Block and Royden, 1990) on the mechanics of core complex formation. Bialas et al. (2007), Rey et al. (2010), and Whitney et al. (2013) considered the effects of non-uniform crustal and lithospheric thickness but did not analyze the details of the mechanical consequences like the interaction between lower crustal flow and faulting. Huet et al. (2011) used a wedge-shaped layering of the crust without initial topography, Moho relief, or mid-crustal shear zone. In addition, they did not systematically vary the strength of the lower crust.

Another important but often-ignored possibility in lithospheric extension is that a weak mid-crustal shear zone can decouple upper crust from lower crust and mantle. The presence of such a decoupling zone is supported by the inference of the dip of subhorizontal mylonitic shear zone near the base of brittle crust using GPS measurements (Velasco et al., 2010) and by subhorizontal detachment surface detected in seismic reflection profiles such as the S reflector in the Iberia margin (Reston et al., 1996). Even in studies that considered the mechanical effect of a decoupling mid-crustal surface on rifting (e.g., Nagel and Buck, 2006; Lavier and Manatschal, 2006; Huismans and Beaumont, 2011), the crust-mantle boundary and the topography were assumed to be initially flat.

These overlooked components might have substantial influence on the dynamics of lithospheric extension. For instance, it is very likely that the interaction between regional lower crustal flow and normal faulting in a hot lithosphere can result in different extensional styles with single or multiple zones of active basins and ranges. Previous studies of extension (Buck, 1988, 1991; Lavier et al., 2000) have demonstrated that several weakening and hardening phenomena control whether extension in wide rifts stays localized on a single zone (one MCC or graben) or multiple zones (multiple MCCs or grabens) of extension. The loss of cohesion or frictional strength on a fault competes with the resistance of the brittle upper plate to bending (Lavier et al., 2000) to accommodate extension on multiple normal faults rather than on a single normal fault. Viscous strengthening in response to normal faulting at the base of the brittle upper crust can also occur if the lower crust is strong (Lavier and Buck, 2002). In that case, strengthening lead to the formation of multiple normal faults in the upper crust (Lavier and Buck, 2002). At the scale of the lithosphere, thinning of the crust and the associated mantle upwelling strengthen the lithosphere and force deformation to delocalize over multiple extensional centers (Buck, 1991). If the pressure gradient and the strength of the lower crust are such that the lower crust can flow efficiently and smooth out variations in crustal thickness (Buck, 1991) then strengthening due to mantle upwelling is suppressed and extension should continue on one given extensional center or normal fault. When the shear resistance in a high viscosity lower crust opposes flow, it cannot suppress crustal thinning efficiently and as a result mantle upwelling may occur. This mechanism increases the lithosphere's resistance to extension and causes the formation of multiple rift basins (Buck, 1991; Buck et al., 2009).

In this paper, we explore the effects of lower crustal flow driven by a regional pressure gradient on the decoupling of deformation in the lithosphere and the style of

rifting that the presence or absence of decoupling generates. Specifically, we conducted numerical experiments on the extension of a two- or three-layer crust in wedge-shaped crust (Fig. 2.1). We also studied the effects of the composition of the lower crust and included the effect of a preexisting decoupling shear zone at the brittle ductile transition (BDT). While a two-layer division of the crust (upper and lower crust) may be sufficient for most tectonic settings, the presence of a strong gabbroic lowermost lower crust (termed mafic lower crust throughout the paper) has been inferred in some regions, such as the US Cordillera and some parts of the Variscan orogeny in Europe (McGuire, 1994; Müntener et al., 2000). That motivates us to assume a three-layer crust and analyze the effect of a strong gabbroic lower crust on extension mechanisms and styles.

2.2 SIMPLE ANALYSIS OF DECOUPLING

We seek to describe the capacity of lower crustal flow driven by a pressure gradient imposed by topographic loading and mantle buoyancy, compared with that driven by far field extension applied at the side of the lithosphere. While the simple analysis presente here ignores the complex non-linear interactions between the brittle and ductile deformation, it is a useful guide to the mechanic of the lithosphere and the interpretation of our numerical models.

2.2.1 Definition of coupled versus decoupled deformation

Local isostasy occurs when loading or unloading on the lithosphere is counterbalanced at the same location. In contrast, regional isostasy involves the non-local effects such as elastic strength (flexure) and lateral ductile flow over a large distance. Compensation becomes local when the flexural strength of the lithosphere is small so that flexural wavelength is much smaller than the scale of loading and ductile flow is not fast enough (Watts, 2001). In the case of local compensation, brittle deformation in the upper

crust is typically compensated by local mantle stretching and upwelling and the deformation appears to be coupled. When the lithosphere has a large flexural rigidity and/or ductile flow is intense, deformation in the brittle upper crust is regionally compensated. Since the regional compensation would involve vigorous lateral flow of the ductile lower crust even for a highly localized deformation of the brittle upper crust (Watts, 2001), the deformation of the upper crust and the mantle lithosphere would appear decoupled.

Here we assume that decoupling and regional compensation occur when the flow rate in the ductile lower crust is greater than the far field boundary conditions. Ductile flow in the lithosphere is generated by horizontal and vertical pressure gradients. The intensity of the flow may exceed the kinematic boundary conditions when excess loading from gradients in crustal thickness are preexisting. It may also be larger if a weak shear zone or decoupling surface is present at the BDT. Another very important factor controlling the rate of ductile flow is the variation in channel thickness in the lower crust (McKenzie et al., 2000). For example, if the channel thickness decreases in the direction of the flow, the flow rate increases in order to conserve mass.

2.2.2 Decoupling ratio

We provide a simple analysis of the effect of lower crustal viscosity and loading from topography and Moho relief on the decoupling of the deformation. We ignore the effects of both channel thickness and weak shear zones for simplicity. Lower crustal flow occurs along the width of the lithosphere, W, along the BDT along a surface of length $W/\cos\alpha$ and along the Moho along a surface of length $W/\cos\beta$, where α is the slope angle of BDT and β is the slope angle of the Moho, and both are small, i.e., <5-10°. We propose that the intensity of decoupling of lower crust with respect to upper crust and

mantle can be roughly expressed as the ratio (D) of the mean horizontal velocity ($\bar{u}$) of the pressure gradient-driven channel flow in the lower crust to the boundary velocity (v_x). If the channel velocity is significant (i.e., $D \geq 1$) then the deformation is decoupled while coupled if the channel velocity is negligible (i.e., $D \ll 1$).

In a wedge-shaped crust where both regional topography and Moho relief are present (Fig. 2.1) and the BDT is assumed to be subhorizontal, the pressure gradient along the base of wedge-shaped brittle crust is (Bird, 1991):

$$\nabla P_x^{topo} \approx \rho_c \; g \frac{\partial h_t}{\partial x} \cos\alpha \approx \rho_c \; g \frac{\partial h_t}{\partial x} \tag{2.1}$$

where ρ_c is the averaged density of upper crust, g the gravity, $\partial h_t/\partial x$ the gradient of topography and $\cos\alpha \approx 1$ ($\alpha < 10°$). Similarly, a contribution from the Moho relief to the pressure gradient in the lower crust is:

$$\nabla P_x^{moho} \approx (\rho_m - \rho_c) \; g \frac{\partial h_m}{\partial x} \cos\beta \approx (\rho_m - \rho_c) \; g \frac{\partial h_m}{\partial x} \tag{2.2}$$

where h_m is the Moho relief and $\cos\beta \approx 1$ ($\beta < 10°$). The mean velocity in the lower crust is:

$$\bar{u} = \frac{h^2}{12\eta_{lc}} \left(\nabla P_x^{moho} + \nabla P_x^{topo} \right) \tag{2.3}$$

where h is the channel thickness and η_{lc} is the viscosity of lower crust. The decoupling ratio D is defined as:

$$D = \frac{|\bar{u}|}{v_x} = \frac{h^2}{12\eta_{lc} v_x} |\nabla P_x| = \frac{h^2 g}{12\eta_{lc} v_x} \left| \rho_c \frac{\partial h_t}{\partial x} + (\rho_m - \rho_c) \frac{\partial h_m}{\partial x} \right| \tag{2.4}$$

We proceed to compute D using Eq. (2.4) for a 200 km-wide crustal wedge. We assumed a topographic relief of 3 km and a corresponding Moho relief of 14 km under local isostasy (Fig. A1). The decoupling factor, D, is plotted with respect to viscosity of the lower crust ranging 10^{19}-10^{23} Pa s and for 3 values of channel thickness (10 km, 20 km and 30 km) (Fig. 2.2). The plot shows that D decreases markedly as the lower crust's viscosity increases. D is nearly negligible when the viscosity is greater than 10^{21} Pa s regardless of the channel thickness. The plot also shows that when the thickness of the

channel increases, the degree of decoupling would increase. The simple analysis presented in Fig. 2.2 suggests that the viscosity and thickness of the lower crust has to be smaller than $\sim 10^{20}$ Pa s and greater than 10 km, respectively, to allow for significant decoupling. A sufficiently large pressure gradient may cause deformations other than the lower crustal flow but such a case is beyond the premises of this simple calculations. Varying the width of the lithosphere (W) from 100 km to 300 km, the topographic relief from 1 km to 5 km, and correspondingly Moho relief from 5 km to 24 km (local compensation) generates a maximum topographic and Moho gradient of 5.7° and 13° respectively. These values still allow us to make the same approximations as in Eq. (2.4). Therefore changing the wedge geometry in this range of dimensions does not significantly affect the decoupling analysis.

2.2.3 Factors contributing to decoupling

Several other factors will play a significant role on the decoupling ratio: 1) The thinning of the lower crustal channel from high to low elevation (Fig. 2.1) contributes significantly to the intensity of lower crust flow. As the lower crust enters a thinner channel the intensity of the flow increases so that mass is conserved. As a result the decoupling ratio should increase significantly as strain rate increases. 2) When present, the weak shear zone at the BDT is a very narrow channel with low viscosity ($\sim 10^{19}$ Pa s at ~300-400 °C). Our simple analysis cannot take these parameters into account. We therefore run numerical experiments to analyze the effect of lower crustal strength and the presence of a weak mid-crustal shear zone.

The existence of mid-crustal shear zones is supported by geological and geophysical evidence (e.g., Jolivet et al., 1998; Lister and Davis, 1989) and numerical models (e.g., Lavier and Manatschal, 2006; Regenauer-Lieb et al., 2006). One difficulty,

however, is to differentiate preexisting shear zones from the ones developed during extension. Here we choose to consider that mid-crustal shear zones always exist in the crust; however, they may be weak, strong, or even completely annealed depending on the geological conditions. To incorporate a full dynamic evolution of the shear zone during extension is out of the scope of this work. Finally when the weak shear zone behaves in a brittle manner whether it slips or not depends on its cohesional and frictional strengths. We will also analyze the effects of the shear zone frictional strength.

2.3 MODEL SETUP

Both regional scale flow (Bird, 1991) and flow driven by emerging differential crustal thickness (Block and Royden, 1990) are simulated in our models (Figs. 2.1 and 2.3). The mechanism for normal faulting used in the models follows an elasto-plastic constitutive update with a Mohr-Coulomb yield criterion (Lavier et al., 1999, 2000) that is consistent with Andersonian fault mechanics (Anderson, 1951). We decreased the fault strength as a function of plastic strain to simulate weakening of the normal faults (Lavier and Buck, 2002; Lavier and Manatschal, 2006). We present experiments with and without preexisting decoupling shear zone. In both sets of experiments we explore the effect of the lower crustal strength as a function of rheological composition (Fig. 2.3). We investigated a two-layer division of the crust using two sets of models (Fig. 2.3A and B, with and without a decoupling layer, respectively) as well as a three-layer crustal structure with two sets of models (Fig. 2.3C and D). Finally, the numerical models are compared to continental extension in several regions around the world to test whether they are developing patterns of deformation that are similar to those observed in natural examples.

We limited the number of numerical experiments and computing time by choosing fixed dimensions and initial thermal structure for the lithosphere that correspond to the wedge described in Fig. 2.1A. We set the thermal age of the lithosphere at 50 Myr with a constant geotherm to set the initial thermal structure. We tested bottom boundary temperature from 600 °C to 1000 °C with an interval of 50 °C in our early simulations. The changes of the bottom boundary temperature in the range only slightly affect our models. Moreover a temperature of 700-800 °C matches best the geotherm imposed by the thermal age of 50 Myr. We used constant boundary temperatures at the bottom (800 °C) and surface (10 °C) and zero heat flux boundary conditions for the sides of the model for all the numerical experiments presented here. Fig. 2.3 shows the initial lithospheric strength profile corresponding to parameters given in Table 2.1. To avoid mesh errors at the surface, a very small amount of erosion and sedimentation are simulated to avoid the development of sharp corners and overhangs. We applied divergent boundary conditions on the sides with a constant overall speed of 1.25 cm yr^{-1}. To simulate regional isostasy, we use a Winkler foundation at the base of the models.

The decoupling layer is modeled as a thin (~2 km) shear zone at the base of upper crust in models with two- and three-layer crust (Fig. 2.1B and D), respectively. It is initially behaving in a ductile manner and is assumed to have low viscosity (~10^{19} Pa s at ~300-400 °C, see supplementary Figs. A1A, C and A2). When the shear zone is included (Fig. 2.1B and D), we varied its frictional strength from very weak to very strong with frictional angle, θ, ranging from 5° to 25° when it enters the brittle field. The rheology of the lower crust is difficult to specify because it depends on the mineral composition, grain size, thermal structure and the presence/absence of fluids/magmas. For each setup in Fig. 2.1, we varied the rheology of the lower crust from low to high viscosity (Fig. 2.3) to study its effect on the intensity of lower crustal flow and

decoupling of the deformation between crust and mantle lithosphere. In models with a two-layer crust, we use the creep law for dry quartz, wet quartz, and wet quartz with 0.12% added water (Jaoul et al., 1984) for strong (high viscosity), intermediate (low viscosity), and weak (minimum viscosity) lower crust (red, green, and blue in Fig. 2.3A and B), respectively. In models with a three-layer crust, we used creep law for plagioclase (Ranalli, 1995) as a reference, and systematically reduced the activation energy term in the creep law, so that lower crustal viscosity varied from high for cold crust to the minimum viscosity for hot crust (red, green, and blue in Fig. 2.3C and D), respectively.

We used a modified version of PARAVOZ (Poliakov et al., 1993; Tan et al., 2012) to carry out the numerical modeling. We used a fine mesh of 500 m by 500 m. We mainly varied the viscosity of the lower crust, and the frictional strength of the mid-crustal shear zone if included. All the other parameters are kept the same across all the models (Table 2.1).

2.4 RESULTS

2.4.1 2-layer models

After 50% of extension models without (Fig. 2.4A-C) and with (Fig. 2.4D-F and Movs. A1-A3) a mid-crustal shear zone show that mantle upwelling is more intense on the highland side of the models (zone of high strain in red), and that as lower crustal strength increases the extensional style changes from lower crustal exhumation dominated to upper-crustal faulting dominated. In models with no mid-crustal shear zone (Fig. 2.4A-C), brittle deformation does not necessarily focus in the thin part of upper crust and even tend to break the highland part of the model. In contrast, when a

weak mid-crustal shear zone is present, upper-crustal deformation always starts in the lowland (Fig. 2.4D-F).

With a weak lower crust (Fig. 2.4A) but no mid-crustal shear zone, lower crustal exhumation in a ~50 km wide gneiss dome dominates the deformation pattern. It generates symmetric a gneiss dome flanked by two active normal faults. For intermediate strength lower crust (Fig. 2.4B), thinning of the crust is more closely related to mantle upwelling as indicated by the upwardly warped Moho. In this case, the isostatic response renders the gneiss dome (Fig. 2.4B) similar to a narrow rift exhuming lower crustal material. With a strong lower crust (Fig. 2.4C), a series of adjacent half-grabens develop over the upwelling mantle and connect together to form a structure similar to a thinned continental margin.

When the mid-crustal shear zone is present (Fig. 2.4D-F and Movs. A1-A3) upper crustal deformation for the weak to intermediate strength lower crust develops rolling-hinge normal faults exhuming lower crust in structures similar to MCCs (Buck, 1988). However, when the lower crust is weak, one single very wide (~100 km) gneiss dome forms (Fig. 2.4D) and lower crustal flow forms a symmetric pattern of exhumation. For a stronger lower crust (Fig. 2.4E), two core complexes 30 km and 50 km wide form separated by major crustal blocks, deformation is more asymmetric and strain in the lower crustal flow is less intense. When the lower crust is strong (Fig. 2.4F) a single 50 km wide core complex forms. However more distributed extension occurs in the upper crust forming a thin crustal layer on top of the exhuming and upwelling lower crust and a zone of highly extended upper crust with domino style faulting develops over the mid-crustal shear zone (Fig. 2.4F).

2.4.2 3-layer models

The models with a three-layer crust behave similarly to the two-layer crust models (Fig. 2.5). One apparent difference is that, when the mid-crustal shear zone is absent and the lower crust is very weak (Fig. 2.5A), continuous exhumation of lower crust occurs along a large offset normal fault in a way similar to that predicted by the rolling hinge model (e.g., Buck, 1988; Lavier et al., 1999; Choi et al., 2013). The corresponding 2-layer model (Fig. 2.4A) produces symmetric massifs bounded by high-angle normal faults. When compared to models in Fig. 2.4 (2-layer models), the Moho is exhumed to 15-25 km depth in case A, B, D and E (Fig. 2.5) showing that crustal thinning is more intense. Crustal thinning is particularly intense in the model 5C (Fig. 2.5C) where crustal stretching and mantle upwelling thin the crust to less than 3 km. Finally, in all the 3-layer models (Fig. 2.5), the strong mafic lower crust is thinned to a negligible thickness under the highland where mantle upwelling is largest.

2.4.3 Effects of the frictional strength of the mid-crustal shear zone

The internal friction angle of the mid-crustal shear zone was changed from 5° to 15° and 25°. As expected, Fig. 2.6A is identical to Fig. 2.5E since the same parameters are used in both simulations. However, as θ_s increases (15°, and 25° for Fig. 2.6B and C, respectively), more core complexes form but they are narrower (from 70 km to 20 km wide). All other parameters being constant, as the frictional strength of the mid-crustal shear zone increases, we find that extension is more distributed and results in the formation of multiple closely spaced rolling hinges with normal faults accumulating smaller offsets. Not all core complexes exhume lower crust to the surface and the deformation migrates towards the highland with increasing extension similar as shown in Mov. A2.

2.5 DISCUSSIONS

2.5.1 Effects of the lower crustal strength

2.5.1.1 In the absence of a weak mid-crustal shear zone

The models without a preexisting shear zone show systematic changes with increasing strength of the lower crust (Figs. 2.4A-C and 2.5A-C) in terms of the spacing of extensional centers, normal fault offsets, and style of rifts and half grabens. Transition from localized to distributed deformation encapsulates the main change associated with increasing lower crustal strength. As a result, the number of small offset normal faults increases and they accommodate a greater proportion of total extension as the lower crust gets stronger. Finally, increasing viscosity of the lower crust decreases the degree of decoupling (Eq. 2.4).

In the 3-layer models, the presence of a high viscosity mafic lower crust increases lower crustal strength. As a result the strength of the lithosphere allows for the formation of a thinner viscous channel. According to our channel flow-based analysis (Fig. 2.2), the reduction in channel thickness, *l*, allows for more coupling. However in the outlier case (Fig. 2.5A), even though the channel thickness is smaller, the lower crustal viscosity is so low that the upper crustal deformation appears decoupled (Fig. 2.2) and a large massif exhuming lower crust forms in the low land. In the other cases, coupling across a thin lower crustal channel leads to more intense and focused crustal thinning, which also implies that compensation is more local. In this framework of degree of decoupling, hardening of the lithosphere is supposed to determine whether deformation stays localized on one large-offset fault or is distributed over multiple faults. Therefore, processes such as crustal thinning, viscous strengthening of the lower crust due to

increased strain rates and bending of the upper crust are likely to dominate the deformation processes as was proposed by Buck et al. (1999).

2.5.1.2 Effects of the weak mid-crustal shear zone

The inclusion of a weak mid-crustal shear zone (frictional angle, θ_s = 5° and viscosity of 10^{19} Pa s when ductile, at ~ 300 - 400 °C, see supplementary Fig. A1-A2) makes the crust accommodate extension more by lower crustal flow rather than upper-crustal faulting (Figs. 2.4D-F, 2.5D-F). All six models in Figs. 2.4D-F and 2.5D-F develop large-offset low-angle normal faults. The extension is generally decoupled (Figs. 2.44D-F, 2.5D-F and Movs. A1-A3) and the regional lower crustal flow from thick to thin crust is intense. Common to all models is the regional migration of the deformation from thin to thick crustal domains and the formation a model-wide subhorizontal Moho discontinuity (Movs. A1-A3, corresponding to Fig. 2.4D-F). The weak mid-crustal shear zone is highly effective in decoupling upper crustal and mantle lithosphere deformation and thus significantly enhances lower crustal flow, smoothing out the crustal relief generated by thinning in all cases.

When the mid-crustal shear zone is present, strength of the lower crust determines the distance up to which thinning of brittle upper crust propagates. For instance, the brittle deformation always starts from the thinnest part but it appears to stop propagating towards the highland at 75, 100 and 125 km in the 2-layer models with weak, intermediate and strong lower crust (Fig. 2.4D-F). This correlation must reflect the balance between increase in brittle strength towards the thicker portion of the crustal wedge and viscous stress involved in the flow of lower crust. When the lower crust is weak, the associated viscous stress must be comparable to the brittle strength of the upper crust at the distance of 75 km; when the lower crust is strong, the viscous stress must be

as large as the brittle strength of the thicker portion of upper crustal at the distance of 125 km. Although not as clear as in the 2-layer models, the same trend is found in the 3-layer models (Fig. 2.5D-F) and the distance traveled by deformation front toward the highland is overall greater compared to that of the corresponding 2-layer model. Lower degree of decoupling due to the smaller channel thickness of the 3-layer models can explain this difference.

Both weak ductile crust and the mid-crustal shear zone favor decoupled extension of a wedge shaped crust. However, decoupled extension would require a very weak ductile crust without a mid-crustal shear zone. The results are in agreement with our simple analysis (Fig. 2.2). While both weak shear zone and weak lower crust can decouple the brittle upper crust from the lower crust, a shear zone is particularly effective in facilitating sub-horizontal shear flow and inducing decoupling in the crustal wedge.

2.5.1.3 Style of MCC formation

The models suggest that the strength of the lower crust controls the style of MCC formation. We found that extension with a weak lower crust favors symmetrical structures similar to gneiss domes in which extension is accommodated by ductile flow while extension with a stronger lower crust leads to the formation of asymmetric MCCs in which extension is accommodated by both ductile flow and distributed stretching over a detachment surface.

The mechanism of the formation of gneiss domes in the models with weak lower crust (Fig. 2.4D and 2.5D) corresponds to the crustal flow or intracrustal isostasy model proposed by Gans (1987) and Block and Royden (1990). Gneiss domes indicating extrusion of deep lower crust by such a process have been observed in the Menderes massif, Turkey (Hetzel et al., 1995; Gessner et al., 2001), NW Rhodope, the Aegean

(Gautier et al., 1999), and Papua New Guinea (Martinez et al., 2001). Intermediate strength of lower crust appears to produce MCCs by the rolling-hinge mechanism (Figs. 2.4E, 2.5E, and Fig. 2.6) and exhumes lower crust to the surface (Lavier et al., 1999; Choi et al., 2013). The process of MCC formation in the strong lower crust models (Fig. 2.4F and 2.5F) would correspond to the flexural uplift model (Spencer, 1984), in which stretching of the upper crust over a flowing and thickening lower crust eventually leads to the exhumation of lower crust. This model is still used to explain core complexes similar to the Whipple Mountains in the Basin and Range province (Spencer 1984).

The main characteristics of Cenozoic tectonics in the Basin and Range and the Aegean are: 1) that both systems were young orogenic belts at the initiation of extension (Wernicke, 1985; Jolivet and Brun, 2010), 2) that they both developed core complexes (Davis and Coney, 1979; Coney et al., 1980; Jolivet and Brun, 2010), and 3) that the Moho is rather continuous and regionally subhorizontal (Klemperer et al., 1986; McCarthy et al., 1991) in the extended region. The numerical models including a weak mid-crustal shear zone (Fig. 2.4D-F, 2.5D-F, 2.6A-C) do fit well with these general features. The numerically produced detachment structure is also in agreement with those observed in the thermally re-equilibrited lithosphere, such as the Norwegian margin (Osmundsen and Ebbing, 2008), Iberia margin (e.g., Reston et al. 1996), and South China Sea (e.g., McIntosh, K. et al., 2014).

The migration of extension seems to conform to the Death Valley region (Miller and Pavlis, 2005), which is comparative in scale, and the Elba to the Adriatic coast (Barchi et al., 1998). However it should be bear in mind that our model might still be in a local-regional scale compared to the Aegean and the Basin and Range. In addition we did not consider arc migration, magma generation, and delamination, which may affect the migration of extension, and may compete with our implied conditions.

2.5.2 Modes of extension of wedge-shaped crust

We found that the lithospheric wedge extends in one of the following two ways: (1) by lower crustal flow, crustal and mantle lithosphere thinning in response to the extension applied at the model boundaries, (2) by intense extension of the highland and the associated upward flow of asthenosphere to compensate for flow of lower crust towards the lowland.

The intensity of lower crustal flow is mainly controlled by the strength of the lower crust and the presence of a weak mid-crustal shear zone at the BDT in the crust. The mid-crustal shear zone is weaker than the lower crust, and when the lower crust is weak (wet quartz rheology) as well, lower crustal flow is intense. As a result, upper crustal extension is localized and accommodated by the exhumation of lower crust to the surface as seen in Figs. 2.4D-E, 2.5D-E and 2.6A-C. These behaviors are also characteristics of intracrustal isostasy (e.g., Block and Royden, 1990). When lower crustal flow is less intense, extension is accommodated by distributed brittle deformation in the upper crust such as domino style faulting (Fig. 2.4F and 2.5F), which in turn indicates upward warping of a detachment fault by mostly vertical flow of the lower crust (Spencer, 1984). Upper crustal deformation migrating toward the highland seen in our models with a weak mid-crustal shear zones (Figs. 2.4D-F, 2.5D-F, and 2.6A-C) are reminiscent of passive margins like Iberia (Ranero and Perez-Guyssenie, 2010; Reston et al., 1996; Nagel and Buck, 2006). Finally the weak mid-crustal shear zone predominantly records sub-horizontal simple shear as is typically observed in mylonitic shear zones at metamorphic core complexes (MCCs) (e.g., Spencer, 1984). Because these characteristics persist even when the shear zone behave in a brittle manner (Fig. 2.6 and supplementary Figs. A4, A6 and A8) we believe that it behaves in a way akin to a detachment fault (Davis and Lister, 1988).

2.5.3 Implications for the continental margin development

The Atlantic margins developed in Caledonian to Variscan orogenic belts (Reston et al., 1996; Lavier and Manatschal, 2006) show 1) multiple tilted high-angle normal fault blocks and few detachment faults, 2) the thinning of the crust compensated in the mantle, and 3) the convex upward Moho that is even exhumed at the seafloor in some places. These characteristics agree with the coupled extension that occurred in our models with strong lower crust and without a mid-crustal shear zone (Figs. 2.5B-C and 2.6B-C). These conditions might be realized in cooler lower lithosphere of long-lived orogenic belts and annealed mid-crustal shear zone inherited from the previous orogenesis. The modeling results also suggest that the presence of reflectors (S reflector in Iberia, Reston et al., 1996) interpreted as detachment at passive margins is not a preexisting weak mid-crustal shear zone but rather the result of shear and thinning at the brittle ductile transition as suggested by Lavier and Manatschal (2006).

2.6 SUMMARY

A wedge shape of crust at the beginning stage of extension is an often-ignored possibility in numerical models. We studied the influence of mid-crustal shear zone and lower crustal strength on the extension of a wedge-shape crust using two-dimensional numerical models. When there is a weak mid-crustal shear zone, we identify three distinct modes of extension determined by the strength of the lower crust, which are characterized by: 1) significant exhumation of lower crust that leads to the formation of massifs in the weak lower crust models, 2) rolling-hinges with large offset faults in the models with intermediate-strength lower, and finally 3) intensive domino style normal faulting and negligible thinning of the lower crust in the case of the models with strong lower crust. This results shows that different types of core complex may form in a crustal wedge and that the different models for the formation of core complexes (e.g., Buck,

1988; Block and Royden, 1990; Axen, 1988) are not mutually exclusive and are representative of a change in the strength and intensity of lower crustal flow versus upper crustal faulting in the wedge. A frictionally stronger mid-crustal shear zone does not change the overall model behaviors but extension occurred over multiple rolling-hinges. Without the mid-crustal shear zone, transition from localized to distributed deformation style occurs as lower crustal strength increases. The associated changes include decrease in the spacing of extensional centers, decrease in offsets and increase in number of normal faults, and transition of regional to local isostatic compensation. This changes lead to the formation of structure similar to those observed at highly extended non-volcanic continental margins (e.g. Ranero and Pérez-Gussinyé, 2010).

Our numerical models cover a wide range of continental extensions observed around the world, and have promising applications. We propose that the presence of a mid-crustal shear zone at the base of the upper crust focuses shear flow subhorizontally in a way similar to what is inferred for a décollement. Finally we show that the styles of extension in a crustal wedge are dependent on the ratio, *D* of rate of lower crustal flow to the far field rate of extension. As explained above, this ratio depends strongly on lower crustal strength and the potential presence of a weak mid crustal shear zone at the brittle ductile transition. This additional parameter allows us to capture the combined influence of the temperature, viscosity, rate of extension and initial lithospheric structure into one non-dimensional number, *D*. When *D* is large enough, extension in the upper crust is compensated by lateral flow of lower crust, which corresponds to regional isostasy. If *D* is small, local isostasy becomes dominant, in which on-site crustal thinning and mantle upwelling compensate extension in the upper crust.

Phase	ρ (kg m^{-3})	θ (°)	θ' (°)	C (MPa)	A (MPa^{-n} s^{-1})	E_a (J mol^{-1})	n	C_p (J/KgK)	h_r (W/kg)
Upper crust	2700	30	15	40	0.125	2.76×10^5	3.05	1000	10^{-9}
Weak lower crust (2-layer crust)	2800	30	15	40	2.5×10^{-3}	1.63×10^5	1.8	1000	10^{-9}
Intermediate lower crust (2-layer crust)	2800	30	15	40	1.85×10^{-6}	1.63×10^5	2.8	1000	10^{-9}
Strong lower crust (2-layer crust)	2800	30	15	40	1.37×10^{-6}	1.84×10^5	2.8	1000	10^{-9}
Weak lower crust (3-layer crust)	2800	30	15	40	0.125	1.8×10^5	3.05	1000	10^{-9}
Intermediate lower crust (3-layer crust)	2800	30	15	40	0.125	2.4×10^5	3.05	1000	10^{-9}
Strong lower crust (3-layer crust)	2800	30	15	40	0.125	2.76×10^5	3.05	1000	10^{-9}
Mafic lower crust (3-layer crust)	3000	30	15	40	0.125	3.5×10^5	3.05	1000	10^{-9}
Mid-crustal shear zone	2800	5-25	5-25	4	0.125	1.76×10^5	3.05	1000	10^{-9}
Mantle	3300	30	15	40	7.0×10^4	5.2×10^5	3.0	1000	-

- Abbreviation in column headings: ρ (density), θ (initial frictional angle), θ' (frictional angle after weakening), C (cohesion), A (coefficient in the creep law), E_a (activation energy in creep law), n (exponential component in the creep law), C_p (heat capacity), h_r (radioactive heating)

- See caption of Fig. 2.3 for references.

Table 2.1: Summary of model parameters.

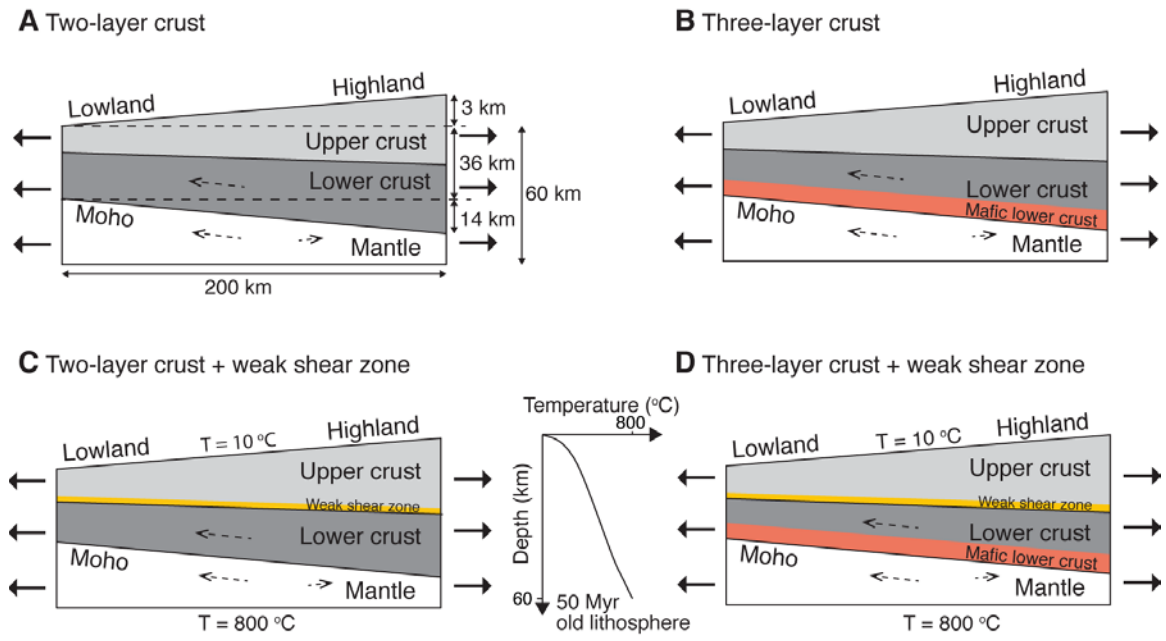

Figure 2.1: Model setups. The modeled domain is 200 km wide with overall extension rate of 1.25 cm yr^{-1} (i.e., 0.625 cm yr^{-1} at both sides) for the numerical models. See supplementary Figs. A1 and A2 in Appendix A for temperature and viscosity of the numerical models at very early stage.

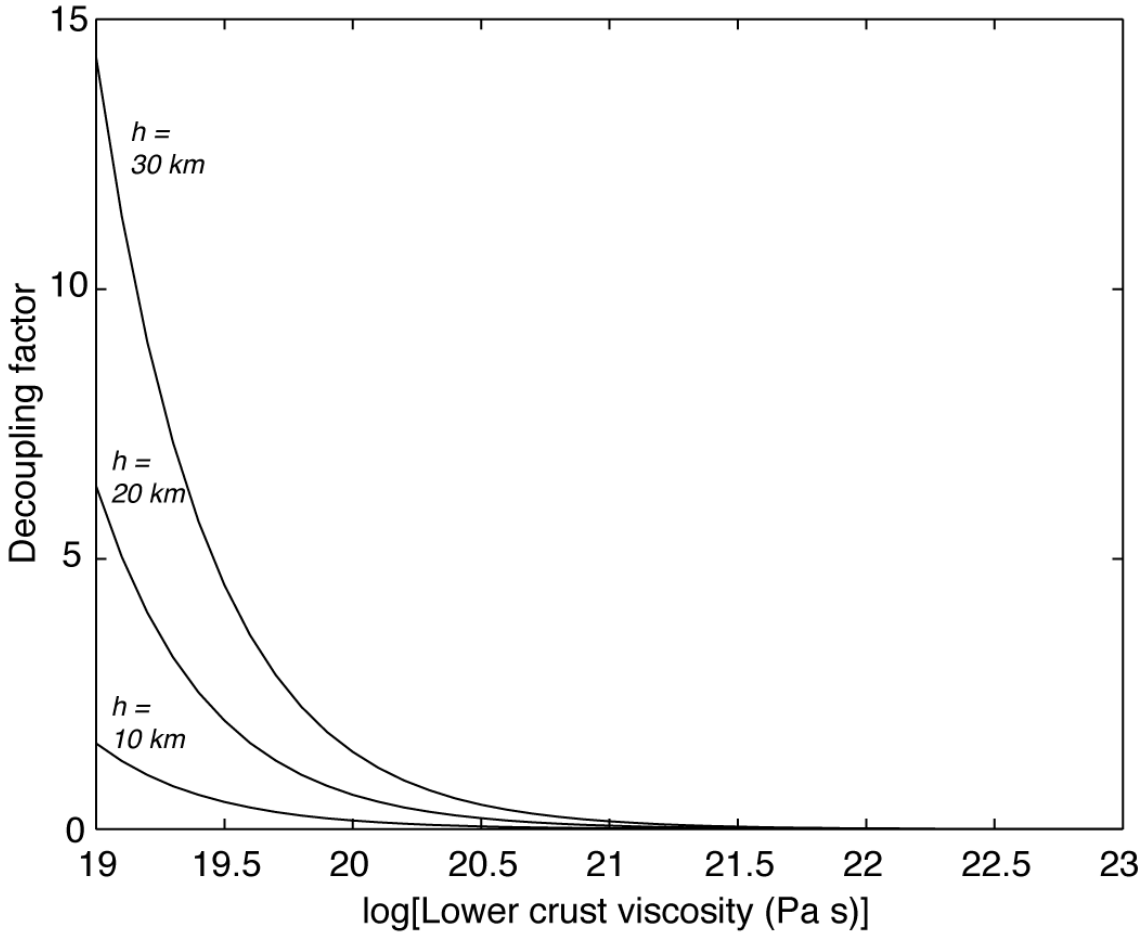

Figure 2.2: Intensity of decoupling induced by topographic loading and mantle buoyancy as a function of viscosity, η_{lc}, and thickness, *h*, of the lower crustal channel.

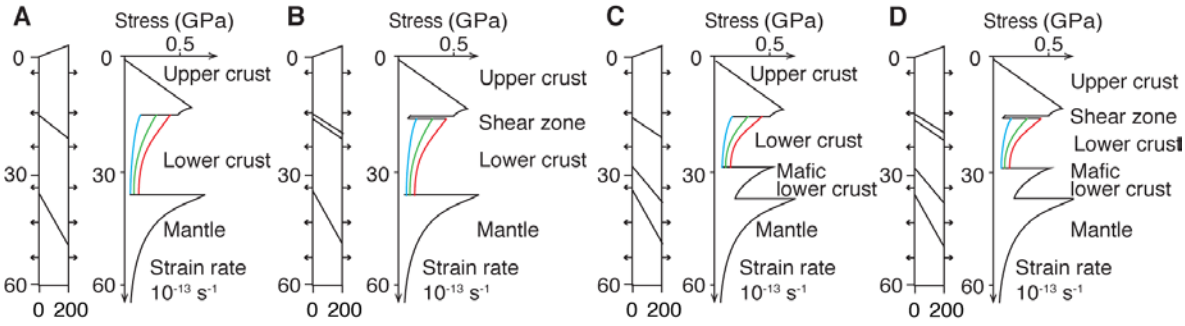

Figure 2.3: Strength envelope for the crust and lithospheric mantle. The model domain is 200 km wide with a 60 km thickness at left side and additional 3 km topography at the right side. A, B: A two-layer crust and plagioclase rheology (Ranalli, 1995) for the upper crust, dry quartz, wet quartz, and wet quartz added with 0.12% water (Jaoul et al., 1984) for strong, intermediate, and weak lower crust (red, green, and blue curve in the strength envelope), respectively, and olivine for the mantle (Kirby and Kronenberg, 1987). C, D: A three-layer crust and plagioclase rheology (Ranalli, 1995) for the upper crust, plagioclase (Ranalli, 1995), weakened plagioclase and strongly weakened plagioclase for strong, intermediate and weak lower crust (red, green, and blue curve in the strength envelope), respectively, strengthened plagioclase (Ranalli, 1995) for the mafic lower crust, and olivine for the mantle (Kirby and Kronenberg, 1987). The shear zone in B and D is ~2 km thick, and is of low viscosity when ductile, and low frictional angle (θ_s, 5°-25°) when brittle. See Table 2.1 for detailed parameters.

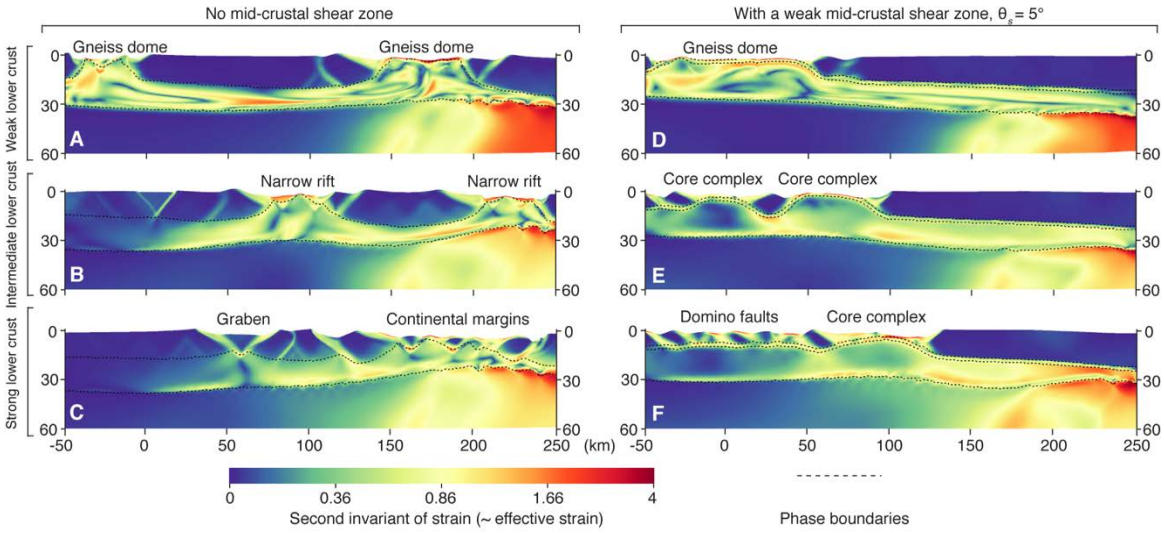

Figure 2.4: Second invariant of strain (i.e. effective strain) of the numerical models with a 2-layer crust, without (A-C) and with (D-F) a mid-crustal weak shear zone. The shear zone friction angle is 5°. All the models are shown at 50% extension corresponding to a stretching factor β = 1.5 after 8 Myrs of evolution. See Appendix A for Movies A1-A3 corresponding to D-F, respectively, and Figs A3 and A4 for corresponding temperature and effective viscosity.

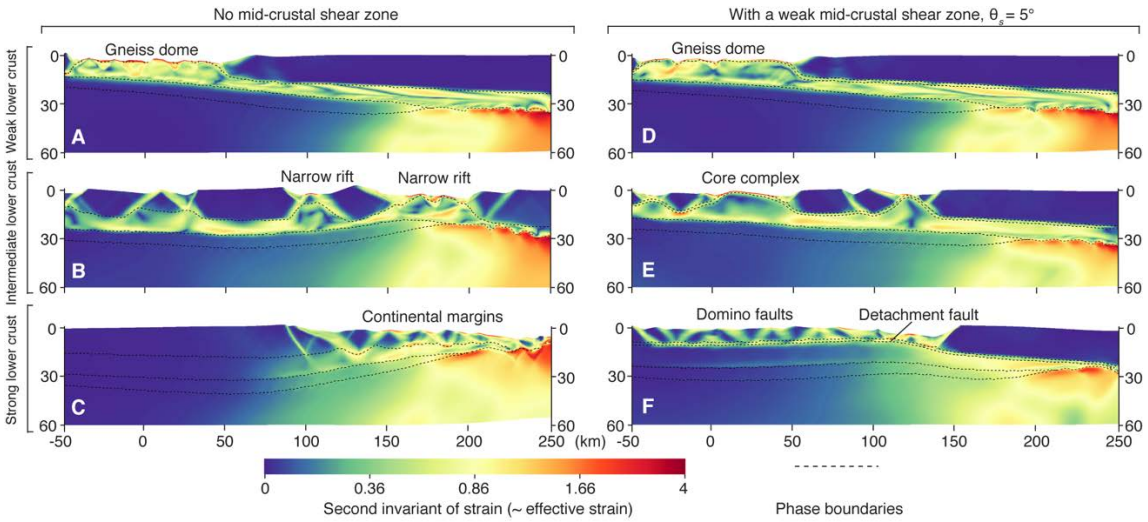

Figure 2.5: Second invariant of strain (i.e., effective strain) of the 3-layer models without (A-C) and with (D-F) a mid-crustal weak shear zone. The shear zone friction angle θ_s is 5°. The deformation style is very similar to that described in Fig. 2.4, with the exception of case A (see text for detailed explanation). All the models are at 50% extension (i.e., stretching factor β = 1.5) with 8 Myrs of extension at 1.25 cm yr^{-1}. See Figs. A5 and A6 in Appendix A for corresponding temperature and effective viscosity.

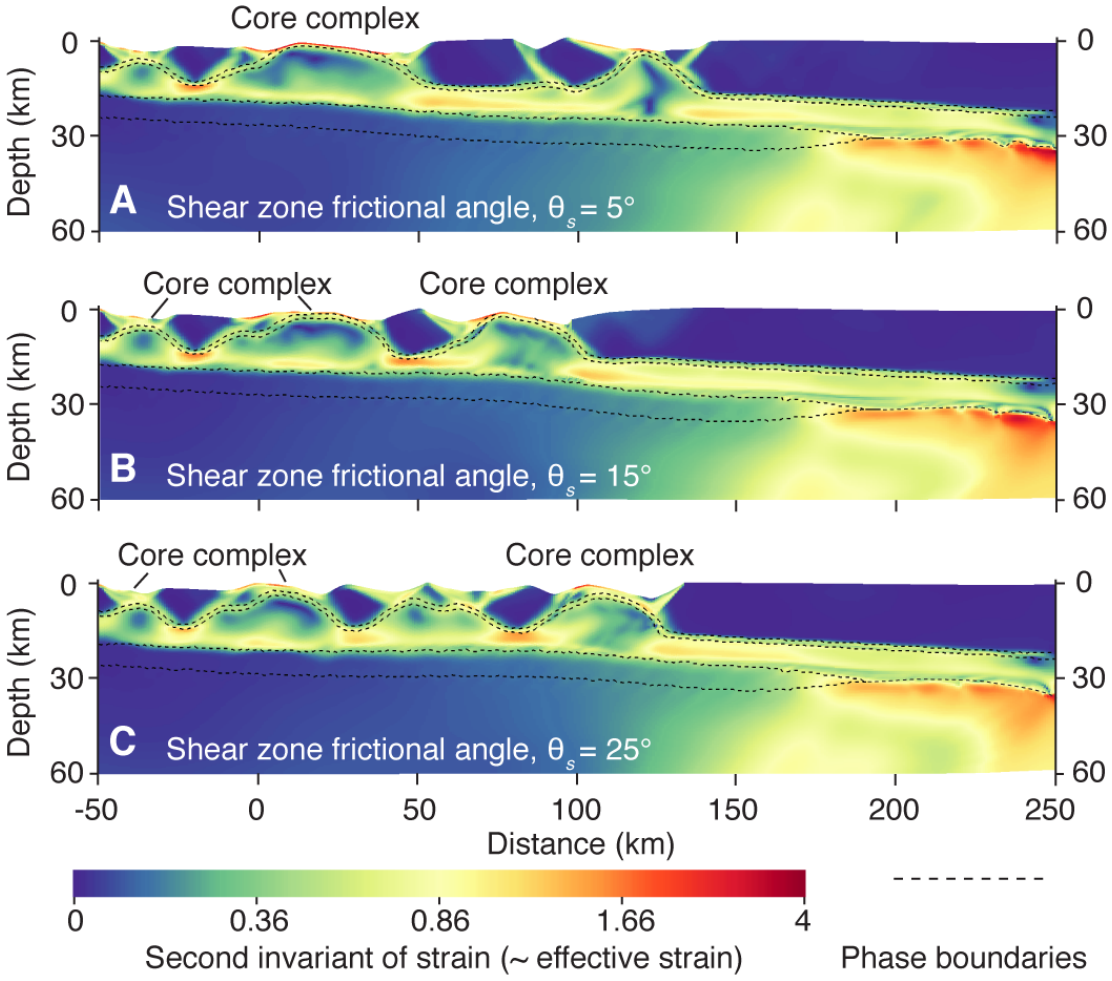

Figure 2.6: Second invariant of strain (i.e., effective strain) from 3-layer models with the intermediate-strength lower crust and the mid-crustal shear zones. The shear zone frictional angle, θ_s, is A. 5°, B. 15°, and C. 25°. All the models are at 50% extension (i.e., stretching factor β = 1.5) with 8 Myrs of extension at 1.25 cm yr^{-1}. See supplementary Figs. A7 and A8 in Appendix A for corresponding temperature and effective viscosity.

Chapter 3: The origin of continental core complexes and detachment faults

[2]

ABSTRACT

Core complexes are observed regionally in the US Cordillera and the Aegean Sea. Despite significant progress, the debate regarding the origin of core complexes and whether detachment faults slip at low angle persists. The clustered distribution of core complexes in orogenic belts leads us to link its origin to post-orogenic extension. We devise thermo-mechanical simulations on a simplified wedge-like orogenic hinterland (or thrust belt) that has initial topography, Moho relief, and a preexisting mid-crustal shear zone that can accommodate shear at very low angles (< 20°). We mainly vary the strength of the lower crust and the frictional strength of the preexisting mid-crustal shear zone. With increasing lower crustal strength, we recognize varying extensional features characterized by bivergent metamorphic massifs, classic Cordilleran metamorphic core complexes, multiple consecutive core complexes (or boudinage structures), and a flexural core complex underlined by a large subsurface low-angle detachment fault with a small convex curvature. We find that the strength of the lower crust, and the existence and strength of a preexisting shear zone significantly affect the formation and evolution of core complexes. Topographic loading and mantle buoyancy forces, together with divergent boundaries, drive a regional lower crustal flow that leads to the exhumation of

---

[2] AUTHORS: Guangliang Wu[a,b,*] and Luc L. Lavier[a,b]

[a] Institute for Geophysics, University of Texas at Austin, 10100 Burnet Rd., Austin, TX 78758, United States

[b] Department of Geological Sciences, University of Texas at Austin, 2225 Speedway, Stop C1160, Austin, TX 78712, United States

[*] Corresponding author: glwu@utexas.edu (G. Wu)

the lower crust where intensive faulting induces strong unloading. The detachment fault is a decoupling zone that accommodates large displacement and accumulates sustained shear strain at very low angle between upper and lower crust. The decoupling can last for more than 10 Myrs for a model with a strong lower crust and an overall divergent boundary velocity at 1.25 cm yr^{-1}. The shear strain in the detachment fault is predominantly simple shear. We find that the preexisting weak shear zone in the crustal wedge induces slip and intense shear at the base of the brittle upper crust, thereby rotating the principal stress away from the vertical axis and inducing a non-Andersonian state of stress that facilitates slip at a low angle on the detachment faults. The modeled thermal history of the exhumed detachments suggests rates ranging from rapid exhumation of less than 1 Myr for some bivergent metamorphic massifs and metamorphic core complexes to relatively slow exhumation rate of more than 10 Myrs for flexural core complexes. Our new models provide a view that is consistent with geological and geophysical observations on how core complexes form and evolve. We discuss the tectonic significance and implications of core complexes in the US Cordillera and the Aegean Sea.

3.1 INTRODUCTION

Continental core complexes have drawn great interest since their first discovery about 40 years ago. They 1) have a distinctive structural style [e.g., *Platt et al.*, 2014], 2) are generally found in orogens such as the US Cordillera and the Aegean [e.g., *Whitney et al.*, 2013], and 3) have important implications for the mechanical properties of crust, stress state, and post-orogenic extension [e.g., *Platt et al.*, 2014]. They typically share three key characteristics (Figure 3.1): 1) a metamorphic core that exposes deep crust from a depth of up to 15-20 km [e.g., *Lister and Davis*, 1989]; 2) a low-angle detachment fault

as a weak layer that contains mylonite, blastomylonite, and microbreccia shattered by closely spaced fractures [*Davis and Coney,* 1979]; and 3) mid-to-high angle hanging wall normal faults lying above the detachment faults [*Davis and Coney,* 1979]. Finally, a nearly flat Moho is typically observed beneath regions where core complexes are found [*Klemperer et al.,* 1986; *McCarthy et al.,* 1991; *Sodoudi et al.,* 2006]. These features provide end-member observations that allow us to explore the ways by which faults slip, strain localizes and partitions. They also shed light on the evolution of the thermal structure and rheology of the crust.

Several models have been proposed to explain the origin of core complexes or detachment faults. Stress rotation induced by basal shear or basal normal forces [e.g., *Yin*, 1989; *Spencer*, 1989; *Melosh*, 1990] has been analytically shown to allow the formation of low-angle normal faults (LANFs), although debate persists on whether the resulting stress field allows slip on a low-angle detachment fault [*Wills and Buc*k, 1997]. The presence of an initial weak zone has been shown not only to rotate the regional stress but also reduce the minimum angle for slip on a fault surface [*Faulkner et al.,* 2006; *Collettini et al.,* 2009]. Finally, crustal flow [*Block and Royden*, 1990; *McKenzie et al.*, 2000] and magmatic activity [*Gans and Bohrson*, 1998] have also been shown to play a significant role in the formation of core complexes. Each of these models contribute to explain aspects of the evolution of core complexes, but none simultaneously explains the three main characteristics described above or the presence of a subhorizontal Moho. For instance, the current most widely accepted rolling-hinge model [*Buck*, 1988; *Lavier et al.*, 1999; *Choi et al.*, 2013] successfully predicts the geometry of core complexes in the oceans, however, it gives little information on the nature of continental detachment faults, the mechanisms controlling lower crustal flow, or the exhumation of a metamorphic core and the presence of normal fault earthquakes slipping at very low angle [e.g., *Wernicke*,

1995]. Moreover, it predicts that the detachment fault is of high-angle origin, a point that contradicts the fact that some detachment faults such as the Whipple Mountains [e.g., *Colletini et al.,* 2011] and Black Mountains [e.g., *Hayman et al.,* 2003] are primary. The flexural model [*Spencer,* 1984] is still largely a schematic model based on geological reconstructions and assumes an initial low-angle detachment with correlated domino normal faults as a prerequisite. Again, it provides little information on the nature of the detachment, ductile flow in the deep crust, or slip mechanisms.

The clustered distribution and striking similarities of continental core complexes in orogenic belts such as US Cordillera and the Aegean Sea motivates us to investigate their origin in the context of post-orogenic extension. The US Cordillera and the Aegean are young Mesozoic/Cenozoic orogenic belts that have undergone intense Cenozoic post-orogenic extension mainly due to slab retreat and collapse [e.g., *Wernicke,* 1992; *Jolivet and Brun,* 2010; *Jolivet et al.,* 2013]. Both the Cordilleran and Aegean Sea can be categorized as Andean-type orogeny [*Dewey and Bird,* 1970], consisting of forelands, hinterlands (and thrust belts), and a plateau. Orogenic hinterlands (and thrust belts) have wedge-shaped geometry with topography and Moho relief. The lithosphere is hot and their formation is typically accompanied by magmatism that is consistent with a weak rheological structure [*Whitney et al.,* 2004]. The geometry, rheology and boundary conditions of orogenic hinterlands (and thrust belts) might significantly affect subsequent extension. It is probable that the extension of an orogenic hinterland due to far-field boundary relaxations naturally leads to formation of core complexes [e.g., *Rey et al.,* 2009].

Here we hypothesize that the presence of a rheologically weak crustal wedge [*Platt et al.,* 2013] including a preexisting crustal-scale décollement [*Faulkner et al.,* 2006; *Collettini et al.,* 2009] provide the necessary elements to consistently predict the

formation of a metamorphic core along a detachment system with mid- to high-angle hanging wall normal faults rooted in the detachment fault. The dip angle of the detachment system can be small, i.e., < 15°, and it varies with depth and across different models. We assume that the décollement is low-angle, weak, foliated, and was formed during the previous phase of Andean-type orogenesis.

To test our hypothesis, we provide a numerical analysis of lower crustal flow driven by topographic loading and mantle buoyancy. We devise numerical simulations of the extension of a crustal wedge that resembles an orogenic hinterland (and thrust belt) in a short-lived orogenic belt [see *Wu et al*., 2015]. We do not assume any orientation of our crustal wedge in an orogen. We simply take a cross section from a region with high topography (termed highland) to a region with low topography (termed lowland) in an orogenic hinterland. Here, we focus on the mechanics of detachment faulting, the associated upper-crustal normal faults and the dynamic evolution of core complexes. We propose a series of numerical models for the evolution of core complexes, compare them with the major core complexes in the US Cordillera and the Aegean, and discuss their characteristics. We use physical and rheological properties that are measured in laboratory experiments or deduced from field observations [e.g., *Collettini et al.*, 2009; *Behr and Platt*, 2011] as well as the traditional Mohr-Coulomb elastoplastic model to simulate the formation and slip of normal faults [*Lavier et al.*, 2000]. We also use classical creep law [e.g., *Burgman and Dresen*, 2009] to simulate the flow of ductile material in the lithosphere.

3.2 METHODS

3.2.1 Analysis of lower crustal flow

Lower crustal flow as channel flow has been analyzed in both compressional and extensional settings [*Block and Royden*, 1990; *Bird*, 1991; *Nagel and Buck*, 2006], however, in the case of a crustal wedge including both topography and Moho relief and two viscous layers, it has not been analyzed in detail. Here, before proceeding with the presentation of our numerical models, we provide an updated solution of lower crustal flow in a crustal wedge [*Wu et al.*, 2015]. This forms a theoretical basis for our model setup and a better framework for the presentation of our model results. We assume that 1) both the regional topography and Moho relief are subhorizontal (< ~ 10°), 2) no slip occurs along the boundaries, 3) the shear zone is initially at a depth of > 15 km, i.e., it is viscous, 4) constant viscosity for both the shear zone and lower crust, 5) a topographic gradient of $\partial h_t/\partial x$ and a Moho relief gradient of $\partial h_m/\partial x$. The flow of the lower crust and shear zone may be idealized as the channel flow of two immiscible incompressible viscous fluids under horizontal pressure between two fixed horizontal rigid plates (Figure 3.2a).

The overall horizontal pressure gradient in the lower crust and shear zone of a crustal wedge induced by topographic loading and mantle buoyancy can be expressed [*Wu et al.*, 2015],

$$\nabla P_x \approx \rho_c g \frac{\partial h_t}{\partial x} + (\rho_m - \rho_c) g \frac{\partial h_m}{\partial x} \quad (3.1)$$

, where ρ_c is the density of crust, and ρ_m of the mantle. Following procedures in *Bird et al.* [2002], the velocity in the shear zone is,

$$v_s = \frac{\nabla P_x}{2\mu_s}\left[h_s^2 + \frac{\mu_s h_{lc}^2 - \ \mu_{lc} h_s^2}{\mu_{lc} h_s + \ \mu_s h_{lc}}(h_s - \ z) - z^2\right], 0 \ \leq z \leq h_s \tag{3.2}$$

and in the lower crust it is,

$$v_{lc} = \frac{\nabla P_x}{2\mu_{lc}}\left[\frac{h_s^2 \mu_{lc}}{\mu_s} + \frac{\mu_s h_{lc}^2 - \ \mu_{lc} h_s^2}{\mu_{lc} h_s + \ \mu_s h_{lc}}(\frac{h_s \mu_{lc}}{\mu_s} - \ z) - z^2\right], -h_{lc} \leq z \leq 0 \tag{3.3}$$

, where h_s and h_{lc} are the thicknesses of the shear zone and the lower crust, respectively, and η_s and η_{lc} are the viscosity of the shear zone and the lower crust, respectively. Without the shear zone, the lower crust forms a channel of single viscous layer, with a velocity of,

$$v_{lc}{}' = \frac{\nabla P_x}{4\mu_{lc}}(h_{lc} - z^2), \ -h_{lc}/2 \ \leq z \leq h_{lc}/2 \tag{3.4}$$

Therefore the average velocity in the lower crust with the shear zone is,

$$\overline{v_{lc}} = \frac{\nabla P_x}{12\mu_{lc}\mu_s}\frac{\mu_s^2 h_{lc}^3 + \ 4\mu_s \mu_{lc} h_s h_{lc}^2 + 3\mu_s \mu_{lc} h_s^2 h_{lc}}{\mu_s h_{lc} + \mu_{lc} h_s} \tag{3.5}$$

, and that without the shear zone,

$$\overline{v_{lc}{}'} = \frac{\nabla P_x h_{lc}^2}{12\mu_{lc}} \tag{3.6}$$

The schematic velocity profile (Figure 3.2a) shows that a weak shear zone significantly enhances the flow of the upper part of the lower crust, and that the strain in the weak shear zone is significant, and predominately simple shear. We assume a value of 2 km for the shear zone thickness and 16 km for the lower crust, and using equations 3.1, 3.5 and 3.6 we plot the average velocity of the lower crust with respect to viscosity (varying from 10^{19} Pa s to 10^{23} Pa s) using a fixed viscosity of 10^{19} Pa s for the shear zone. The results show that the lower crustal velocity is very sensitive to the viscosity of the lower crust, and that the existence of a weak shear zone greatly enhances

the lower crustal flow (Figure 3.2b). For a reasonable tectonic velocity of ~2 cm yr^{-1} it is clear that lower crustal flow is driven by the pressure gradient induced by topographic loading and mantle buoyancy. It can be greater or comparable to the tectonic velocity if the lower crust is weak enough, i.e., generally weaker than 3×10^{20} Pa s (Figure 3.2b). If the velocity of the lower crust is greater than the tectonic velocity, then the lower crustal flow may decouple from the deformation occurring in the upper crust and mafic lower crust (and mantle), and the regional isostasy will control flow and deformation in the crustal wedge [*Wu et al.*, 2015].

3.2.2 Model setup

We use FLAC [*Poliakov et al.*, 1993; *Tan et al.*, 2012] for numerical simulations. The method is described in Wu et al., 2015. In short, we use a crustal wedge (Figure 3.3) to approximate a representative orogenic hinterland and vary the strength of the lower crust across different models [*Wu et al.*, 2015]. We include a preexisting shear zone between the upper and lower crust at the beginning of extension, assuming it was formed during the preceding orogeny. The regional continuous shear zone, which in reality is far more complex, is a model simplification. The detailed model setup is shown in Figure 3.3a, and its strength profile and physical parameters are shown in Figure 3.3b and Table 3.1, respectively.

We set a constant temperature of 10 °C and 800 °C for the surface and bottom, respectively and zero heat-flow boundary conditions on both sides of the model. In the model, we do not consider the dynamic evolution of the brittle and mylonitic shear zone. Instead we imposed a given frictional strength when it is brittle and specific low cut-off viscosity (~10^{19} Pa s) when it is ductile. Processes such as magmatic activity and delamination are not simulated. We test various parameters, such as topographic gradient,

Moho relief, and bottom boundary temperature [*Wu et al*., 2015] before focusing on the frictional strength of shear zone and the viscosity of the lower crust. We find those to be the most important controlling factors. To vary the viscosity of the lower crust, we systematically change the activation energy term in the dislocation creep law for plagioclase [*Ranalli,* 1995] so that it is in the regime of wet quartz with partial melting (very weak), wet quartz (intermediate strength), or plagioclase (strong) (Figure 3.3b). We use Mohr-Coulomb yield criteria for upper crust and most commonly accepted dislocation creep laws for the mafic lower crust and mantle [*Ranalli and Murphy,* 1987; *Kirby and Kronenberg,* 1987]. We varied the frictional strength of the shear zone by changing the internal frictional angle of the Mohr-Coulomb failure envelope in different models. Spreading that would be caused by gravitational rollback is simulated by divergent boundary conditions, gravity-driven relaxation of the topography, and changes in crustal thickness. It is not clear how each contributes to the extension, however, we know that the divergent extension rate typically ranges from 1 - 2 cm yr^{-1} [e.g., *DeMets et al.*, 2010], and that a reasonable regional topographic gradient is typically < 0.03. Setting an extension rate as well as a variation in crustal thickness simulates the contributions of both extensional divergence and crustal buoyancy in the numerical simulation. We used an overall extension rate of 1.25 cm yr^{-1} for all the models presented here.

3.3 RESULTS

In a previous study [*Wu et al.*, 2015], we found that a pre-existing sub-horizontal shear zone (detachment fault) or possibly one developed during extension is critical to the development continental core complexes that are consistent with observations of their three key elements and the subhorizontal Moho. If the detachment structure between the upper and lower crust is absent, structures more characteristic of rifted margins such as

half-grabens and tilted blocks form. Extension in a crustal wedge leads to the formation of continental margins unless the lower crust is very weak [*Wu et al.*, 2015]. We propose here that core complexes are the product of the feedback between extension along the detachment system and fast lateral lower crustal flow during post-orogenic extension in a crustal wedge. We present a suite of models and an analysis of their characteristics in an attempt to substantiate our hypothesis.

3.3.1 Detachment systems

Distinct detachment systems arise in our numerical models. Here, we take the liberty to propose three types of model detachment system, defined as a shear zone across which significant displacement, strain accumulation and partitioning occur (Figure 3.4). Type-I is a convex upward detachment fault that behaves as a brittle shear zone at shallow depth and transitions to a ductile shear zone at greater depth. In Figure 3.4a the brittle domain of the detachments or normal faults is indicated by a continuous red line and the ductile domain by a fading transitional red dashed line. All the detachments initiate in the preexisting shear zone and underlie a hanging wall populated with normal faults rooted in the detachment. Type-I detachment requires a weak to intermediate strength lower crust so that lower crustal flow is intense enough to exhume the detachment to the surface (Figure 3.4a). A shear zone is required but not necessarily weak when it is brittle. For example, the shear zone in Figure 3.4a is relatively strong with a friction coefficient of 0.47 in the brittle domain (< 13 km depth) and transitions to a viscosity of ~10^{19} Pa s in the ductile domain (> 13 km depth).

Type-II is defined as a listric detachment fault constituted of a brittle listric normal fault in the crust which soles out into the preexisting shear zone at depth. The brittle part of the shear zone transitions to a basal ductile shear zone at depth (Figure

3.4b). The listric normal fault is of high-angle origin and is progressively rotated to mid-to-low angle as extension progresses. The listric detachment fault exerts a strong control over the structure of the extended region. Type-II typically forms when the lower crust fails to exhume to the surface. They require intermediate strength lower crust and the brittle strength of the preexisting shear zones may vary.

Type-III is a subsurface one that is mainly a sub-horizontal brittle shear zone which transitions to a ductile shear zone at greater depth (Figure 3.4c,). As shown in Figure 3.4c, a LANF with a dip angle of 20° is also predicted at the range front, changing to 40° at deeper depth.

From type-I to type-III, upper- and lower crustal extension becomes more coupled, and the intensity of the exhumation and lateral flow of the lower crust decreases. This is consistent with our analytic calculations (Equations 3.2 and 3.3). The frictional coefficients (0.09 - 0.46) of the shear zone used in our models are reasonable and consistent with those of common minerals in shear zones [Table 3 in *Collettini*, 2011]. In all of these cases, the models show that the orientation of the principal stresses in the detachment fault is rotated away from the vertical axis (Figure 3.4, σ_1 orientation). The stress is strongly rotated in the regions adjacent to the brittle and ductile detachment and close to the surface where a steep topographic gradient exists (Figure 3.5). The rotation of the principal axis away from the vertical establishes a non-Andersonian state of stress that facilitates slip along the generally low angle detachment faults. Figure 3.5 shows that the non-Andersonian stress persists even in the zone where the detachment fault behaves in a brittle manner following Mohr-Coulomb yield criterion (inset with plastic strain ~ brittle deformation). The non-Andersonian stress extends in the ductile part of the detachment. The σ_1, however, is still largely vertical in the brittle upper crust except in the regions mentioned above (Figure 3.5).

3.3.2 Hanging wall normal faults

The normal faults forming in the hanging wall of the detachment faults have different styles defined by the overall flow in the lower crust and the corresponding type of detachment fault. Overlying type-I detachment faults, the normal faults form a chaotic mosaic, in which synthetic and antithetic normal faults overprint each other (Figure 3.4a). This is partially due to the extreme thinning of the upper crust and to continuous slip along the convex basal detachment. The normal faults develop in a process similar to that predicted by the rolling-hinge model [*Wernicke*, 1992; *Lavier et al.*, 1999; *Choi et al.*, 2013]; however, in our models a given generation of faults may be active simultaneously and alternate its activity with another group of faults. Normal faults may get locked as they rotate to dip angles unfavorable to continuous extension and as the detachment fault becomes sub-horizontal [Choi and Buck, 2012; *Choi et al.*, 2013]. Following locking a new generation of normal faults forms closer to the range front (Figure 3.4).

The normal faults in the hanging wall of type-II detachments are connected to the master listric fault and behave mainly as antithetic faults (Figure 3.4b). The hanging-wall of type III detachments is populated by domino style sets of synthetic normal formal faults (Figure 3.4c). The dip angle of the faults depends on the degree of rotation, but they generally slip at mid-to-high angle (30° - 50°).

The slip rate along the detachment exerts control over the style of hanging wall normal faults. We found that the normal faults in the hanging wall of the detachments dip in the same direction when the slip rate of the detachment fault is high (e.g., Figure 3.5). When the slip rate of the detachment fault is low, conjugate normal faults are formed. In other words, the strain rate in the shear zone must be large enough to cause significant enough basal shear stress to favor domino faults dipping in the same direction. For example, hanging wall normal faults consecutively form and dip in the same direction

when the slip rate of the detachment fault is high during the fast exhumation of the lower crust (Figures 3.4c and 3.5).

3.3.3. Core complex evolution

We present four models that generate different type of core complexes (Figure 3.6) defined as a domal structures including multiple detachment faults with their corresponding hanging wall fault systems (Figures 3.7-3.10). In the following, we distinguish the highland and lowland (Figure 3a) as the areas of high and low topography in the initial structure of the crustal wedge, respectively.

3.3.3.1. Bivergent core complexes or metamorphic massifs

Bivergent core complexes develop with a very weak lower crust, featuring a type-I detachment system and mosaic synthetic and antithetic hanging wall normal faults (Figures 3.6a and 3.7). It has the features of a bivergent set of detachment faults similar to the central Menderes core complex [*Gessner et al.,* 2001]. The detachment fault formed on the highland side of the crustal wedge accumulates extension continuously, while the detachment fault on the lowland side passively adjusts to the overall extension (Figure 3.7). Mid-to-high-angle normal faults may develop in the massif when the lower crust is exhumed and has cooled to a temperature low enough for brittle deformation to occur (Figure 3.7c). Once the upper crust breaks up, the lower crust exhumes and accommodates most of the extension with stable highland and lowland upper-crustal blocks slipping along the detachment faults on both sides of a massif and defining a core complex. The exhumation rate of lower crust is very high. In the model shown in Figure 3.7 the shear zone and lower crust are exhumed from approximately 16 km depth to the surface over 1 Myr of extension.

The presence of a very weak lower crust (wet quartz regime with partial melting) is crucial for the development of the bivergent core complex since it allows for rapid lateral flow and exhumation of the lower crust. In that case the topographic gradient can support a very fast flow in the lower crust driven by the overall topographic gradient (Figure 3.7). The presence of a preexisting sub-horizontal detachment fault significantly facilitates the exhumation of lower crust through continuous extension along the detachment system as predicted by the analytic model (Figure 3.2). Most of the extension in the bivergent core complex is accommodated by the exhumation of the lower crust. The Moho relief varies between 20 km below the lowland and 30 km under the highland and has therefore been significantly reduced after 8 Myrs of evolution (Figure 3.7c).

3.3.3.2. Metamorphic core complexes

This model generates core complexes with characteristics observed in the Basin and Range and the Aegean Sea [e.g., *Coney et al.*, 1980; *Whitney et al.*, 2013] (Figure 3.1a, c, e and f). The core complexes feature type-I detachment faults, sequentially developed synthetic and antithetic normal faults, and an exhumed asymmetric lower crustal dome (Figure 3.6b). On the lowland side of the model, a type-III detachment fault has formed above a 20 km wide dome of lower crust that has failed to exhume to the surface (Figure 3.6b, zone 1 and Figure 3.8). On the highland side, another small lower crustal dome has formed that could potentially develop into another core complex if more extension were to accumulate in the model (Figure 3.8c). As opposed to the bivergent massif, both upper-crustal thinning and lower crustal exhumation play an equivalent role in accommodating extension (Figure 3.6b and 3.8). Furthermore, detachment faults also accommodate significant extension. The size of the core complexes ranges from 50 km to

more than 100 km, and the exhumation rate is intermediate. In Figure 3.8, the shear zone is exhumed from 15-20 km deep to near the surface and in about 2-3 Myr.

The model has an intermediate lower crust (wet quartz regime) and a weak shear zone (with low frictional strength < 0.2). In its early stage, a type-II detachment fault develops which is critical for the later evolution by forming an active feedback between exhumation of lower crust and extension along the detachment system. Once formed, it dominates the extension, however, it might or might not be able to develop into a fully evolved metamorphic core complex.

3.3.3.3 Boudinage structures

This model resembles the metamorphic core complex in that it is characterized by similar detachment fault and hanging wall normal faults form (Figures 3.6b-c, 3.9). The boudinage structures differ from the metamorphic core complexes in their inability to exhume the lower crust to the surface. Core complexes are typically less than 50 km and have typical boudinage structures. The boudins develop a series of lower crustal domes and upper crustal swells that start in the lowland and propagate to the highland as extension continues (Figures 3.6c, 3.9). The boudinage mode is associated with a lower crust (wet quartz regime) and a shear zone of intermediate strength (with intermediate frictional coefficient ~ 0.2 - 0.46).

3.3.3.4. Flexural core complexes

This type of model generates a type-III detachment fault. It also features sequentially developed hanging-wall normal faults which are synthetic, mid-to-high-angle and in domino style that sole into the detachment fault. Underlying the type-III detachment fault is a dome of lower crust with low uplift curvature (Figures 3.6d and 3.10). If the strain rate in the shear zone is high enough to favor strongly non-

Andersonian stress, a series of synthetic domino style normal faults form. Otherwise a system of conjugate synthetic and antithetic hanging wall normal faults form. Both the upper crust and lower crust accommodate extension to equivalent degree. Exhumation of the lower crust is very slow, and it requires ~10s Myrs for flexural core complex to form. In the model shown in Figure 3.10 the shear zone is exhumed from a depth of 18 km to 6 km in approximately 6 Myrs.

Flexural core complexes have a strong lower crust (dry quartz or plagioclase creep regime) and a weak-intermediate preexisting shear zone (frictional coefficient < ~ 0.46). However, a stronger shear zone inhibits the formation of the lower crustal dome with a smaller curvature. The extension in the upper crust through domino style faulting dominates the evolution of the deformation in the upper crust, and the exhumation of lower crust is subdued due to its high viscosity. Even with a detachment fault, a decoupling between the upper and lower crust does not occur, as predicted by the analytic model (Figure 3.2).

3.3.4. Lower crustal flow and intracrustal isostasy

Crustal and mantle flow during the formation of the different core complexes generate two kinds of feedback: 1) between faulting and stretching in the upper crust and lower crustal flow along a detachment fault, 2) between regional crustal thinning and lithospheric mantle necking. The first one controls the stretching style of the crust while the second governs how the mantle isostatically compensates for crustal thinning.

In all the numerical models presented (Figures 3.7-3.10) the lower crust flows from highland to lowland, and necking occurs in areas where faulting in the upper crust is active. When the lower crust is weak and/or the preexisting detachment is weak, the flow decouples the upper crustal deformation from the deformation in the lower lithosphere

along a detachment fault, a result consistent with the theoretical predictions (Figure 3.2 and Wu et al, 2015). Necking of the lithospheric mantle is small as long as the lower crustal flow is not activated. When lower crustal flow occurs from highland to lowland, the mantle flows asymmetrically towards the highland to compensate for the depletion of lower crust. As a result, lower crustal flow largely compensates extension in the upper crust, while mantle upwelling beneath the highland compensates for the regional flow of lower crust towards the lowland. A very long-wavelength isostatic compensation coexists with intracrustal isostasy. The intracrustal compensation wavelength increases as decoupling between upper crustal deformation and lower crustal flow decreases. This occurs as the lower crustal strength and detachment strength increase from bivergent, to metamorphic, to flexural core complexes. The long wavelength regional isostasy leads to the formation of a smooth subhorizontal Moho. The two coexisting wavelengths of local crustal and regional lithospheric isostasy are consistent with theoretical predictions [*Zuber et al.*, 1986]. As a consequence of the flow, the mafic lower crust is sheared away from the highland.

3.3.5. Thermal history

In Figure 3.11 we plot the thermal history of a material particle attached to the detachment fault for the bivergent core complex, metamorphic core complex, boudinage structures and the flexural core complex (black star or dot in Figures 3.7-3.10). The temperature of the detachment faults decreases from 300-400°C to around 20-50°C. This is consistent with samples from natural core complexes [e.g., *Kounov et al.*, 2015]. The exhumation rate is fastest for the bivergent case, cooling 250°C cooling over 1 myr (Figure 3.11i). Metamorphic and boudinage cases also cool rapidly, decreasing 250-300 °C over 1.5 to 2 Myrs (Figure 3.11ii-iv). Flexural uplift cases cool much slower,

decreasing ~125°C over 6 Myrs (Figure 3.11v). The trend is generally consistent with cooling rate of natural core complexes [e.g., Fig. 6 in *Whitney et al.*, 2013], however our models may not be able to capture the magnitude of the temperature history as we are not accounting for magmatic processes (partial melting and fluids migration) or the complex thermal history associated with the orogenic processes preceding the extension. However, the models do clearly show that as the strength of lower crust and of the detachment increases from the bivergent to the flexural core complex, the time window for the formation of core complexes is greatly lengthened, and the cooling history is significantly longer (Figure 3.11).

3.4. DISCUSSIONS

3.4.1. Preexisting shear zone at mid-crustal depth

Mylonitic shear zones are observed in almost every known continental core complex [e.g., *Bartley and Wernicke*, 1984; *Brown and Solar*, 1998], although debate persists regarding their origin. They typically display a complex deformational history, for instance, the microstructures in the mylonite shear zone of the Buckskin-Rawhide detachment fault in west-central Arizona indicate two opposing senses of slip [*Singleton*, 2013], and display several weakening mechanisms, such as fluid-assisted granular flow and grain size reduction [e.g., *Oliot et al.*, 2013; *Smith et al.*, 2011; *Platt and Behr*, 2011]. Though our model may be quite simple, it is supported by the discrepancy between the mechanical responses of the brittle upper crust and ductile lower crust which inevitably generates a zone of strong strain localization, i.e., a mid-crustal shear zone [e.g., *Gueydan et al.*, 2004]. In addition, recent reports show intriguing examples of mid-crustal shear zones characterized by weak anastomosed phyllonitic shear bands rich in phengite and quartz which accommodate significant amount of shortening in the Alps [*Bellanger et*

al., 2014]. A core complex can be modeled without an explicit shear zone when the lower crust is very weak [e.g., Buck et al., 2005; Wu et al., 2015]. Such a case might be suitable for oceanic core complexes but seems not for continental core complexes.

In our models, the shear zone is assumed crustal-scale, mid-crustal, and viscously weak when extension starts, and is formed during previous orogenisis. It is a long-lived decoupling zone between upper and lower crust [e.g., *Gueydan et al.,* 2004]. Preexisting shear zones in the crust also include 1) a preexisting thrust fault [e.g., *Banks and Warburton*, 1991] and 2) a recently formed detachment by semibrittle processes [e.g, *Lavier and Manatschal*, 2006]. A natural shear zone could be one or any combination of these shear zones at different depths and times. Due to their weak nature, such shear zones are able to accumulate large amount of shear strain, generating attenuated structures [e.g., *Brown and Solar*, 1998] and releasing energy through aseismic creep events instead of catastrophic earthquakes. They may potentially be the origin of very LANF earthquakes [e.g., *Wernicke*, 1995], although most normal fault earthquakes slip at a high dip angle [e.g., *Jackson and White*, 1989].

Our theoretical analysis and numerical models reinforce the idea that the shear zone is both geologically and geophysically significant, especially during postorogenic extension. Hence, we believe that a crustal scale shear zone of variable strength always exists at mid-crustal depth, although, it may not be spatially continuous as assumed in our models. In addition, the strong shear strain suggests that a shear zone along the Moho is also highly probable (Figures 3.7-3.10). However, the origin of shear zones in the lithosphere and their tectonic significance need further investigation.

3.4.2. Detachment systems and low-angle slip

The detachment systems described in our models are zones of localized deformation with high strain rate that can accumulate very large amount of strain (10s kilometers of extension). Both upper-crustal brittle and lower crustal ductile deformation occur in these zones of high strain accumulation, although the amount of extension accumulated in a brittle or ductile manner varies as a function of the strength contrast and decoupling between the upper and lower crust (Figure 3.2, Wu et al., 2015).

Our models also show that a brittle detachment can accumulate strain at very low-angle. In an elastoplastic layer yielding according to the Mohr-Coulomb criterion, the slip on a normal fault at dip angle lower than 30° is inhibited even for low coefficients of static friction [*Anderson*, 1951; *Wills and Buc*k, 1998]. Rather than slip on the preexisting LANF, a new high-angle normal fault forms in the layer to accumulate strain [e.g., *Wills and Buc*k, 1998; *Lavier et al*., 2000]. However in the cases presented here two factors are simultaneously at play: 1) the initially weak preexisting shear zone acts as a heterogeneity that can slip at low angle as long as the state of stress in the hanging wall has not reached yield (Figure 3.12), and 2) the shear flow enhanced by the regional topographic gradient (Figure 3.2) at the base of the detachment rotates the principal stresses away from the vertical axis [*Melosh*, 1990], inducing a non-Andersonian state of stress and facilitating normal slip at low-angle.

An analysis of the Mohr-Coulomb circle (Figure 3.12) illustrates how a weak preexisting shear zone allows for the initiation and slip along the detachment faults even at unusually low angles while resisting the formation of a new detachment system in the hanging-wall. The presence of a preexisting weak brittle and ductile shear zone in the crustal wedge acts as a low angle heterogeneity at the base of the upper crust. The detachment and upper crustal yield stress envelope are represented with a Mohr-Coulomb

circle corresponding to a hypothetical state of stress in the crustal wedge (Figure 3.12). The detachment has already yielded (black dot on the circle) while the upper crust has not yet yielded. Therefore, the formation of new faults in the upper crust is delayed by the weak preexisting shear zone as well as the rotation of the stresses to a non-Andersonian state allowing further slip a low-angle.

These effects are modulated by the rotation and exhumation of the lower crust when deformation is decoupled (bivergent and metamorphic core complexes). For low coupling and weak detachment faults, slip along the detachment is initially facilitated by the state of stress and later by the rotation of the detachment to a higher dip angle during lower crustal exhumation. When coupling increases, slip over the detachment fault is more difficult since the coefficient of static friction is larger (boudinage structures). Since the frictional strength of the brittle part of the detachment fault is higher and resists continuous slip, it eventually locks up when the dip of the detachment becomes too low. As a result, multiple zones of active faulting and exhumation form, sequentially generating the pinch and swell structures characteristic of crustal scale boudinage. Finally, when the strength of the upper crust is similar to that of the lower crust, the brittle detachment accommodates shear at low angle before high-angle normal faults form. When high-angle normal fault are rotated to a dip angle unfavorable to slip, the detachment slips again. Detachment faults and hanging wall normal faults work intermittently to accommodate extension. Sometimes slip is accommodated along the detachment a low angle, at other time it is accommodated by a set of hanging-wall normal fault slipping at high angle.

The origin of detachment faults in our models is a sub-horizontal crustal-scale mid-crustal shear zone that is warped and exhumed to variable degrees in the brittle and/or ductile regimes (Figures 3.4, 3.7-3.10). The characteristic LANF at the range front

(75 – 90 km in Figure 3.5b) forms because of the large topographic gradient forcing a high degree of rotation of the maximum principle stress (σ_1) from the vertical direction (non-Andersonian). Primary detachment fault as well as faults which rotate from high to low angles are generated in our numerical models. The models therefore suggest that both high-angle origin and primary detachment faults are probable. The numerical models also suggest that the visible parts of the detachment faults with extremely low-angle dip overprint shear zones that are originally ductile. The results are consistent with geological observations in many core complexes. Finally, it is possible that most of the exhumed shear zones were aseismic and creeping with very small earthquakes. Therefore seismicity on LANFs is rare, and most of recorded seismicity in the extended region indicates mid-to-high angle dip.

3.4.3. Lower crustal flow and intracrustal isostasy

Lower crustal flow effectively transports hot lower crust from the stable highland towards the extended lowland. The flow is driven by the topographic loading and mantle buoyancy, thereby reducing both topography and Moho relief in the highland [*Wu et al.*, 2015]. The decreasing thickness of lower crust from highland to lowland also intensifies the lower crustal flow due to restrictions imposed by mass conservation. As a result, intracrustal isostasy predominates when the lower crust is weak enough. For a specific crustal wedge, the driving forces are determined once the geometry and boundary conditions are set [*Wu et al.*, 2015]. The biggest factor affecting crustal flow is then the viscosity of the ductile lower crust [*Wu et al.*, 2015]. A weak lower crust facilitates flow, while a strong one resists it (Figure 3.2). Strong decoupling and depth-dependent extension is observed with a weak-to-intermediate lower crust (Figures 3.7-3.9). Strong crustal flow enhances intracrustal isostasy, and largely inhibits mantle flow for

compensation. The mantle passively adapts to the overall deformation pattern of the crust, and leads to upwelling below the highland domain of the crustal wedge. The relative strength of crustal flow when compared with extension driven by divergent boundary conditions affects both the style of extension and compensation, as is evident in Figures 3.7-3.10 (see Wu et al., 2015 for details).

3.4.4. Geological and geophysical observations

Each core complex or detachment fault in our models has its natural counterpart, particularly in the US Cordillera and the Aegean Sea (See Figures 3.1, 3.7-3.10 and references therein). The bivergent core complex model resembles geological reconstruction of southwest Rhodope in the Aegean [*Gautier et al.*, 1999] and the Menderes Massif in Turkey [*Hetzel et al.,* 1995] where extensional shearing partly localize in a décollement and the exhumation rate is high. The strong and fast intrusion of middle and lower crust suggest they are weak, which is consistent with our numerical model. Our model, however, further suggests that the two detachment systems take different roles: one is more “active”, and the other passively adapts to the overall extension. The metamorphic core complex model is consistent to the Whipple Mountains [*Davis,* 1980], Harcuvar Mountains [*Rehrig and Reynolds*, 1980], and Snake Range core complex [e.g., *Miller et al.*, 1983; *Bartley and Wernicke,* 1984; *Wernicke,* 1992] in the Basin and Range. The modeled boudinage structures resemble the Death Valley turtlebacks [*Miller and Pavlis,* 2005] in the Basin and Range. Finally, the modeled flexural core complex resembles those reconstructed for the Elba-Adriatic coast [*Collettini et al.*, 2006]. The Crete core complex in the Aegean Sea [*Gautier et al.*, 1999] shares characteristics of bivergent and metamorphic core complexes. Temperature histories and exhumation rates extracted from the models are consistent with most natural

core complexes [e.g., Table 2 in *Ketcham,* 1996; *Gautier and Brun,* 1993; *Kounov et al.*, 2015]. The numerical models could be used to interpret a broad range of core complexes known to date.

The style and migration of extension, the bulk thinning of the crust, and the associated intracrustal compensation predicted by our models could be used to interpret the regional evolution of the Basin and Range [*Dickinson,* 2004]. The earlier stage generates many core complexes when the lower crust is hot and fluids/magma activity is strong with predominantly basaltic volcanism. The later stage, where mid-to-high-angle normal faults predominate, occurrs when the lower crust has cooled and the magmatic activity and fluid migration have been replaced by mostly rhyolitic to bimodal volcanism. The strain partitioning in the crust [e.g., *Wernicke,* 1992] seems to be consistent with our model predictions. Our models are also consistent with the observations of sub-horizontal Moho in the Basin and Range and Western Europe where intensive extensions occurred [*Klemperer et al.,* 1986; *McCarthy et al.,* 1991; *Sodoudi et al.,* 2006].

The detachment faults are by far the most controversial feature in the interpretation of core complexes. Geological or seismological evidence suggests detachment faults dip at angles between 10° - 30° [*Collettini,* 2011]. The models predict they can slip at dip lower than 10° and that primary detachment faults have their probable origin in Cretaceous orogenic belts for the Basin and Range province. The Black Mountains and the Whipple Mountains where hanging wall grabens are made up of and/or filled with tertiary sediments and volcanic rocks [*Hayman et al.,* 2003; *Miller and Pavlis,* 2005; *Davis,* 1980] suggest that these visible detachments have a more recent origin than those exhumed from the lower crust. However, type-I and type-II detachment faults, where large amounts of principal stress rotation occur near the surface, would allow slip at low angle at the contacts between the sediments and exhumed lower crust.

This mechanism has the effect of rejuvenating the detachment surface and is consistent with the observations.

Finally, we use an upper and lower divisions for the crust, but we should point out that the exhumed deep crust in our models are principally exhumed from mid-crustal level, which in some literature is termed middle crust.

3.5. CONCLUDING REMARKS

Our models predict that core complexes are natural products of the decoupling between the extension in the upper crust and the lateral flow and exhumation of lower crust along a detachment. We presented three types of detachment faults and four types of core complexes based on numerical models. A crustal wedge with a very weak lower crust leads to the development of a bivergent core complex (or metamorphic massif). An intermediate strength lower crust (wet quartz regime) leads to the development of classic Cordilleran metamorphic core complexes as interpreted in the Basin and Range and the Aegean Sea. A strong lower crust leads to the formation of a flexural core complex for which little lower crustal exhumation occurs. A weak preexisting shear zone is also critical for the development of metamorphic core complexes. Our models suggest that detachment faults develop in hot young orogens where strong fluids/magma activity and a preexisting weak interface or décollement exist.

Our models provide a consistent view of post-orogenic extension, and produce structural characteristics that bear striking resemblance to core complexes observed in the Basin and Range, the Aegean, and likely elsewhere.

Phase	ρ (kg m^{-3})	θ (°)	θ' (°)	C (MPa)	A (MPa^{-n} s^{-1})	E_a (J mol^{-1})	n	C_p (J $Kg^{-1}K^{-1}$)	h_r (W kg^{-1})
Upper crust	2700	30	15	40	0.125	2.76×10^5	3.05	1000	10^{-9}
Weak lower crust	2800	30	15	40	0.125	1.8×10^5	3.05	1000	10^{-9}
Intermediate lower crust	2800	30	15	40	0.125	2.4×10^5	3.05	1000	10^{-9}
Strong lower crust	2800	30	15	40	0.125	2.76×10^5	3.05	1000	10^{-9}
Mafic lower crust	3000	30	15	40	0.125	3.5×10^5	3.05	1000	10^{-9}
Mid-crustal shear zone	2800	5-25	5-25	4	0.125	1.76×10^5	3.05	1000	10^{-9}
Mantle	3300	30	15	40	7.0×10^4	5.2×10^5	3.0	1000	-

- Abbreviation in column headings: ρ (density), θ (initial frictional angle), θ' (frictional angle after weakening), C (cohesion), A (coefficient in the creep law), E_a (activation energy in creep law), n (exponential component in the creep law), C_p (heat capacity), and h_r (radioactive heating).
- See main text for references.

Table 3.1: Summary of key model parameters.

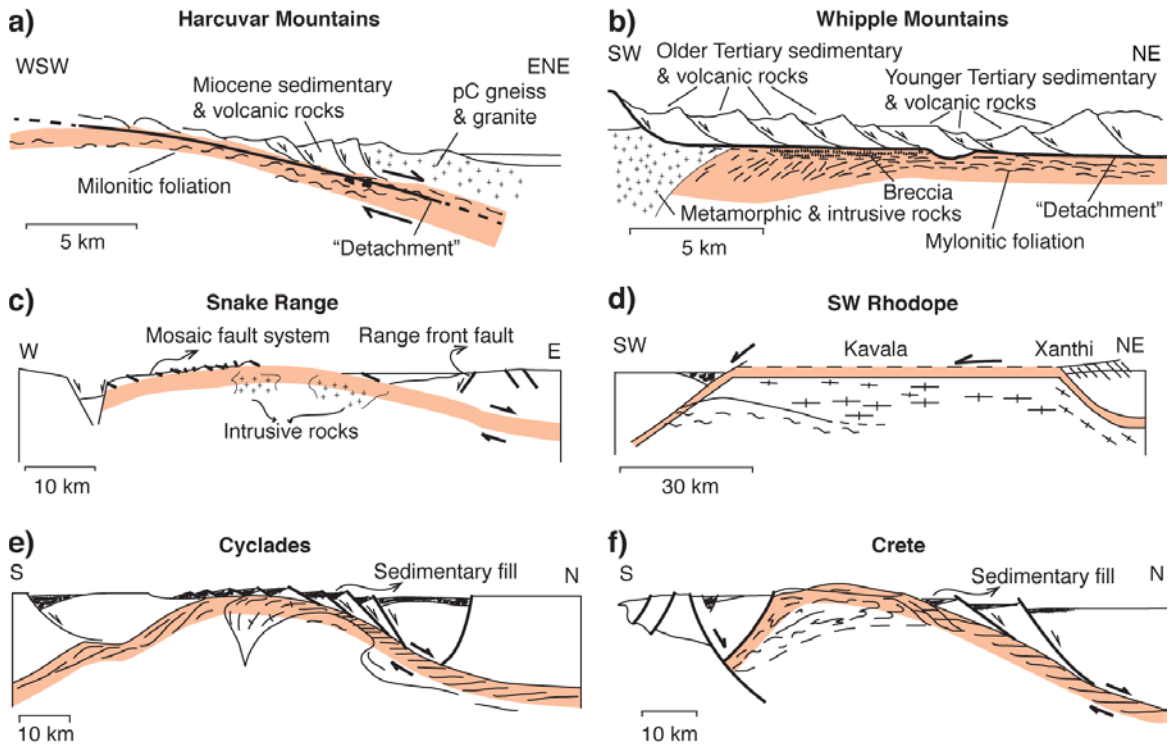

Figure 3.1: Geological and geophysical reconstructions of core complexes in the US Cordillera and the Aegean showing the characteristic detachment faults, overlying upper-crustal normal faults, and underlying exhumed lower crust: (a) Harcuvar Mountains [*Buck*, 1988; after *Rehrig and Reynolds*, 1980]; (b) Whipple Mountains in California, with inferred dome on the left side removed [*Buck*, 1988; after *Davis*, 1980]; (c) the Snake Range [after *Miller et al.*, 1983]; (d) SW Rhodope massif [after *Gautier et al.*, 1999]; (e) the Central Cyclades [after *Gautier et al.*, 1999]; (f) Crete [after *Gautier et al.*, 1999]. In all of these cross sections, the Moho is sub-horizontal.

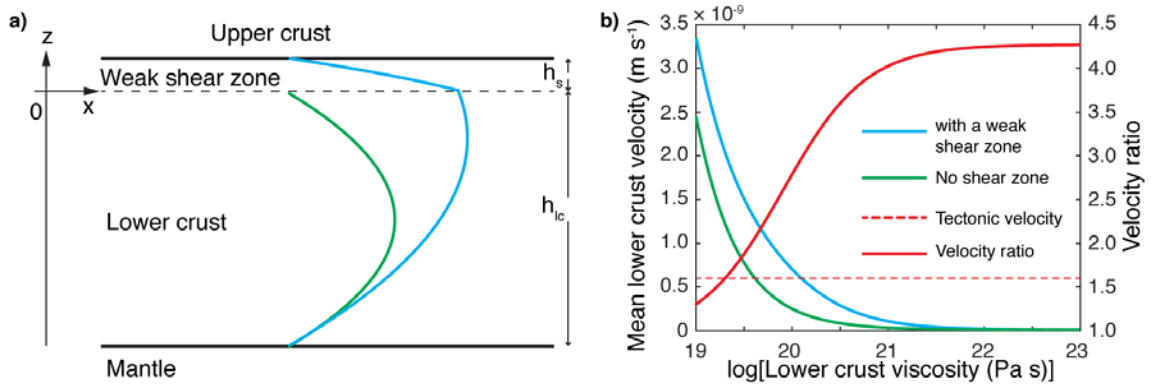

Figure 3.2: (a) Idealized shear zone and lower crust as two immiscible fluids between two rigid plates of upper crust and mantle. The scaled velocity profile (blue) in the weak shear zone (10^{19} Pa s) and lower crust (10^{20} Pa s) is shown with magnitude being greater toward the right side. The profile for the lower crust with the same thickness but without a weak shear zone is shown in green. (b) Mean velocity of lower crust with respect to the viscosity of lower crust with and without a weak shear zone, and ratio of mean velocity with/without a weak shear zone (10^{19} Pa s). The red dashed line indicates a tectonic velocity of 6×10^{-10} m s^{-1} (~2 cm.yr^{-1}). The velocity is calculated with 2 km for h_s, and 16 km for h_{lc}.

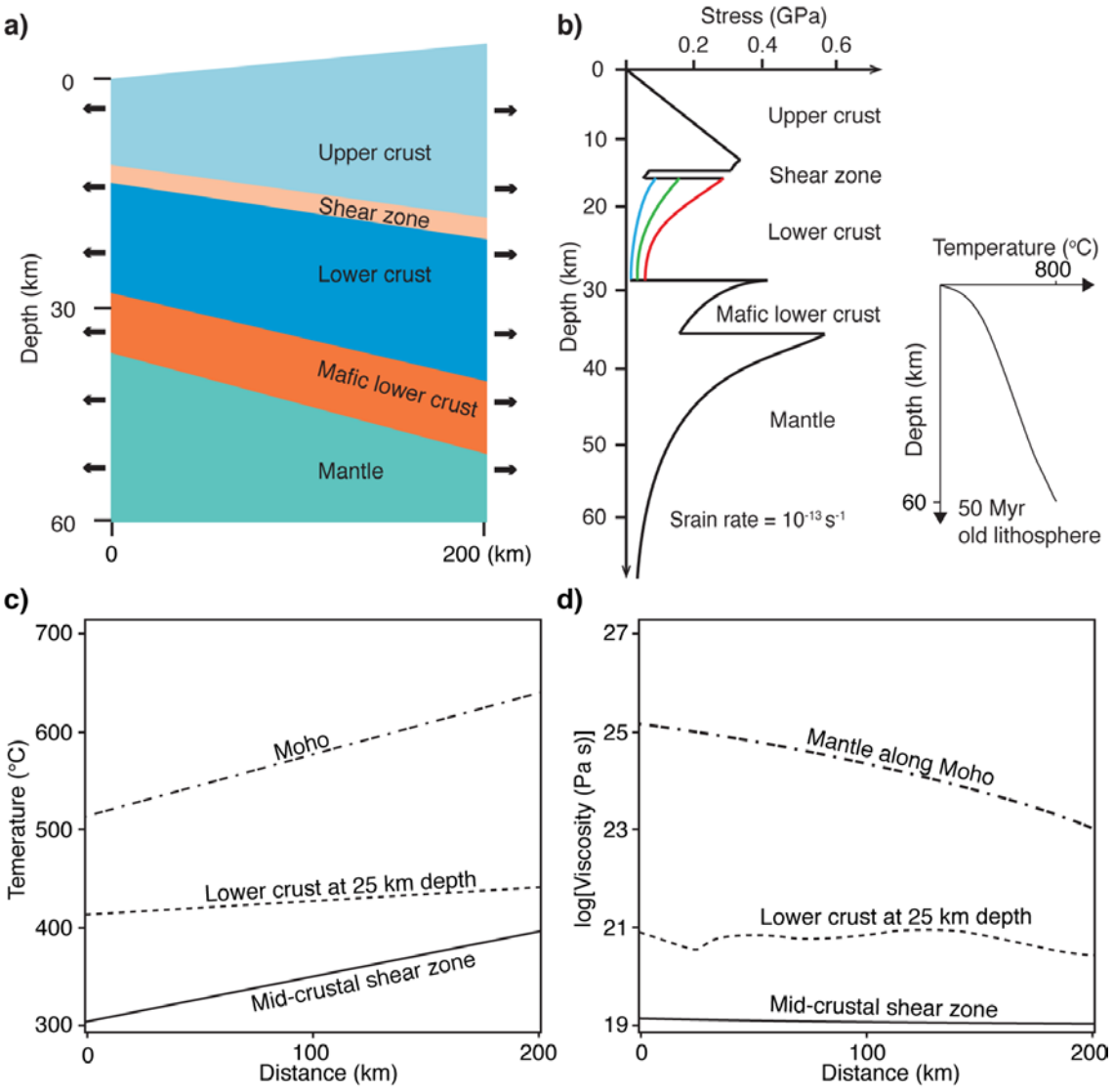

Figure 3.3: (a) Model setup. The shear zone thickness is initially 2 km. The temperature for the top surface is 10 °C, and bottom 800 °C. There is no heat flow boundary conditions on either side of the model. (b) Strength profiles across the left side of the modeled crustal wedge based on the parameters in Table 3.1, with three characteristic strengths of lower crust: (1) wet quartz with partial melting, (2) wet quartz, and (3) plagioclase. (c) Plot of temperature in the mid-crustal shear zone, at 25 km depth in the lower crust, and Moho after 0.1 Myr of model run with intermediate lower crust. (d) Plot of viscosity in the mid-crustal shear zone, at 25 km depth in the lower crust, and in the mantle along the Moho discontinuity for a model with intermediate lower crust.

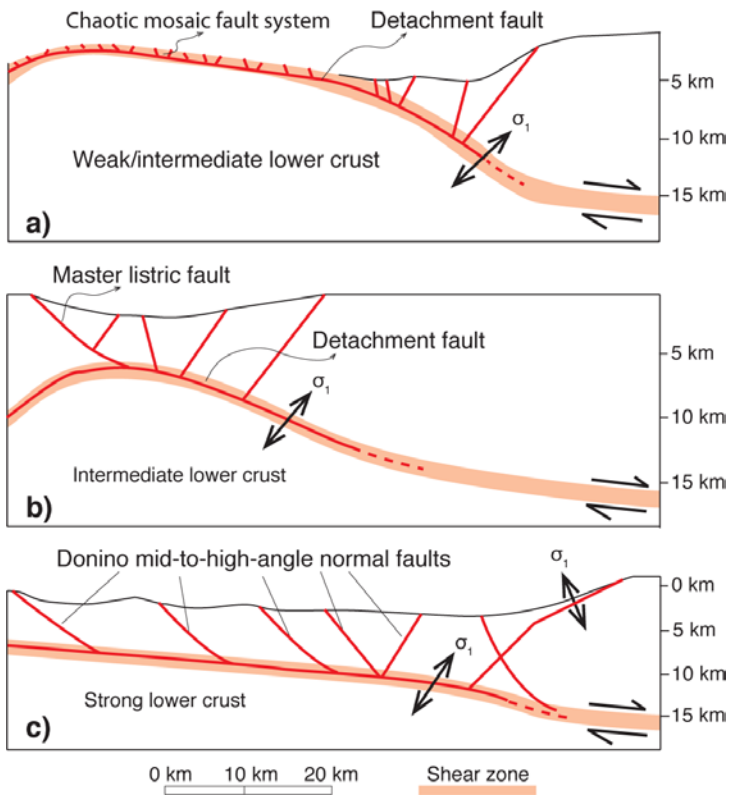

Figure 3.4: Three distinct detachment systems and their associated hanging wall normal faults based on numerical simulations. Principal stress is non-Andersonian in the shear zone and in the regions where topographic gradient is large. (a) A type-I detachment fault consists of a detachment fault residing in the brittle domain or close to the surface that bears ductile inheritance, and a ductile shear zone as a continuation of the brittle shear zone. (b) A type-II detachment fault is a listric normal fault soling into a detachment fault residing in the brittle domain and extending as a ductile shear zone a deeper depth. (c) A type-III detachment fault is a subsurface fault zone, which has a subhorizontal dip in the brittle domain and transitions slowly to a ductile shear zone at depth.

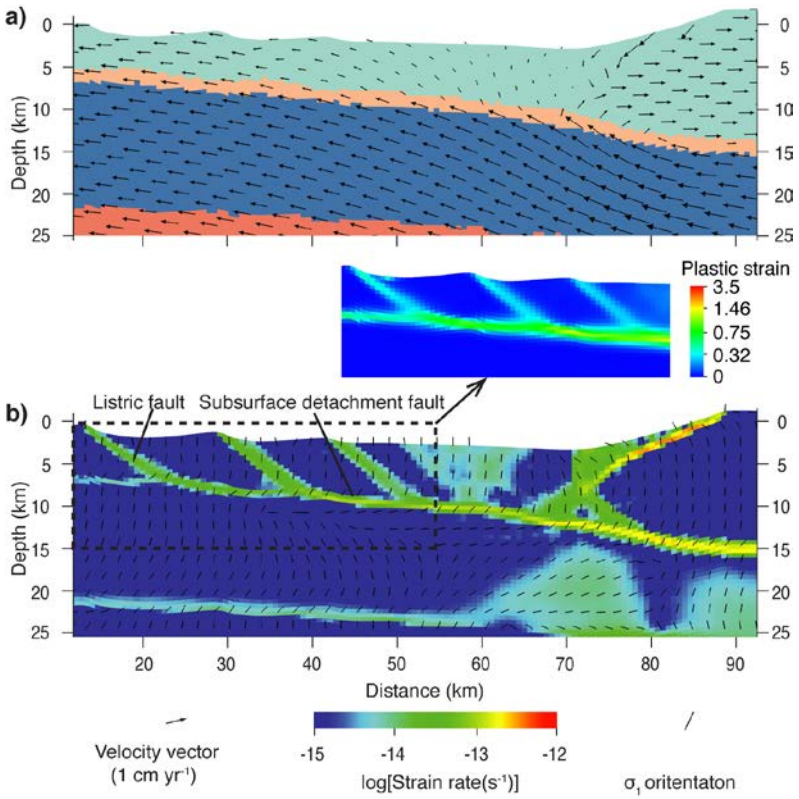

Figure 3.5: Snap shots of velocity vector and principle stress (σ_1) numerical model with relatively strong lower crust and a weak shear zone. (a) Velocity vectors show that the upper crust and lower crust is decoupled. (b) The σ_1 significantly deviates from vertical direction (non-Andersonian state of stress) in the regions adjacent to the shear zone and in regions with high topographic gradient (range front). The plastic strain inset shows the brittle low-angle detachment fault with its associated hanging wall normal faults.

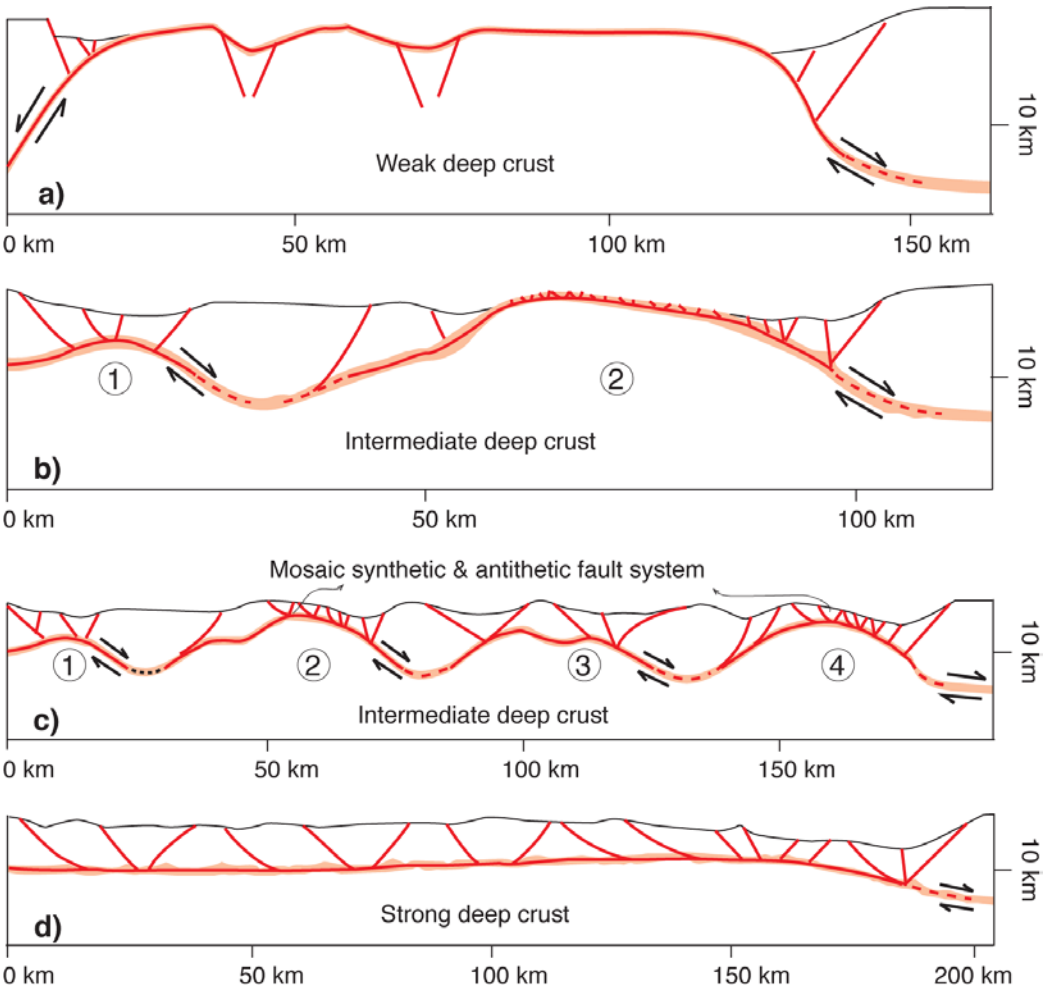

Figure 3.6: Typical core complexes and detachment systems generated by the numerical models. (a) A bivergent core complex with an exhumed metamorphic massif (type-I). (b) A metamorphic core complex or classic Cordilleran core complex (numbered 2) including a type-I detachment system and a classic asymmetric lower crustal dome. Another core complex (numbered 1) has a type-II detachment system and a lower crustal dome not yet exhumed to the surface. (c) Boudinage structures consisting of several consecutive core complexes with typical type-II detachment systems. (d) The type-III detachment system overlying a flexural core complex with lower crustal dome exhibiting a very small curvature.

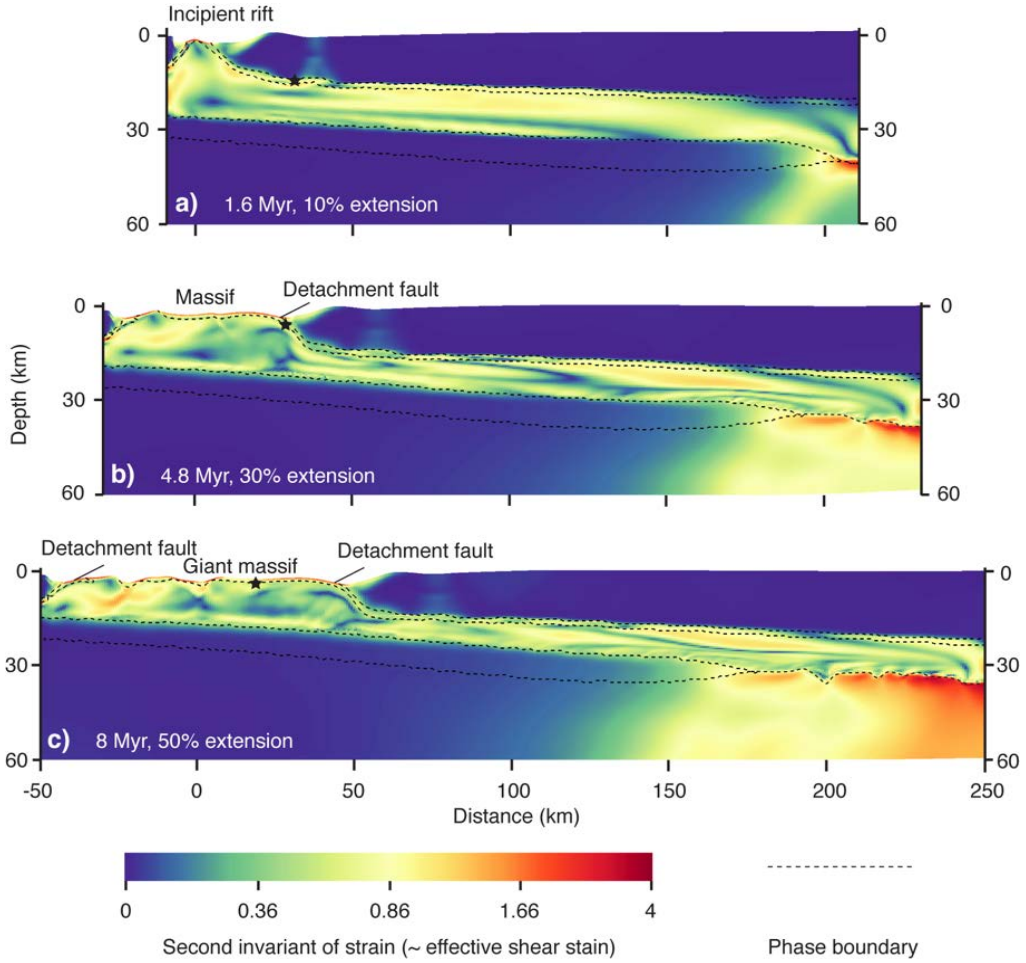

Figure 3.7: Bivergent core complex. The model has a weak lower crust and a weak mid-crustal shear zone (frictional angle, 5°). It develops bivergent detachment faults (Type-I) and a large massif (or batholith).

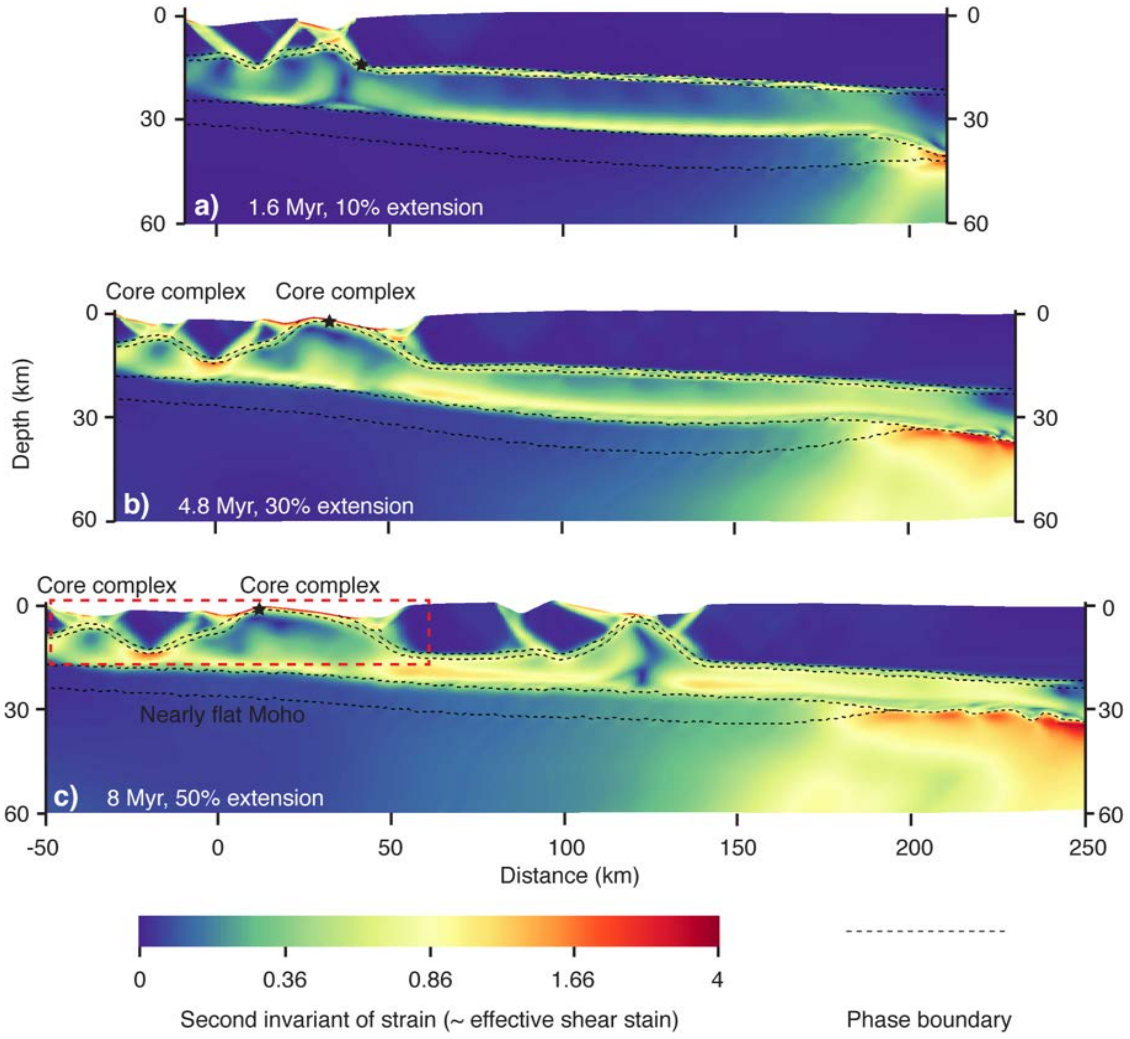

Figure 3.8: Metamorphic core complex. The model has an intermediate strength lower crust (wet quartz regime) and a weak mid-crustal shear zone (frictional angle, 5°). It generates the classic Cordilleran core complex (Red rectangle in c) as well as type-I and type-II detachment faults.

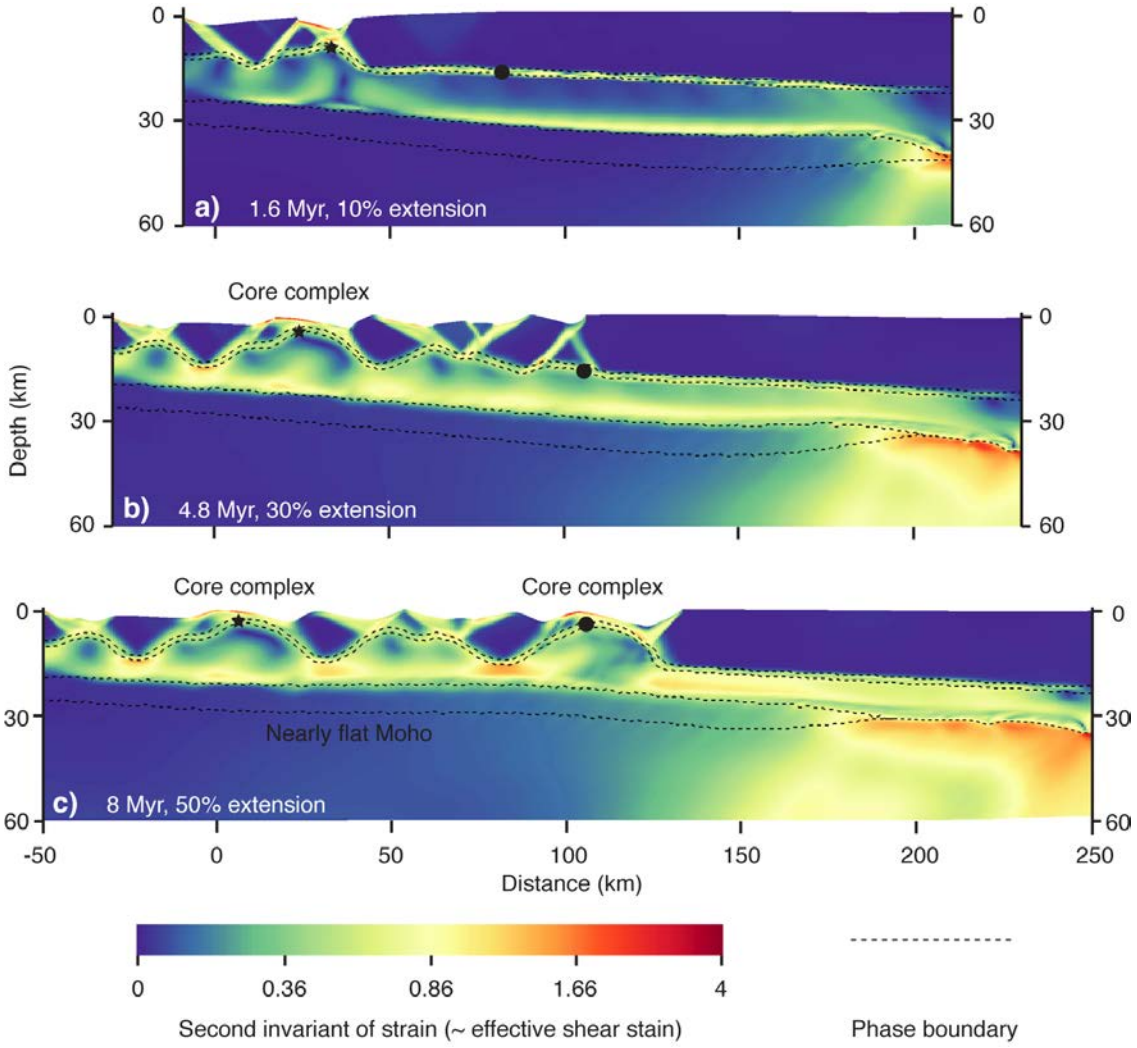

Figure 3.9: Boudinage structures. The model has an intermediate strength lower crust (wet quartz regime) and a strong mid-crustal shear zone (frictional angle, 25°). It develops a series of small core complexes as well as type-I and type-II detachment faults.

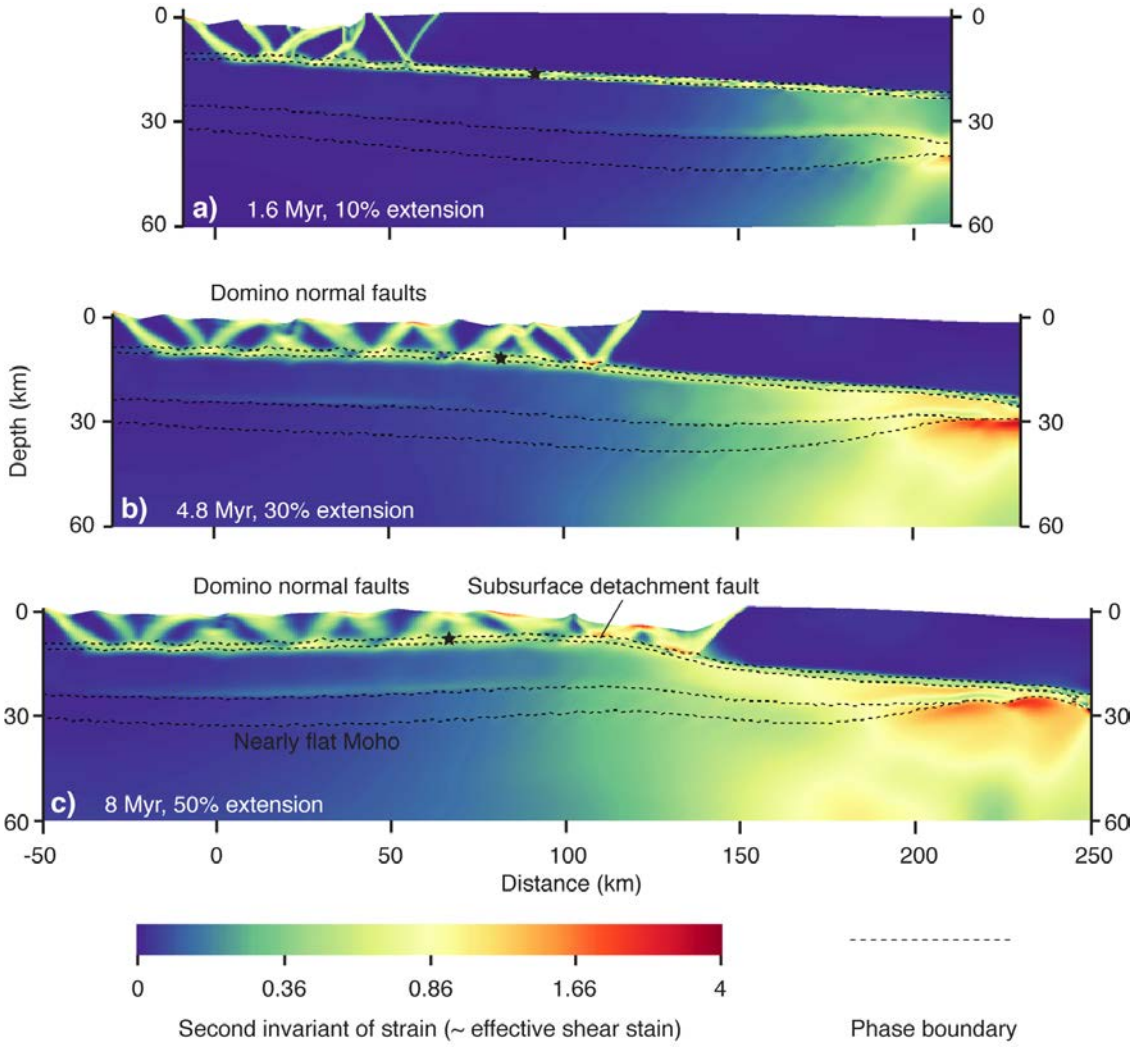

Figure 3.10: Flexural core complex. The model has a strong lower crust (dry quartz regime), and a weak mid-crustal shear zone (frictional angle, 5°). It generates a subsurface detachment fault (Type-III) and a series of domino style hanging wall normal faults.

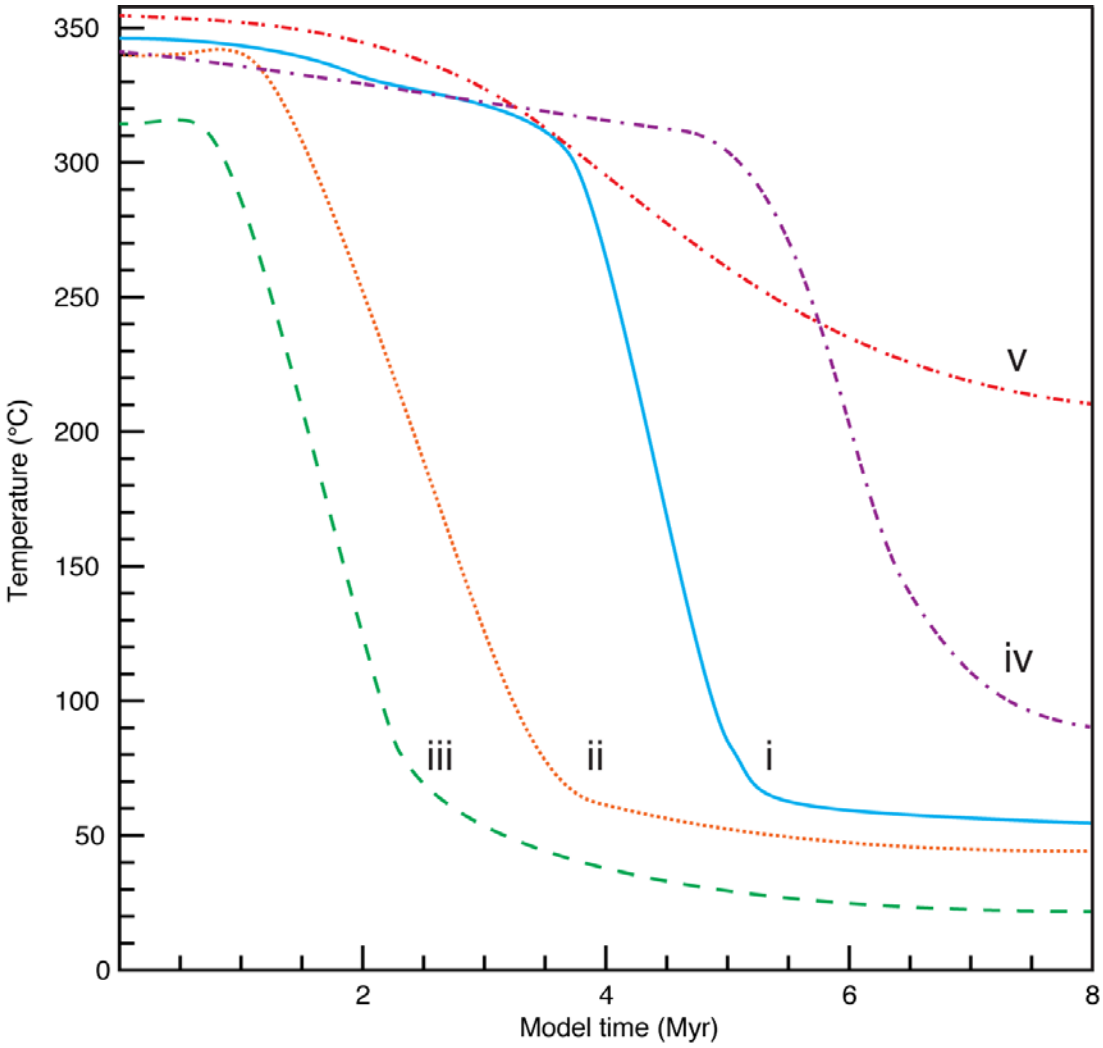

Figure 3.11: Thermal history of sampled particles in the shear zones of modeled core complexes: (i) Metamorphic massif in the model shown in Figure 3.8 (star); (ii) Metamorphic core complex in the model shown Figure 3.9 (star); (iii) Metamorphic core complex in the model shown in Figure 3.9 (star); (iv) Boudinage structure in the model shown in Figure 3.9 (dot); (v) Flexural core complex in the model shown in Figure 3.10 (star).

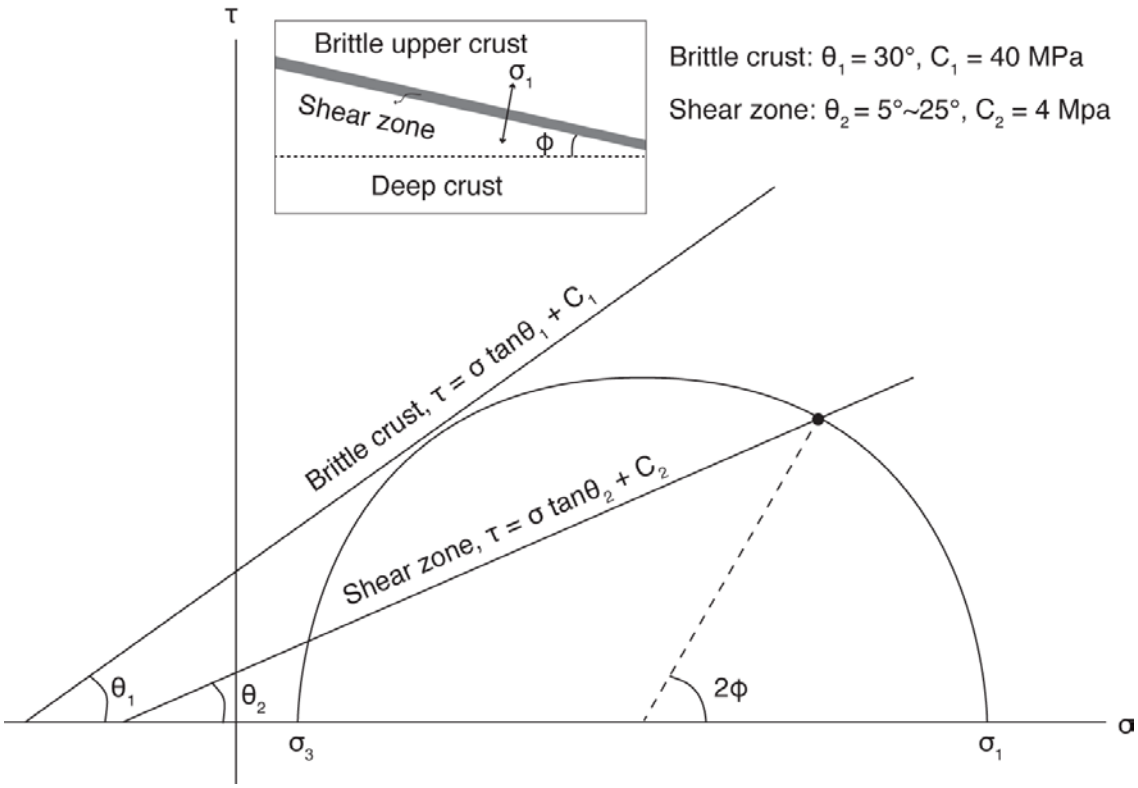

Figure 3.12: Mohr-Coulomb analysis with a preexisting weak subhorizontal shear zone. The yield stress of the shear zone has crossed the Mohr-Coulomb (MC) circle and failed, while the failure envelope in the hanging wall has not yet crossed. The heterogeneity allows the low angle detachment fault residing below the hanging wall to slip as along as the hanging wall has not yielded.

Chapter 4: Two-phase postorogenic extension: A working hypothesis for the South China Sea margins

[3]

Note: Supplementary methods and figures are included in Appendix B.

ABSTRACT

Based on a synthesis of data and numerical models, we develop a two-phase scenario for the extension of an orogenic belt to explain the formation of the margins of the South China Sea (SCS). We use concept first outlined in Wu et al., 2015 for the extension of a crustal wedge to define the characteristics of these 2 phases. During phase 1, deformation in the crust is decoupled from the mantle lithosphere. The resulting structure is asymmetric with a series of large rift basins and ranges mainly in the current South China margin. These structures become younger towards the South. Lower crustal flow driven by topographic loading and mantle buoyancy towards the low lying part (lowland) of the crustal wedge plays a critical role in two ways: 1) it permits rifting to initiate in the lowland, and propagate towards the topographically high area of the crustal wedge (highland), and 2) it reduces both topography and Moho relief in the highland. The process ultimately becomes unsustainable as the crust in the highland is highly attenuated and heated by the upwelling mantle. Phase 2 initiates near the site of the last active rift in the highland. In phase 2, crustal and lithospheric mantle deformation are coupled and symmetric, generating conjugate margins characterized by domino style normal faults

[3] AUTHORS: Guangliang Wu[a,b,*] and Luc L. Lavier[a,b]

[a] Institute for Geophysics, University of Texas at Austin, 10100 Burnet Rd., Austin, TX 78758, United States

[b] Department of Geological Sciences, University of Texas at Austin, 2225 Speedway, Stop C1160, Austin, TX 78712, United States

[*] Corresponding author: glwu@utexas.edu (G. Wu)

dipping seaward, and finally leading to breakup and seafloor spreading. Each phase may include multiple episodes of extension. Thermal cooling and subsidence during a tectonically quiescent period between the two phases probably occurred at the transition between them. The model presented is a highly simplified version of the rather complicated evolution of the SCS margins, but it helps illustrate what we believe are the key processes.

4.1 INTRODUCTION

The mechanisms of post-orogenic continental extension are usually attributed to a combination of the following processes: 1) plate-boundary forces induced by migrating subduction zones (e.g., Malinverno and Ryan, 1986; Holloway, 1982), 2) tectonic escape associated with large continental scale collisions (e.g., Tapponnier et al., 1982), 3) the removal of the lower part of the lithosphere by delamination (e.g., Bird, 1978) or by convection (e.g., Houseman et al., 1981), and to 4) extensional collapse driven by the excess buoyancy in a mountain belt (e.g., Platt and Vissers, 1989). Extension is believed to preferentially initiate in orogenic belts because of their thicker crusts, higher thermal gradients, weak crustal strength, structural heterogeneities and sharp gradients in topography and Moho relief (e.g., Coney et al., 1980; Dewey, 1988; Buck, 1991; Beaumont et al., 2001).

The Basin and Range in the Western US, for example, began extension ~40 Ma, shortly after the end of the Laramide orogeny (Christiansen et al., 1992). Though extension varies in time regionally, 2 phases of extension can be generally distinguished. Phase 1 is dominated by directional lower crustal flow exemplified by formation of core complexes where exhumed lower crusts juxtapose upper-crustal rocks along detachment faults (e.g., Wernicke, 1992). Phase 2 is marked by the formation of upper crustal high-

angle normal faults developing the characteristic Basin and Range style. The exact mechanisms for extension are probably different, but the SCS region seems to undergo a similar process that develops much further and eventually leads to seafloor spreading.

In this paper, we propose a two-phase postorogenic extensional scenario for the evolution of the SCS margins based on a synthesis of data and numerical models. We do not aim to resolve the detailed history of the tectonic evolution but rather focus on the mechanisms controlling the different structural styles observed in the SCS margins.

4.2 TECTONIC SETTING

The SCS lies in the Westernmost Pacific region and is bounded to the North by the South China margin, to the southeast by the southeastern SCS margin and Palawan orogenic belt, to the west by the Ailao Shan-Red River strike-slip fault system, and to the east by the Manila trench and the Taiwan orogenic belt (Fig. 4.1). Before extension, the region was an Andean-type orogenic belt (e.g., Taylor and Hayes, 1983). Extension began in latest Cretaceous, perhaps influenced by a combination of the tectonic escape of the India-Eurasia collision (e.g., Tapponnier et al., 1982; Briais et al., 1993), the subduction in the Western Pacific (e.g., Holloway, 1982; Taylor and Hayes, 1983) and/or a suspected proto-SCS (e.g., Taylor and Hayes, 1983). Intracontinental forces generated by buoyancy are induced by topographic gradients, Moho relief and slab rollback. The SCS underwent multiple episodes of extension since the Late Mesozoic (e.g., Ru and Piggot, 1986), eventually leading to seafloor spreading starting at ~33 Ma (Li et al., 2014).

4.3 TWO-PHASE POSTOROGENIC EXTENSION – A WORKING HYPOTHESIS

Though complex, the rifting in the SCS region seems to display a first order pattern (e.g., Sun et al., 2009). An earlier phase, ~65 Ma - ~33 Ma, is characterized by the

formation of large metamorphic massifs and grabens probably overlying detachment faults (Sun et al., 2009; Cullen et al., 2010) in the distal part of both the Northern and Southeastern SCS margins (e.g., thick dash lines in Fig. 4.1). A later phase, ~33 Ma - ~16 Ma, is dominated by seafloor spreading and domino style normal faults dipping towards the SCS (Fig. 4.2). The fact that the North Palawan block is continental, and was previously contiguous with mainland South China (e.g., Taylor and Hayes, 1983) suggests a two-phase postorogenic extension of an orogenic belt dipping Northwest with the North Palawan block to the Southeast. Even though each phase is probably composed of multiple episodes of extension, we focus on understanding the mechanism of formation of the structural styles during the 2 main phases (e.g., Ru and Piggot, 1986; Cullen et al., 2010).

Phase 1 extension is more focused on the Northern SCS margin than the Southeast margin (Cullen et al., 2010). Beginning in the latest Cretaceous ~65±10 Ma (Taylor and Hayes, 1983), it was asymmetric, and sequentially generated the Beibu Gulf Basin, the Northern Pearl Mouth River Basin (PMRB), the Qiongdongnan Basin starting at ~65 Ma, ~59 Ma, and ~44 Ma, respectively (e.g., Sun et al., 2009). These basins are characterized by half-grabens or strongly asymmetric grabens, most are bounded by southward-dipping master faults. The basins are characterized by boudinage structures where domes of mid-crust are bounded by very large asymmetric grabens/basins formed by normal faulting and detachment faults (e.g., Hu et al., 2009; Sun et al., 2009 and references therein). The observations seem to be consistent with models of continental extension in a crustal wedge characterized by a weak lower crust and strong detachment faults (Wu et al., 2015). Intense regional lower crust flow and a shear zone that is weak when viscous but strong when brittle are necessary to develop such a structural style (Wu et al., 2015). Such an extensional style is not sustainable as it attenuates the crust, reduces

topography and Moho relief and eventually reduces the force driving the regional lower crustal flow (Wu et al., 2015). It may transition to more symmetric extension when 1) the topographic loading and mantle buoyancy become insufficient to drive a regional crustal flow from the highland to the lowland and 2) lithospheric necking in the highland localize extension. A potential period of tectonic quiescence in the SCS (e.g., Ru and Piggot, 1986) may further drive extension towards a more symmetric style of deformation as thermal cooling and subsidence occurs during the quiescence. It inhibits regional flow by increasing the viscosity of the lower crust and decreasing the topographic gradient, respectively.

Phase 2 probably began not long before seafloor spreading. When phase 2 started, the crust was already significantly attenuated. Subsurface detachment faults developed from shear zones formed in proceeding Andean-type orogenesis may have been present beneath the regionally seaward-dipping normal faults (Fig. 4.2 and references therein). Phase-2 structures are best observed close to ocean basins, such as in the southern part of PMRB (e.g., Sun et al., 2009) and towards the tip of NE subbasin (e.g., Lester et al., 2014) and the tip of SW subbasin (e.g., Franke et al., 2014) where opening occurs later in time (e.g., Pautot et al., 1986; Li et al., 2014). Phase 2 extension is more localized and symmetric (e.g., Franke et al., 2014). It occurs in the part of the orogeny that was most likely the highland of the crustal wedge and where upwelling of the mantle was the most intense (Wu et al., 2015).

As phase 1 evolves, the rift basins formed earlier in the lowland cool down and become stronger than the undeformed Southeastern region in the highland. This area was originally the weakest, stayed the most consistently weak, and was most likely the last one to deform. This may explain why phase 2 and seafloor spreading are mainly localized in the regions that were originally the thickest part of the orogeny. The transition between

the 2 phases is likely continuous, and may vary across regions. However, phase 1 is found in the proximal margin (thick dash lines in Fig. 4.1), while phase 2 occurred in the distal margin (Fig. 4.2). The presence of the same two phases of extension in the SE margin is difficult to infer as the margin has been subducted beneath Borneo (e.g., Taylor and Hayes, 1983).

4.4 NUMERICAL MODELS

To test whether we can reproduce distinct phases of extension with distinct structural styles in a crustal wedge, we designed a series of numerical experiments (see Appendix B for methods). Our aim is not to reproduce the complete evolution of the SCS but to test whether the geometry and properties of crustal wedges akin to orogenic hinterland can appropriately predict some of the features observed in the SCS margins.

Phase 1 is modeled as an Andean-type orogenic belt approximated by a single crustal wedge with a preexisting décollement acting as an initially weak mid-crustal shear zone (Fig. B1, Table B1). Phase 1 is essentially crustal extension decoupled from extension in the lithospheric mantle. Depending on the strength of the lower crust and frictional strength of the mid-crustal shear zone, the extensional style resembles those described in Wu et al. (2015). Fig. 4.3A shows a model with intermediate strength lower crust in the wet quartz regime after 10 Myr of extension at 1.25 cm yr^{-1}. The evolution and structure of the asymmetric massifs and large grabens that form sequentially from the NW to the SE is consistent with observations in the northern SCS margin (e.g., thick dash lines in Fig. 4.1). Lower crustal flow plays an important role in attenuating the crust and propagating extension towards the SE. After ~9 Myr, the crust is already severely attenuated, the 600 °C isotherm has a convex shape (See Fig. B2 in Appendix B), and the whole region probably reached a regional isostatic equilibrium. Crustal attenuation and

mantle upwelling began to localize extension in the SE at the forefront of the propagating extension.

Phase 2 is modeled identically, but without the mid-crustal shear zone (Fig. B1 and Table B1). We assume that the mid-crustal shear zone is either very strong or completely annealed after a long period of inactivity, or that it was never present in the thickest part of the orogeny. Fig. 4.3B shows a model with a strong lower crust in the dry quartz regime at 10 Myr with 1.25 cm yr^{-1} extension. The extension begins in the highland and localization occurs early and proceeds quickly (See Fig. B3 in appendix B). It is characterized by seaward-dipping normal faults, extreme thinning of the lower crust, a missing mafic lower crust in the intensively extended region, and strong mantle upwelling that may even lead to mantle exhumation. A shear zone, preexisting or formed during extension through fluids assisted weakening or grain-size reduction, may lead to the formation of domino faults sitting above detachment faults through a mechanism similar as the model shown in Fig. 5F of Wu et al. (2015). We believe however, that the extension in the far SE side may differ from what is shown in Fig. 4.3B, as a larger highland or plateau on its SE side may affect the extension.

4.5 DISCUSSION

The SCS margins can be approximated by juxtaposing an extended back-arc regions made up of phase 1 model on the left and phase 2 on the right with extended forearc regions represented by North Palawan and Reed (Taylor and Hayes, 1983). We therefore propose a two-phase postorogenic extension for the formation of SCS margins (Fig. 4.4). Phase 1 starts in the lowland of a large back-arc orogenic belt with topography dipping towards North. Phase 1 extension migrates south and simultaneously attenuates the crust of the highland through mantle upwelling in the area and lower crustal flow

towards the lowland. The strong mantle upwelling in the highland weakens the lithosphere. As the lowland cools, topographic gradient and Moho relief are reduced. Phase 1 eventually becomes unsustainable, and phase 2 begins in the highland. The geographical boundary between phase 1 and 2 is difficult to pinpoint, but it is expected that phase 2 is more pronounced towards the distal margin.

The extensional style of phase 1 and phase 2 differs significantly and there seems to be a switch in mechanism between the two phases. In phase 1, lower crustal flow plays an important role in attenuating the crust and promoting the migration of extension. Our model of phase 1 is consistent with Clift et al (2001) who found that the lower crust flow is important in Beibu Gulf basin. We suggest that phase 1 represents a characteristic early-phase postorogenic extension. This early phase tends to be localized in the orogenic lowland where thin-skinned orogeny and strong accretion during previous orogenesis has generated a weak décollement and many thrust faults. Intracrustal forces imposed by topographic loading and mantle buoyancy may overcome far-field-driven forces induced by tectonic escape or subduction. In phase 2, mantle upwelling dominates, and eventually leads to seafloor spreading. Phase 2 appears to be akin to back-arc extension, given that 1) it is closely related to the Borneo-Palawan subduction system in term of the timing of seafloor spreading (e.g., Holloway, 1982; Hall, 1997), 2) it involves a significant degree of extension that cannot be solely accounted for by the tectonic escape model (e.g., Cullen et al., 2010), and 3) the extensional style fits well with back-arc extension (e.g., Shuto et al., 2006).

The evolution of the SCS subbasins seems to be diachronous (e.g., Li et al., 2014). For instance, the extension of the SW subbasins is found to propagate sequentially through time from NE to SW (e.g., Li et al., 2014). We suggest that our models may also be used to infer the extensional style in each subbasins. However, the style strongly

depends on whether it occurs before or after the attenuation of the lower crust. The transition between decoupled and coupled deformation (Wu et al., 2015) would correspond to a switch in extensional mechanisms and a transition between phase 1 and 2 extension. The SCS margins have been previously described as Atlantic-type margins (Taylor and Hayes, 1983). Here, we suggest that both phases are akin to what is observed in the Basin and Range province. The SCS was able to transition to a phase of coupled deformation between the crust and the lithospheric mantle, while the Basin and Range is still transitioning to coupled extension.

4.6 CONCLUSION

Based on a synthesis of data and numerical models, we propose a two-phase postorogenic extension model that approximates the SCS margins which could be tested further. Both phases are localized in the loosely defined back-arc region of an orogeny that has an extended ancient forearc comprised of the North Palawan and Reed Bank. Phase 1 is localized in the lowland of the ancient backarc and characterized by lower crustal flow and exhumation that migrates southwards. The directional crustal flow from highland to lowland of the previous orogeny and the strong mantle upwelling in the highland attenuate the highland crust, giving way to phase 2 extension. Phase 2 occurs in the highland, and is characterized by fast mantle upwelling and seaward-dipping normal faults. We further suggest that a transition between decoupled to coupled lithospheric deformation in an orogenic system controls a switch in deformation style and a change from distributed to localized extension.

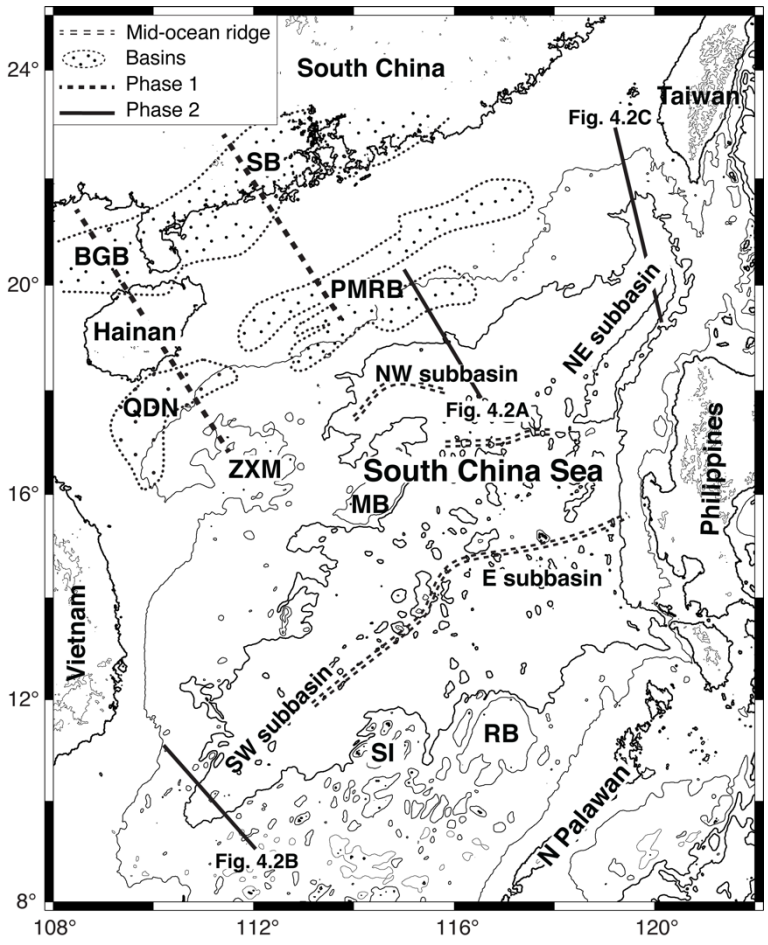

Figure 4.1: The SCS and margins. Major basins (Sun et al., 2009) and relic seafloor spreading centers (double dashed lines, Briais et al., 1993) are delineated. BGB - Beibu Gulf Basin, MB - Maccelesfield Bank, PMRB - Pearl Mouth River Basins, QDN - Qiongdongnan Basin, RB-Reed Bank, SI - Spratly Islands (Nansha), SB - Sanshui Basin, ZXM - Zhongsha-Xisha Massif.

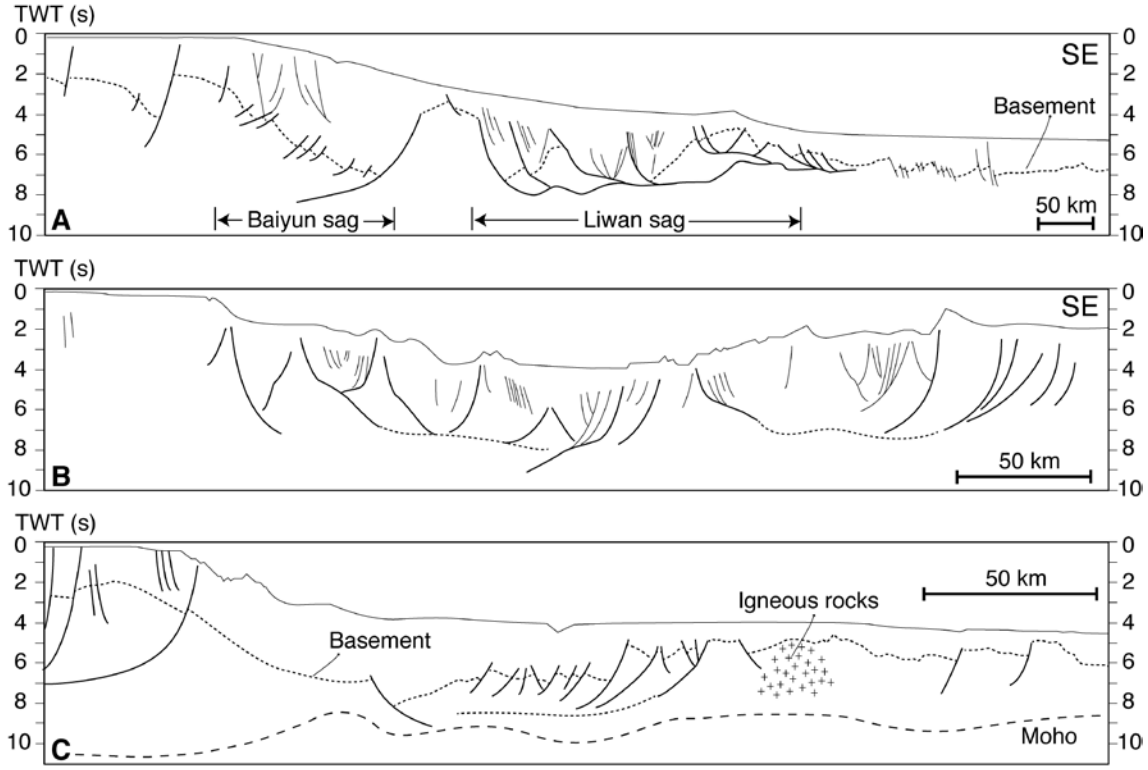

Figure 4.2: Interpreted profiles across SCS margins (location in Fig. 4.1). A: Southern PMRB (after Hu et al., 2009; Sun et al., 2009). B: Nam Con Son Basin in the SW subbasin (after Franke et al., 2014). C: NW margin of NE subbasin (after Lester et al., 2014). The characteristic structure of domino style normal faults soling into a detachment fault is observed in these interpreted profiles.

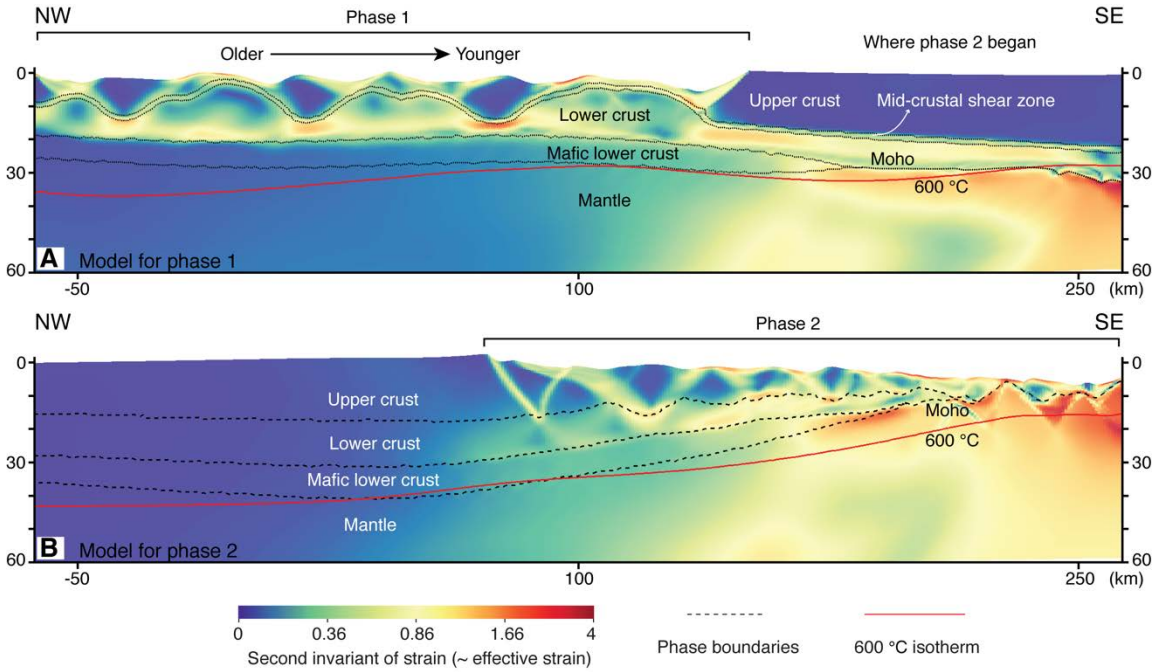

Figure 4.3: Numerical models for phase 1 and 2. A: Model for phase 1 at 10 Myr. The extension initiates in the lowland, and migrates from NW to SE as extension evolves and generates several grabens, half grabens and massifs. It finally begins to localize at the site of last active rifting after ~ 9 Myrs. B: Model for phase 2 at 10 Myr. The extension is highly localized in the highland, and leads to a hyperextended region where the lower crust is extremely thin, the mafic lower crust is missing and the mantle is even exhumed to the surface. On both sides, detachment faults, if developed, helps to facilitate exhumation. See also Fig. B2 and B3 in Appendix B for full evolution.

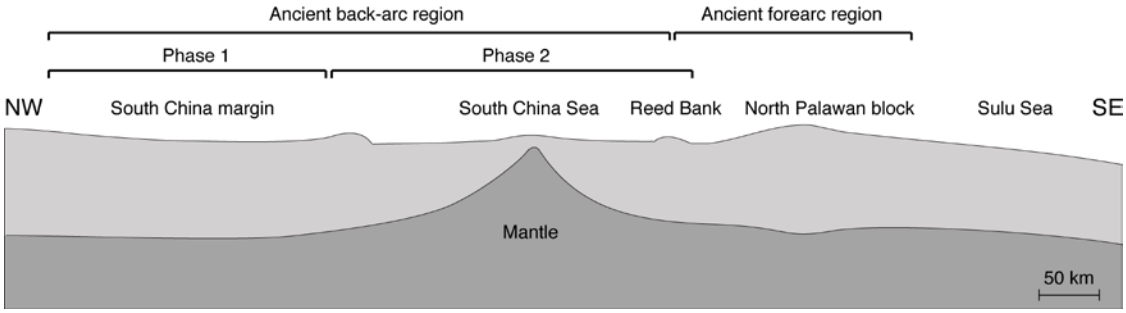

Figure 4.4: Simple illustration of the evolution of the SCS margins. The current SCS margins represent the extended loosely defined ancient back-arc region, with phase 1 localized in the former lowland and phase 2 in the former highland. The Reed Bank and North Palawan block is the extended ancient forearc region (Taylor and Hayes, 1983).

Chapter 5: Concluding remarks

In the dissertation, we systematically explore the idea of continental extension in orogenic belts approximated by a crustal wedge overlying the lithospheric mantle, through both analytical modeling and numerical experiments. We apply these concepts to the origin of core complexes and detachment faults, and the tectonic evolution of the SCS.

In chapter 2, we investigate the physics of lower crustal flow in a crustal wedge in the presence or absence of a preexisting weak mid-crustal shear zone. We analyze how topographic loading and mantle buoyancy drive lower crustal flow, and how the mid-crustal shear zone enhances the lower crustal flow. Using numerical modeling methods, we demonstrate that a weak mid-crustal shear zone effectively decouples upper crustal extension from lower crustal flow, crustal from lithospheric mantle deformation. We find that by increasing the strength of the lower crust, different modes of extension develop in the crustal wedge. We suggest that our models can be used to explain the origin of core complexes and to interpret the structure of some continental margins.

In Chapter 3, we apply our models to the origin of metamorphic core complexes and detachment faults. We present 4 models that provide a view of how core complexes form and evolve through time consistent with the geological and geophysical observations. We show that topographic loading and mantle buoyancy forces, together with divergent boundary, drive a regional crust flow from the highland towards the lowland. The lower crust flows towards the lowland where intense faulting induces strong unloading. The detachment fault is a decoupling zone that accommodates large displacement and accumulates sustained shear strain between upper and lower crust up to more than 10 Myr. We show that detachment faults can slip at low angle as a preexisting

weak brittle shear zone in which the principal stress axes are rotated to a non-Andersonian state by intense lower crustal flow at their base. They also form and slip at low angle in areas of strong topographic gradients such as range fronts.

In chapter 4, we apply these concepts in the more complex context of the SCS. Based on a data synthesis and numerical models, we propose that a two-phase extensional scenario in an orogenic belt that may explain the formation of the SCS margins. Phase 1 is asymmetric, decoupled, and generates a series of large rift basins and uplifts mainly in the current proximal parts of the SCS margin. Phase 2 is symmetric, coupled, and generates conjugate margins characterized with domino normal faults dipping seawards, and finally leads to breakup and seafloor spreading.

We will pursue our effort in addressing issues regarding continental extension in orogenic belts, but there are several issues remained to be answered, such as 1) the dynamics of mid-crustal shear zone including its weakening and strengthening mechanisms and their effects during postorogenic extension, 2) the effects of delamination of a mountain root, 3) the effects of magmatic and fluids activities commonly occurring during postorogenic extension, and 4) the interplay of internal and external forces that drive extension in orogenic belts. In addition, concepts derived in the dissertation may be applied to island arc systems and back-arc extension. The above-mentioned problems may serve as directions for future research.

Appendix A: Supplementary materials for chapter 2

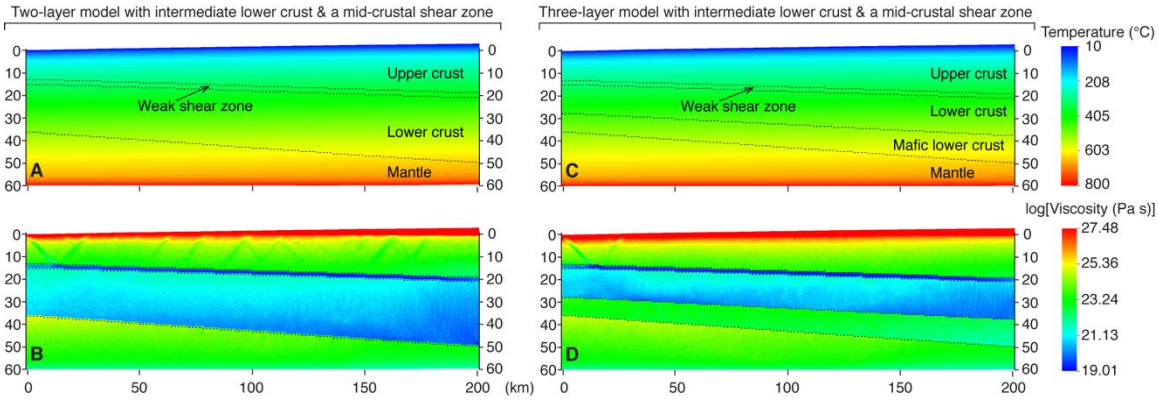

Figure A1: A.C. Temperature of two-layer and three-layer crust models, respectively, with a weak shear zone at the very early stage (0.1 Myr). B.D. Viscosity of two-layer and three-layer crust models, respectively, with a weak shear zone at the very early stage (0.1 Myr).

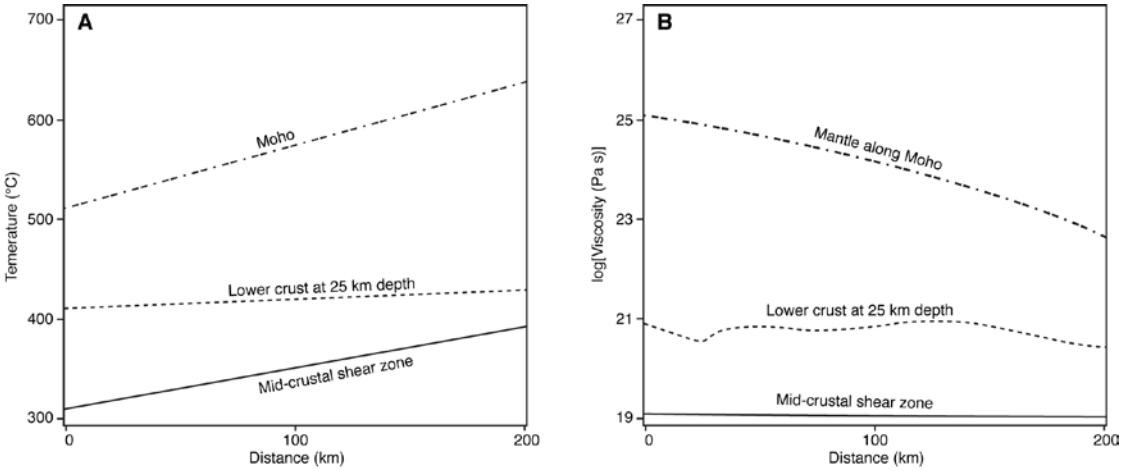

Figure A2: A. Plot of temperature in the mid-crustal shear zone, at 25 km depth in the lower crust, and Moho as shown in Fig. A1C. B. Plot of viscosity in the mid-crustal shear zone, at 25 km depth in the lower crust, and in the mantle along Moho as shown in Fig. A1D.

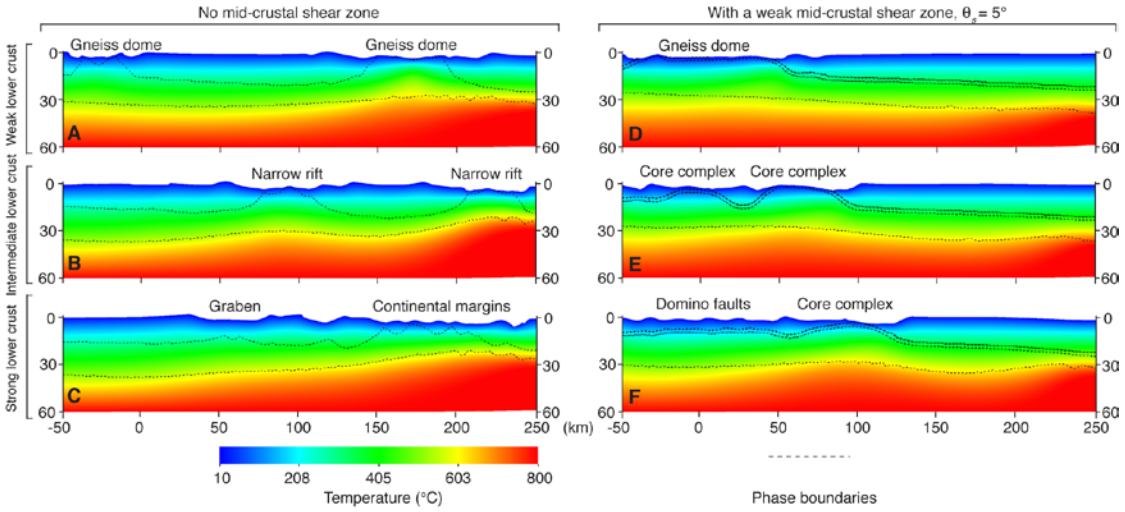

Figure A3: Temperature field of numerical models corresponding to those shown in Fig. 2.4.

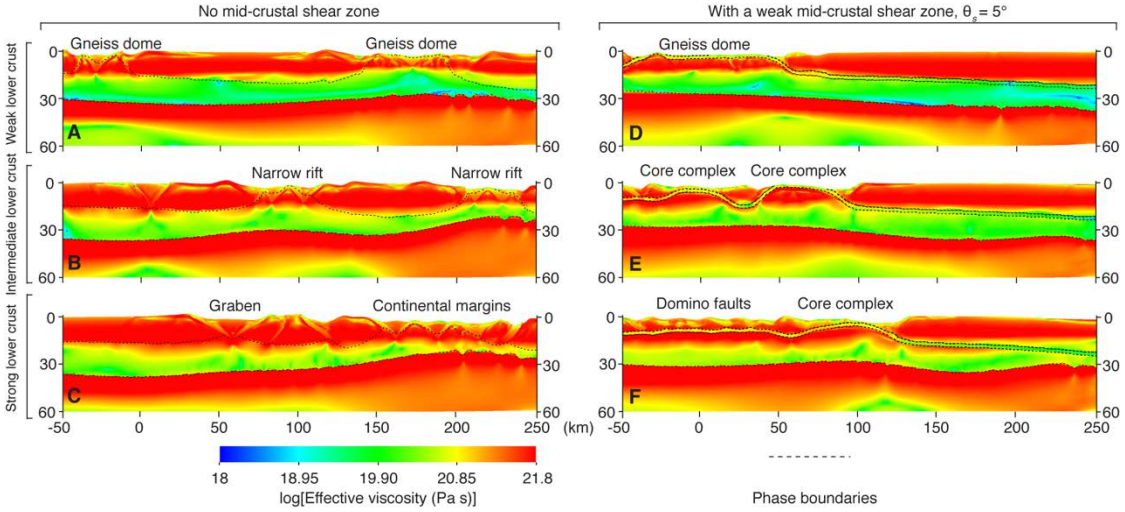

Figure A4: Effective viscosity of numerical models corresponding to those shown in Fig. 2.4.

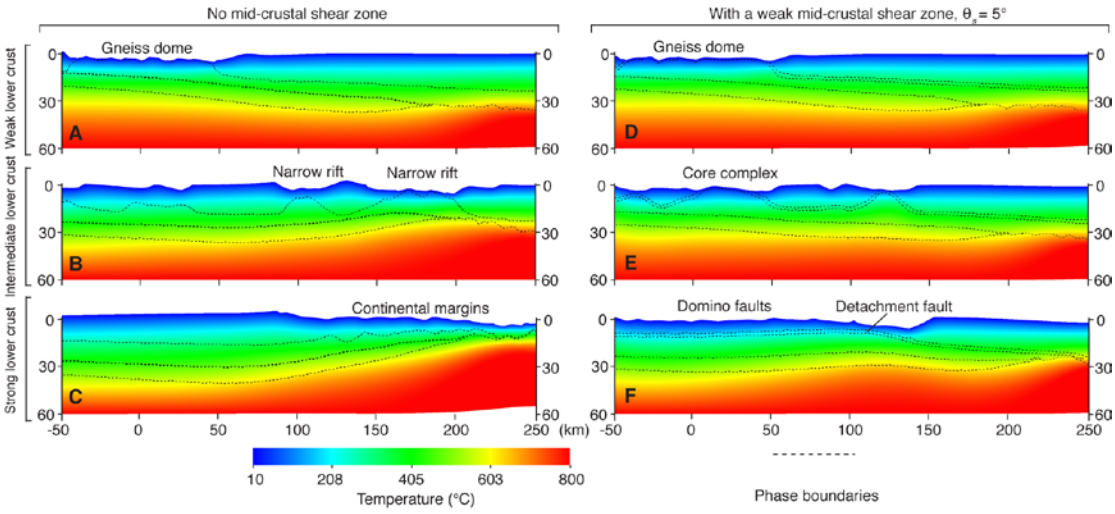

Figure A5: Effective viscosity of numerical models corresponding to those shown in Fig. 2.5.

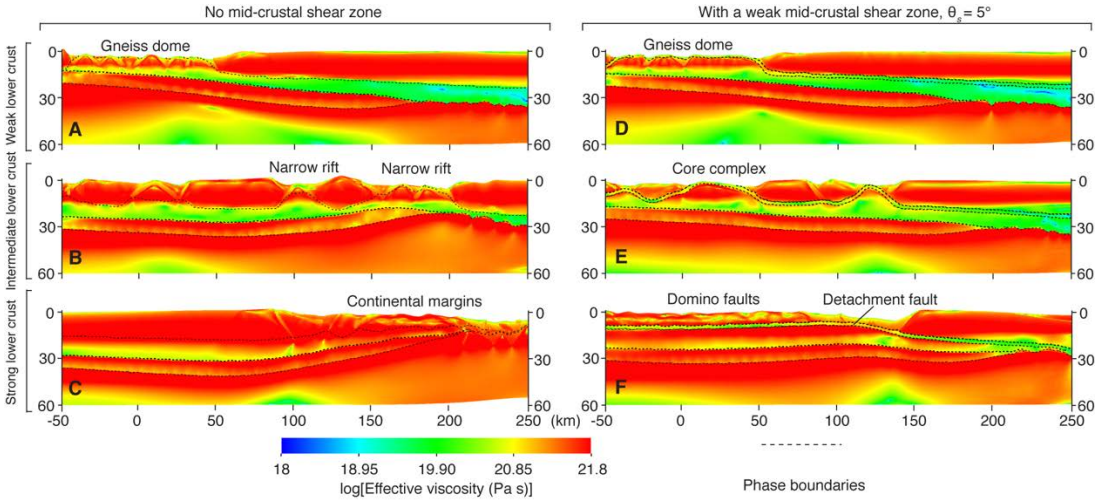

Figure A6: Effective viscosity of numerical models corresponding to those shown in Fig. 2.5.

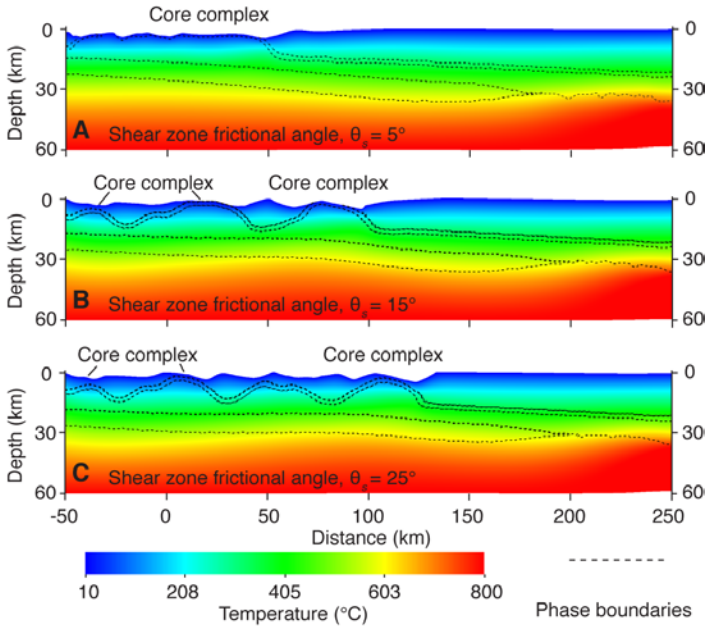

Figure A7: Effective viscosity of numerical models corresponding to those shown in Fig. 2.6.

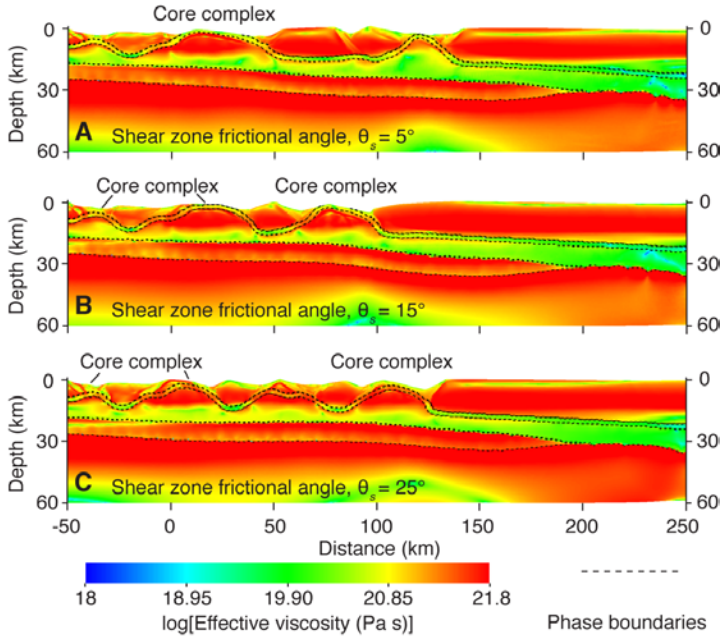

Figure A8: Effective viscosity of numerical models corresponding to those shown in Fig. 2.6.

Note: The following movies can be played back in Adobe Reader 9 or later. For the hard copy version of the dissertation, please find the accompanied CD or see Wu et al. (2015).

Movie A1: Evolution of 2-layer-crust numerical model corresponding to Fig. 2.4D with weak lower crust (wet quartz with 0.12% added water), showing generation of a huge massif through a bivergent detachment system.

Movie A2: Evolution of the 2-layer-crust numerical model corresponding to Fig. 2.4E with intermediate lower crust (wet quartz), showing generation of classic Cordilleran core complexes and migration of extension from lowland towards highland.

Movie A3: Evolution of the 2-layer-crust numerical model corresponding to Fig. 2.4F with strong lower crust (dry quartz), showing generation of migrating domino normal faults, and formation of a core complex through flexural uplift.

Appendix B: Supplementary materials for chapter 4

METHODS

To model phase 1, we used identical methods as described in Wu et al. (2015), but we let the model run a lot longer. The Palawan block before extension is assumed in the SE our modeled region (Fig. B1). The northern South China Sea (SCS) region before Cenozoic extension is assumed to be an orogenic belt regionally dipping towards NW. We varied lower crust from strong to weak using plagioclase (Ranalli, 1995) as reference and systematically reduced its activation energy term of the dislocation creep law. The mid-crustal shear zone is assumed weak when it is viscous (low cut-off viscosity ~ 10^{19} Pa s). Weak to strong mid-crustal shear zones when it is brittle are tested as well by increasing its internal frictional angle. We imposed a constant velocity boundary on both sides at an overall velocity of 1.25 cm yr^{-1}. Key model parameters are shown in Table B1. To model phase 2, we use identical method but excluding the mid-crustal shear zone.

In both phase 1 and phase 2 models, the model results are very sensitive to lower crust rheology as well as frictional strength of the mid-crustal shear zone. We therefore spent significantly amount of time to figure out the best parameters we believe better represent the SCS margins. However, since parameter space is huge, and many parameters may contribute towards the same model results, we can only use qualitative terms such as weak, intermediate or strong to describe the lower crust and the mid-crustal shear zone when it is brittle.

SUPPLEMENTARY TABLES

Phase	ρ (kg m^{-3})	θ (°)	θ' (°)	C (MPa)	A (MPa^{-n} s^{-1})	E_a (J mol^{-1})	n	C_p (J Kg^{-1}K^{-1})	h_r (W kg^{-1})
Upper crust	2700	30	15	40	0.125	2.76×10^5	3.05	1000	10^{-9}
Weak lower crust	2800	30	15	40	0.125	1.8×10^5	3.05	1000	10^{-9}
Intermediate lower crust	2800	30	15	40	0.125	2.4×10^5	3.05	1000	10^{-9}
Strong lower crust	2800	30	15	40	0.125	2.76×10^5	3.05	1000	10^{-9}
Mafic lower crust	3000	30	15	40	0.125	3.5×10^5	3.05	1000	10^{-9}
Mid-crustal shear zone	2800	5-25	5-25	4	0.125	1.76×10^5	3.05	1000	10^{-9}
Mantle	3300	30	15	40	7.0×10^4	5.2×10^5	3.0	1000	-

- Abbreviation in column headings: ρ (density), θ (initial frictional angle), θ' (frictional angle after weakening), C (cohesion), A (coefficient in the creep law), E_a (activation energy in creep law), n (exponential component in the creep law), C_p (heat capacity), and h_r (radioactive heating).

Table B1: Summary of key model parameters for both phase 1 and phase 2.

SUPPLEMENTARY FIGURES

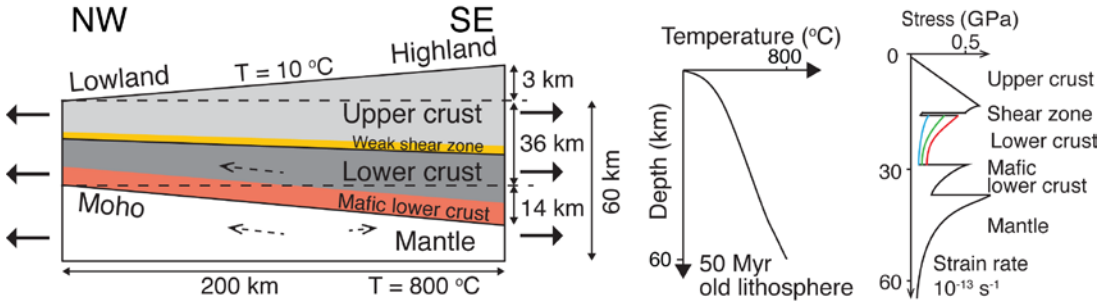

Figure B1: Model setup for phase 1. See table B1 for model parameters. For phase 2, the model set up is identical but excluding the weak shear zone.

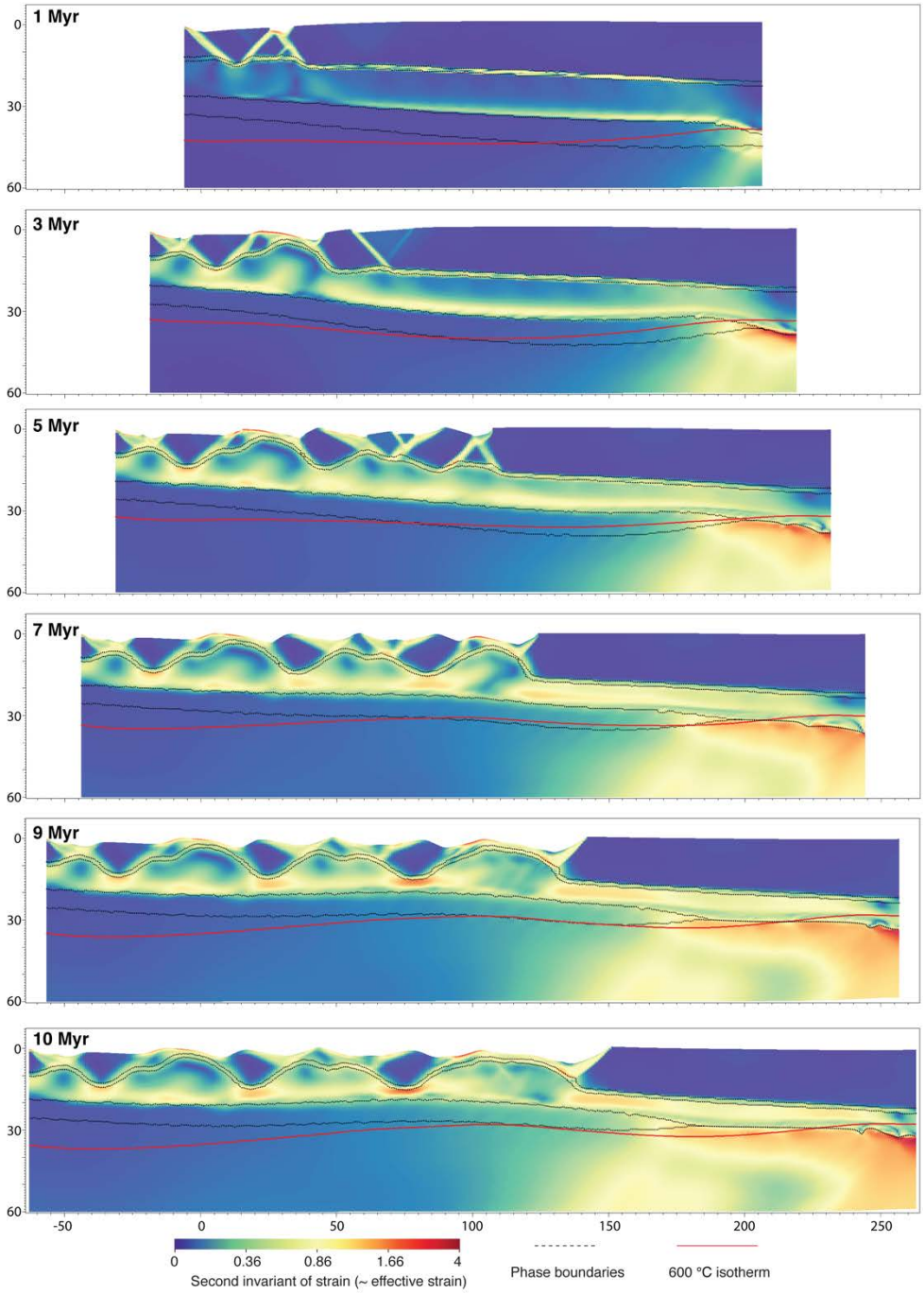

Figure B2: 10 Myr evolution corresponding to model shown in Fig. 4.3A.

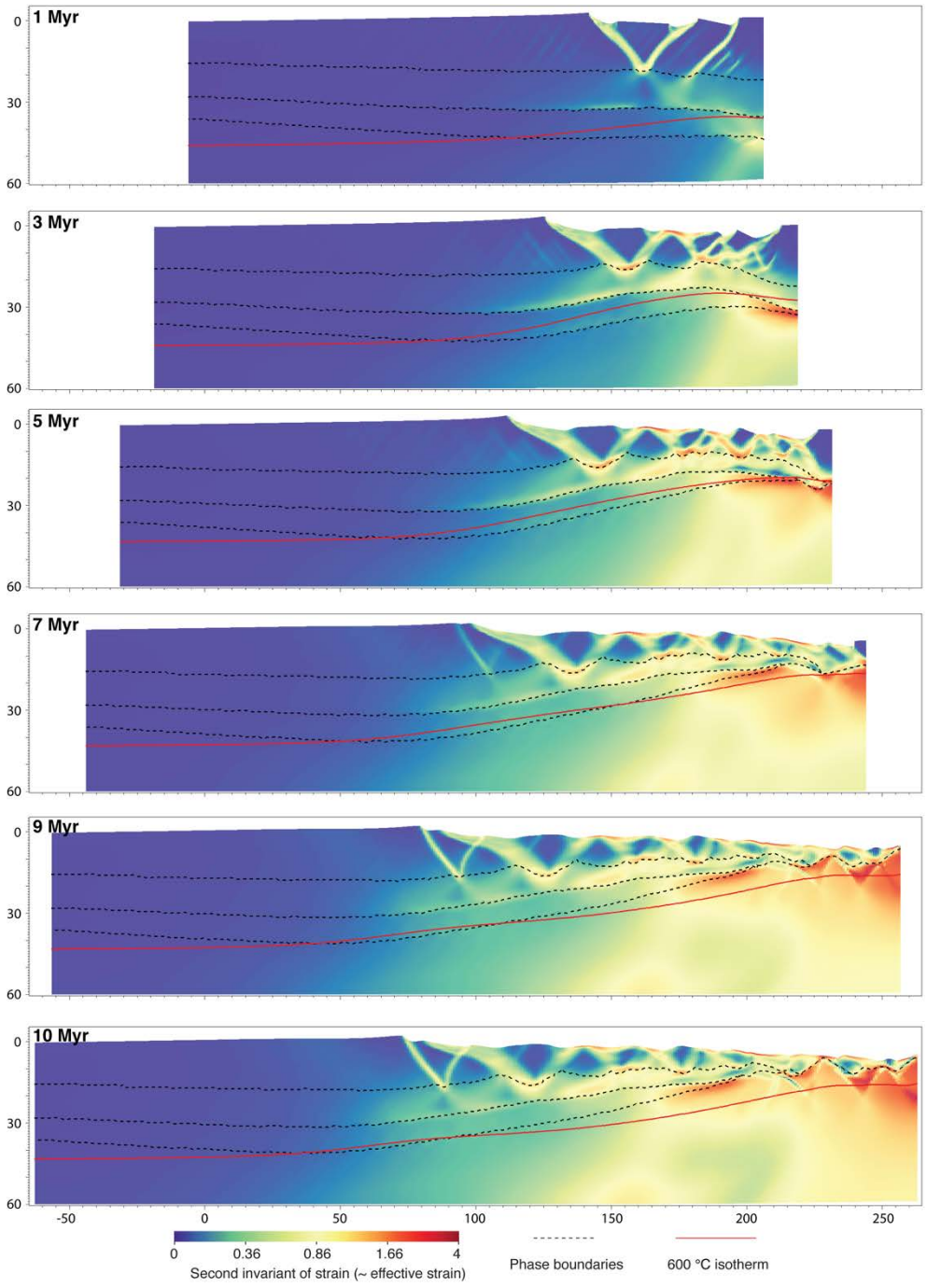

Figure B3: 10 Myr evolution corresponding to the model in Fig.4.3B.

References

Anderson, E. M. (1951), *Dynamics of Faulting*, 2nd ed. Oliver and Boyd, Edinburgh.

Axen, G. J. (1988), The Geometry of Planar Domino-Style Normal Faults above a Dipping Basal Detachment, *J. Struct. Geol.*, *10*(4), 405-411, doi:10.1016/0191-8141(88)90018-1.

Banks, C. J., and J. Warburton (1991), Mid-crustal detachment in the Betic system of southeast Spain, *Tectonophysics*, *191*(3), 275-289.

Barchi, M., G. Minelli, and G. Pialli (1998), The CROP 03 profile: a synthesis of results on deep structures of the Northern Apennines, *Mem. Soc. Geol. Ital*, *52*, 383-400.

Bartley, J. M., and B. P. Wernicke (1984), The Snake Range decollement interpreted as a major extensional shear zone, *Tectonics*, *3*(6), 647-657.

Bassi, G. (1991), Factors controlling the style of continental rifting: insights from numerical modelling, *Earth Planet. Sci. Lett.*, *105*(4), 430-452.

Beaumont, C., R. Jamieson, M. Nguyen, and B. Lee (2001), Himalayan tectonics explained by extrusion of a low-viscosity crustal channel coupled to focused surface denudation, *Nature*, *414*(6865), 738-742.

Behr, W. M., and J. P. Platt (2011), A naturally constrained stress profile through the middle crust in an extensional terrane, *Earth Planet. Sci. Lett.*, *303*(3-4), 181-192, doi:10.1016/j.epsl.2010.11.044.

Bellanger, M., N. Bellahsen, L. Jolivet, T. Baudin, R. Augier, and A. Boutoux (2014), Basement shear zones development and shortening kinematics in the Ecrins Massif, Western Alps, *Tectonics*, *33*(2), 84-111.

Bialas, R. W., W. R. Buck, M. Studinger, and P. G. Fitzgerald (2007), Plateau collapse model for the transantarctic mountains-west Antarctic rift system: Insights from numerical experiments, *Geology*, *35*(8), 687-690, doi:10.1130/G23825A.1.

Bird, P. (1991), Lateral extrusion of lower crust from under high topography in the isostatic limit, *J. Geophys. Res.*, *96*(B6), 10275-10210,10286.

Bird, R. B., W. E. Stewart, and E. N. Lightfoot (2007), *Transport phenomena*, John Wiley and Sons, New York

Block, L., and L. H. Royden (1990), Core complex geometries and regional scale flow in the lower crust, *Tectonics*, *9*(4), 557-567.

Braun, J., and C. Beaumont (1989), A physical explanation of the relation between flank uplifts and the breakup unconformity at rifted continental margins, *Geology*, *17*(8), 760-764.

Briais, A., P. Patriat, and P. Tapponnier (1993), Updated interpretation of magnetic anomalies and seafloor spreading stages in the South China Sea: Implications for

the Tertiary tectonics of Southeast Asia, *J. Geophys. Res. (1978–2012)*, *98*(B4), 6299-6328.

Brown, M., and G. S. Solar (1998), Shear-zone systems and melts: feedback relations and self-organization in orogenic belts, *J. Struct. Geol.*, *20*(2), 211-227.

Buck, W. (2007), Dynamic processes in extensional and compressional settings: The dynamics of continental breakup and extension, *Treatise on Geophysics*, *6*, 335-376. doi:10.1016/B978-044452748-6.00110-3

Buck, W. R. (1988), Flexural rotation of normal faults, *Tectonics*, *7*(5), 959-973.

Buck, W. R. (1991), Modes of Continental Lithospheric Extension, *J. Geophys. Res.*, *96*(B12), 20161-20178, doi:10.1029/91JB01485.

Buck, W. R., L. L. Lavier, and A. N. B. Poliakov (1999), How to make a rift wide, *Philos. Trans. R. Soc. A.*, *357*(1753), 671-690.

Buck, W. R., L. L. Lavier, and A. N. B. Poliakov (2005), Modes of faulting at mid-ocean ridges, *Nature*, *434*(7034), 719-723, doi:10.1038/nature03358.

Buck, W. R., C. Small, and W. B. Ryan (2009), Constraints on asthenospheric flow from the depths of oceanic spreading centers: The East Pacific Rise and the Australian-Antarctic Discordance, *Geochem. Geophys. Geosyst.*, *10*(9).

Burov, E. B., and M. Diament (1995), The Effective Elastic Thickness (T-E) of Continental Lithosphere - What Does It Really Mean, *J. Geophys. Res.*, *100*(B3), 3905-3927, doi:10.1029/94JB02770.

Choi, E., and W. R. Buck (2012), Constraints on the strength of faults from the geometry of rider blocks in continental and oceanic core complexes, *J. Geophys. Res. (1978–2012)*, *117*(B4).

Choi, E., W. R. Buck, L. L. Lavier, and K. D. Petersen (2013), Using core complex geometry to constrain fault strength, *Geophy. Res. Lett.*, *40(15)*, 3863-3867.

Christiansen, R., R. Yeats, S. Graham, W. Niem, A. Niem, and P. Snavely Jr (1992), Post-Laramide geology of the US Cordilleran region, *The Geology of North America*, *3*, 261-406.

Clift, P., and J. Lin (2001), Preferential mantle lithospheric extension under the South China margin, *Mar. Petrol. Geol.*, *18*(8), 929-945.

Collettini, C. (2011), The mechanical paradox of low-angle normal faults: Current understanding and open questions, *Tectonophysics*, *510*(3), 253-268.

Collettini, C., N. De Paola, R. Holdsworth, and M. Barchi (2006), The development and behaviour of low-angle normal faults during Cenozoic asymmetric extension in the Northern Apennines, Italy, *J. Struct. Geol.*, *28*(2), 333-352.

Collettini, C., A. Niemeijer, C. Viti, and C. Marone (2009), Fault zone fabric and fault weakness, *Nature*, *462*(7275), 907-910, doi:10.1038/nature08585.

Coney, P. J. (1980), Cordilleran suspect terranes, *Nature*, *288*, 329-333.

Cullen, A., P. Reemst, G. Henstra, S. Gozzard, and A. Ray (2010), Rifting of the South China Sea: new perspectives, *Petrol. Geosci.*, *16*(3), 273-282.

Davis, G. A., and G. Lister (1988), Detachment faulting in continental extension; perspectives from the southwestern US Cordillera, *Geol. Soc. Am. Spec. Pap.*, *218*, 133-160.

Davis, G. H. (1980), Structural characteristics of metamorphic core complexes, southern Arizona, *Geol. Soc. Am. Mem.*, *153*, 35-78.

Davis, G. H., and P. J. Coney (1979), Geologic development of the Cordilleran metamorphic core complexes, *Geology*, *7*(3), 120.

DeMets, C., R. G. Gordon, and D. F. Argus (2010), Geologically current plate motions, *Geophys. J. Int.*, *181*(1), 1-80.

Dewey, J. (1988), Extensional collapse of orogens, *Tectonics*, *7*(6), 1123-1139.

Dewey, J. F., and J. M. Bird (1970), Mountain belts and the new global tectonics, *J. Geophys. Res.*, *75*(14), 2625-2647.

Dickinson, W. R. (2004), Evolution of the North American Cordillera, *Annu. Rev. Earth Planet. Sci.*, *32*, 13-45.

Dunbar, J. A., and D. S. Sawyer (1989), How preexisting weaknesses control the style of continental breakup, *J. Geophys. Res.*, *94*(B6), 7278-7292.

Faulkner, D., T. Mitchell, D. Healy, and M. Heap (2006), Slip on 'weak' faults by the rotation of regional stress in the fracture damage zone, *Nature*, *444*(7121), 922-925.

Franke, D., D. Savva, M. Pubellier, S. Steuer, B. Mouly, J.-L. Auxietre, F. Meresse, and N. Chamot-Rooke (2014), The final rifting evolution in the South China Sea, *Mar. Petrol. Geol.*, *58*, 704-720.

Gans, P. B. (1987), An Open-System, 2-Layer Crustal Stretching Model for the Eastern Great-Basin, *Tectonics*, *6*(1), 1-12, doi:10.1029/TC006i001p00001.

Gans, P. B., and W. A. Bohrson (1998), Suppression of volcanism during rapid extension in the basin and range province, united states, *Science*, *279*(5347), 66-68.

Gautier, P., J.-P. Brun, and L. Jolivet (1993), Structure and kinematics of upper Cenozoic extensional detachment on Naxos and Paros (Cyclades Islands, Greece), *Tectonics*, *12*(5), 1180-1194.

Gautier, P., J. P. Brun, R. Moriceau, D. Sokoutis, J. Martinod, and L. Jolivet (1999), Timing, kinematics and cause of Aegean extension: a scenario based on a comparison with simple analogue experiments, *Tectonophysics*, *315*(1), 31-72.

Gessner, K., U. Ring, C. Johnson, R. Hetzel, C. W. Passchier, and T. Güngör (2001), An active bivergent rolling-hinge detachment system: Central Menderes metamorphic core complex in western Turkey, *Geology*, *29*(7), 611-614.

Gessner, K., C. Wijns, and L. Moresi (2007), Significance of strain localization in the lower crust for structural evolution and thermal history of metamorphic core complexes, *Tectonics*, *26*(2).

Gueydan, F., Y. M. Leroy, and L. Jolivet (2004), Mechanics of low-angle extensional shear zones at the brittle-ductile transition, *J. Geophys. Res.*, *109*(B12), B12407.

Hall, R. (1997), Cenozoic plate tectonic reconstructions of SE Asia, *Geol. Soc., London, Spec. Pub.*, *126*(1), 11-23.

Hauge, T. A., E. C. Hauser, J. E. Oliver, C. J. Potter, and S. Klemperer (1986), The Moho in the Northern Basin and Range Province, Nevada, Along the Cocorp 40-Degree-N Seismic-Reflection Transect, *Geol. Soc. Am. Bull.*, *97*(5), 603-618, doi:10.1130/0016-7606(1986)97<603:TMITNB>2.0.CO;2.

Hetzel, R., C. W. Passchier, U. Ring, and Ö. O. Dora (1995), Bivergent extension in orogenic belts: the Menderes massif (southwestern Turkey), *Geology*, *23*(5), 455-458.

Hirth, G., and D. Kohlstedt (2003), Rheology of the upper mantle and the mantle wedge: A view from the experimentalists, *Inside the subduction Factory*, 83-105.

Hirth, G., C. Teyssier, and J. W. Dunlap (2001), An evaluation of quartzite flow laws based on comparisons between experimentally and naturally deformed rocks, *Int. J. Earth Sci.*, *90*(1), 77-87.

Holloway, N. (1982), North Palawan Block, Philippines; its relation to Asian mainland and role in evolution of South China Sea, *AAPG Bull.*, *66*(9), 1355-1383.

Houseman, G. A., D. P. McKenzie, and P. Molnar (1981), Convective instability of a thickened boundary layer and its relevance for the thermal evolution of continental convergent belts, *J. Geophys. Res.*, *86*(B7), 6115-6132.

Hu, D., D. Zhou, X. Wu, M. He, X. Pang, and Y. Wang (2009), Crustal structure and extension from slope to deepsea basin in the northern South China Sea, *J. Earth Sci.*, *20*, 27-37.

Huet, B., L. Le Pourhiet, L. Labrousse, E. B. Burov, and L. Jolivet (2011), Formation of metamorphic core complex in inherited wedges: A thermomechanical modelling study, *Earth Planet. Sci. Lett.*, *309*(3-4), 249-257, doi:10.1016/j.epsl.2011.07.004.

Huismans, R., and C. Beaumont (2011), Depth-dependent extension, two-stage breakup and cratonic underplating at rifted margins, *Nature*, *473*(7345), 74-U85, doi:10.1038/nature09988.

Jackson, J., and N. White (1989), Normal faulting in the upper continental crust: observations from regions of active extension, *J. Struct. Geol.*, *11*(1-2), 15-36.

Jaoul, O., J. Tullis, and A. Kronenberg (1984), The Effect of Varying Water Contents on the Creep-Behavior of Heavitree Quartzite, *J. Geophys. Res.*, *89*(NB6), 4298-4312, doi:10.1029/JB089iB06p04298.

Jolivet, L., and J. P. Brun (2010), Cenozoic geodynamic evolution of the Aegean, *Int. J. Earth Sci.*, *99*(1), 109-138.

Jolivet, L., et al. (1998), Midcrustal shear zones in postorogenic extension: Example from the northern Tyrrhenian Sea, *J. Geophys. Res.*, *103*(B6), 12123-12160, doi:10.1029/97JB03616.

Jolivet, L., C. Faccenna, B. Huet, L. Labrousse, L. Le Pourhiet, O. Lacombe, E. Lecomte, E. Burov, Y. Denèle, and J.-P. Brun (2013), Aegean tectonics: Strain localisation, slab tearing and trench retreat, *Tectonophysics*, *597*, 1-33.

Ketcham, R. A. (1996), Thermal models of core-complex evolution in Arizona and New Guinea: Implications for ancient cooling paths and present-day heat flow, *Tectonics*, *15*(5), 933-951.

Kirby, S., and A. Kronenberg (1987), Rheology of the lithosphere: selected topics, *Rev. Geophys.*, *25*(6), 1219-1244.

Klemperer, S. L., T. Hauge, E. Hauser, J. Oliver, and C. Potter (1986), The Moho in the northern Basin and Range province, Nevada, along the COCORP 40 N seismic-reflection transect, *Geol. Soc. Am. Bull.*, *97*(5), 603-618.

Kounov, A., E. Wüthrich, D. Seward, J.-P. Burg, and D. Stockli (2015), Low-temperature constraints on the Cenozoic thermal evolution of the Southern Rhodope Core Complex (Northern Greece), *Int. J. Earth Sci.*, *104*(5), 1337-1352.

Kruse, S., M. McNutt, J. Phippsmorgan, L. Royden, and B. Wernicke (1991), Lithospheric Extension near Lake Mead, Nevada - a Model for Ductile Flow in the Lower Crust, *J. Geophys. Res.*, *96*(B3), 4435-4456, doi:10.1029/90JB02621.

Lavier, L. L., and W. R. Buck (2002), Half graben versus large-offset low-angle normal fault: Importance of keeping cool during normal faulting, *J. Geophys. Res.*, *107*(B6).

Lavier, L. L., W. R. Buck, and A. N. B. Poliakov (2000), Factors controlling normal fault offset in an ideal brittle layer, *J. geophys. Res*, *105*(23), 431–423.

Lavier, L. L., and G. Manatschal (2006), A mechanism to thin the continental lithosphere at magma-poor margins, *Nature*, *440*(7082), 324-328, doi:10.1038/nature04608.

Lavier, L. L., W. Roger Buck, and A. N. B. Poliakov (1999), Self-consistent rolling-hinge model for the evolution of large-offset low-angle normal faults, *Geology*, *27*(12), 1127-1130.

Lester, R., H. J. Van Avendonk, K. McIntosh, L. Lavier, C. S. Liu, T. Wang, and F. Wu (2014), Rifting and magmatism in the northeastern South China Sea from wide-angle tomography and seismic reflection imaging, *J. Geophys. Res.*, *119*(3), 2305-2323.

Li, C. F., X. Xu, J. Lin, Z. Sun, J. Zhu, Y. Yao, X. Zhao, Q. Liu, D. K. Kulhanek, and J. Wang (2014), Ages and magnetic structures of the South China Sea constrained by deep tow magnetic surveys and IODP Expedition 349, *Geochem. Geophys. Geosyst.*, *15*(12), 4958-4983.

Lister, G. S., and G. A. Davis (1989), The origin of metamorphic core complexes and detachment faults formed during Tertiary continental extension in the northern Colorado River region, USA, *J. Struct. Geol.*, *11*(1-2), 65-94.

Malinverno, A., and W. B. Ryan (1986), Extension in the Tyrrhenian Sea and shortening in the Apennines as result of arc migration driven by sinking of the lithosphere, *Tectonics*, *5*(2), 227-245.

Martinez, F., A. M. Goodliffe, and B. Taylor (2001), Metamorphic core complex formation by density inversion and lower-crust extrusion, *Nature*, *411*(6840), 930-934, doi:10.1038/35082042.

McCarthy, J., S. P. Larkin, G. S. Fuis, R. W. Simpson, and K. A. Howard (1991), Anatomy of a metamorphic core complex: Seismic refraction/wide-angle reflection profiling in southeastern California and western Arizona, *J. Geophys. Res. (1978–2012)*, *96*(B7), 12259-12291.

McGuire, A. V. (1994), Southern Basin and Range Province Crust-Mantle Boundary - Evidence from Gabbroic Xenoliths, Wikieup, Arizona, *J. Geophys. Res.*, *99*(B12), 24263-24273, doi:10.1029/94JB01184.

McIntosh, K., L. Lavier, H. van Avendonk, R. Lester, D. Eakin, and C.-S. Liu (2014), Crustal structure and inferred rifting processes in the northeast South China Sea, *Mar. Petrol. Geol.*, *58*, 612-626, doi:10.1016/j.marpetgeo.2014.03.012.

McKenzie, D., F. Nimmo, J. A. Jackson, P. Gans, and E. Miller (2000), Characteristics and consequences of flow in the lower crust, *J. Geophys. Res.*, *105*(B5), 11,029-011,046.

Melosh, H. (1990), Mechanical basis for low-angle normal faulting in the Basin and Range province, *Nature*, *343*, 331-335.

Miller, E. L., P. B. Gans and J. Garing (1983), The Snake Range décollment: An exhumed Mid-Tertiary ductile-brittle transition, *Tectonics*, *2*(3), 239-263.

Miller, M., and T. Pavlis (2005a), The Black Mountains turtlebacks: Rosetta stones of Death Valley tectonics, *Earth-Science Reviews*, *73*(1-4), 115-138, doi:10.1016/j.earscirev.2005.04.007.

Miller, M. B., and T. L. Pavlis (2005b), The Black Mountains turtlebacks: Rosetta stones of Death Valley tectonics, *Earth Sci. Rev.*, *73*(1-4), 115-138, doi:10.1016/j.earscirev.2005.04.007.

Muntener, O., J. Hermann, and V. Trommsdorff (2000), Cooling history and exhumation of lower crustal granulite and Upper Mantle (Malenco, Eastern Central Alps), *J. Petrol.*, *41*(2), 175-200, doi:10.1093/petrology/41.2.175.

Nagel, T. J., and W. R. Buck (2006), Channel flow and the development of parallel-dipping normal faults, *J. Geophys. Res.*, *111*(B8), B08407.

Oliot, E., P. Goncalves, K. Schulmann, D. Marquer, and O. Lexa (2013), Mid-crustal shear zone formation in granitic rocks: Constraints from quantitative textural and crystallographic preferred orientations analyses, *Tectonophysics*, 612 (2014): 63-80

Osmundsen, P., and J. Ebbing (2008), Styles of extension offshore mid-Norway and implications for mechanisms of crustal thinning at passive margins, *Tectonics*, *27*(6). doi:10.1029/2007TC002242

Pautot, G., et al. (1986), Spreading direction in the central South China Sea, *Nature*, *321*(6066), 150-154.

Platt, J., and R. Vissers (1989), Extensional collapse of thickened continental lithosphere: A working hypothesis for the Alboran Sea and Gibraltar arc, *Geology*, *17*(6), 540-543.

Platt, J. P., and W. M. Behr (2011), Grainsize evolution in ductile shear zones: Implications for strain localization and the strength of the lithosphere, *J. Struct. Geol.*, *33*(4), 537-550, doi:10.1016/j.jsg.2011.01.018.

Platt, J. P., W. M. Behr, and F. J. Cooper (2014), Metamorphic core complexes: windows into the mechanics and rheology of the crust, *J. Geol. Soc*.

Platt, J. P., W. M. Behr, K. Johanesen, and J. R. Williams (2013), The Betic-Rif arc and its orogenic hinterland: A review, *Annual Rev. Earth Planet. Sci.*, *41*, 313-357.

Poliakov, A., P. Cundall, Y. Podladchikov, and V. Lyakhovsky (1993), An explicit inertial method for the simulation of viscoelastic flow: an evaluation of elastic effects on diapiric flow in two-and three-layers models, *NATO ASI Ser. C Math. Phy. Sci.*, *391*, 175-175.

Ranalli, G., 1995. *Rheology of the Earth, 2nd ed*. Chapman and Hall, London.

Ranalli, G., and D. C. Murphy (1987), Rheological stratification of the lithosphere, *Tectonophysics*, *132*(4), 281-295.

Ranero, C. R., and M. Perez-Gussinye (2010), Sequential faulting explains the asymmetry and extension discrepancy of conjugate margins, *Nature*, *468*(7321), 294-U180, doi:10.1038/nature09520.

Regenauer-Lieb, K., R. F. Weinberg, and G. Rosenbaum (2006), The effect of energy feedbacks on continental strength, *Nature*, *442*(7098), 67-70, doi:10.1038/nature04868.

Rehrig, W. A., and S. J. Reynolds (1980), Geologic and geochronologic reconnaissance of a northwest-trending zone of metamorphic core complexes in southern and western Arizona, *Cordilleran metamorphic core complexes: Geol. Soc. Am. Mem.*, *153*, 131-157.

Reston, T. J., C. M. Krawczyk, and D. Klaeschen (1996), The S reflector west of Galicia (Spain): Evidence from prestack depth migration for detachment faulting during continental breakup, *J. Geophys. Res.*, *101*(B4), 8075-8091, doi:10.1029/95JB03466.

Rey, P., C. Teyssier, and D. Whitney (2009), Extension rates, crustal melting, and core complex dynamics, *Geology*, *37*(5), 391.

Rey, P. F., C. Teyssier, and D. L. Whitney (2010), Limit of channel flow in orogenic plateaux, *Lithosphere*, *2*(5), 328-332, doi:10.1130/L114.1.

Ru, K., and J. D. Pigott (1986), Episodic rifting and subsidence in the South China Sea, *AAPG Bull.*, *70*(9), 1136-1155.

Shuto, K., H. Ishimoto, Y. Hirahara, M. Sato, K. Matsui, N. Fujibayashi, E. Takazawa, K. Yabuki, M. Sekine, and M. Kato (2006), Geochemical secular variation of magma source during Early to Middle Miocene time in the Niigata area, NE Japan: Asthenospheric mantle upwelling during back-arc basin opening, *Lithos*, *86*(1), 1-33.

Singleton, J. S. (2013), Development of extension-parallel corrugations in the Buckskin-Rawhide metamorphic core complex, west-central Arizona, *Geol. Soc. Am. Bull.*, *125*(3-4), 453-472.

Smith, S., R. Holdsworth, C. Collettini, and M. Pearce (2011), The microstructural character and mechanical significance of fault rocks associated with a continental low-angle normal fault: the Zuccale Fault, Elba Island, Italy, *Geol. Soc., London, Spec. Pub.*, *359*(1), 97-113.

Sodoudi, F., R. Kind, D. Hatzfeld, K. Priestley, W. Hanka, K. Wylegalla, G. Stavrakakis, A. Vafidis, H. P. Harjes, and M. Bohnhoff (2006), Lithospheric structure of the Aegean obtained from P and S receiver functions, *J. Geophys. Res. (1978–2012)*, *111*(B12).

Sonder, L., P. England, B. P. Wernicke, and R. Christiansen (1987), A physical model for Cenozoic extension of western North America, *Geol. Soc., London, Spec. Pub.*, *28*(1), 187-201.

Spencer, J. E. (1984), Role of tectonic denudation in warping and uplift of low-angle normal faults, *Geology*, *12*(2), 95.

Spencer, J. E., and C. G. Chase (1989), Role of crustal flexure in initiation of low-angle normal faults and implications for structural evolution of the Basin and Range province, *J. Geophys. Res.*, *94*(B2), 1765-1775.

Sun, Z., Z. Zhong, M. Keep, D. Zhou, D. Cai, X. Li, S. Wu, and J. Jiang (2009), 3D analogue modeling of the South China Sea: a discussion on breakup pattern, *Journal of Asian Earth Sciences*, *34*(4), 544-556.

Tan, E., L. L. Lavier, H. J. Van Avendonk, and A. Heuret (2012), The role of frictional strength on plate coupling at the subduction interface, *Geochem. Geophys. Geosyst.*, *13*(10).

Tapponnier, P., G. Peltzer, A. Le Dain, R. Armijo, and P. Cobbold (1982), Propagating extrusion tectonics in Asia: New insights from simple experiments with plasticine, *Geology*, *10*(12), 611-616.

Taylor, B., and D. E. Hayes (1983), Origin and history of the South China Sea basin, *Geophy. Monogr. Ser.*, *27*, 23-56.

Tirel, C., J.-P. Brun, and E. Burov (2008), Dynamics and structural development of metamorphic core complexes, *J. Geophys. Res.*, *113*(B4), doi:10.1029/2005JB003694.

Velasco, M. S., R. A. Bennett, R. A. Johnson, and S. Hreinsdottir (2010), Subsurface fault geometries and crustal extension in the eastern Basin and Range Province, western US, *Tectonophysics*, *488*(1-4), 131-142, doi:10.1016/j.tecto.2009.05.010.

Watts, A. (2001), Isostasy and Flexure of the Lithosphere, *Isostasy and Flexure of the Lithosphere*, Cambridge University Press, Cambridge

Wernicke, B. (1981), Low-angle normal faults in the Basin and Range province - Nappe tectonics in an extending orogen, *Nature*, *291*(5817), 645-648, doi:10.1038/291645a0.

Wernicke, B. (1985), Uniform-sense normal simple shear of the continental lithosphere, *Can. J. Earth Sci.*, *22*(1), 108-125.

Wernicke, B. (1992), Cenozoic extensional tectonics of the US Cordillera, *The Cordilleran orogen: Conterminous US: Boulder, Colorado, Geological Society of America, Geology of North America*, *3*, 553–581.

Wernicke, B. (1995), Low-angle normal faults and seismicity: A review, *J. Geophys. Res.*, *100*(B10), 20159-20174.

White, R., and D. McKenzie (1989), Magmatism at rift zones: the generation of volcanic continental margins and flood basalts, *J. Geophys. Res.*, *94*(B6), 7685-7729.

Whitney, D. L., C. Teyssier, P. Rey, and W. R. Buck (2013), Continental and oceanic core complexes, *Geol. Soc. Am. Bull.*, *125*(3-4), 273-298.

Whitney, D. L., C. Teyssier, and O. Vanderhaeghe (2004), Gneiss domes and crustal flow, *Geol. Soc. Am. Spec. Pap.*, *380*, 15-33.

Wills, S., and W. R. Buck (1997), Stress-field rotation and rooted detachment faults: A Coulomb failure analysis, *J. Geophys. Res.*, *102*(B9), 20503-20520,20514.

Wu, G., L. L. Lavier, and E. Choi (2015), Modes of continental extension in a crustal wedge, *Earth Planet. Sci. Lett.*, *421*, 89-97, doi:doi:10.1016/j.epsl.2015.04.005.

Yin, A. (1989), Origin of regional, rooted low-angle normal faults: A mechanical model and its tectonic implications, *Tectonics*, *8*(3), 469-482.

Zuber, M., E. Parmentier, and R. Fletcher (1986), Extension of continental lithosphere: a model for two scales of Basin and Range deformation, *J. Geophys. Res.*, *91*(B5), 4826-4838.